Dynamics of Synaptically Interacting Integrate-and-Fire Neurons

by

Matthew Philip James

A DOCTORAL THESIS

Submitted in partial fulfilment of the requirements

for the award of

Doctor of Philosophy in Mathematics of Loughborough University

April 2002

Summary

Travelling waves of activity have been experimentally observed in many neural systems. The functional significance of such travelling waves is not always clear. Elucidating the mechanisms of wave initiation, propagation and bifurcation may therefore have a role to play in ascertaining the function of such waves. Previous treatments of travelling waves of neural activity have focussed on the mathematical analysis of travelling pulses and numerical studies of travelling waves. It is the aim of this thesis to provide insight into the propagation and bifurcation of travelling waveforms in biologically realistic systems.

There is a great deal of experimental evidence which suggests that the response of a neuron is strongly dependent upon its previous activity. A simple model of this synaptic adaptation is incorporated into an existing theory of strongly coupled discrete integrate-and-fire (IF) networks. Stability boundaries for synchronous firing shift in parameter space according to the level of adaptation, but the qualitative nature of solutions is unaffected. The level of synaptic adaptation is found to cause a switch between bursting states and those which display temporal coherence.

Travelling waves are analysed within a framework for a one-dimensional continuum of integrate-and-fire neurons. Self-consistent speeds and periods are determined from integro-differential equations. A number of synaptic responses (α-function and passive and quasi-active dendrites) produce qualitatively similar results in the travelling pulse case. For IF neurons, an additional refractory mechanism needs to be introduced in order to prevent arbitrarily high firing rates. Different mathematical formulations are considered with each producing similar results. Dendrites are extensions of a neuron which branch repeatedly and the electrical properties may vary. Under certain conditions, this active membrane gives rise to a membrane impedance that displays a prominent maximum at some nonzero resonant frequency. Dispersion curves which relate the speed of a periodic travelling wave to its period are constructed for the different synaptic responses with additional oscillatory behaviour apparent in the quasi-active dendritic regime. These stationary points are shown to be critical for the formation of multi-periodic wave trains. It is found that periodic travelling waves with two periods bifurcate from trains with a single period via a drift in the spike times at stationary points in the dispersion curve.

Some neurons rebound and fire after release from sustained inhibition. Many previous mathematical treatments have not included the effect of this activity. Analytical studies of a simple model which exhibits post-inhibitory rebound show that these neurons can support half-centre oscillations and periodic travelling waves. In contrast to IF networks, only a single travelling pulse wavespeed is possible in this network. Simulations of this biophysical model show broad agreement with the analytical solutions and provide insight into more complex waveforms.

Results of the thesis are presented in a discussion along with possible directions for future study. Noise, inhomogeneous media and higher spatial dimensions are suggested.

Keywords: biophysical models, dendrites, integrate-and-fire, neural coding, neural networks, post-inhibitory rebound, synaptic adaptation, travelling waves

ACKNOWLEDGEMENTS

Contents

Chapter 1

Introduction

An important goal of mathematical biology is to create models which provide precise statements about biological systems. Existing techniques established in mathematical analysis can be utilised to study these models. Mathematical neuroscience is one such area of mathematical biology which has grown rapidly over the last twenty years at both the single cell and network levels. Forming a better understanding of the primary characteristics of mathematical neural models and the parameters which control their behaviour can lead to advances in targetting specific activity in experiments. This will ultimately result in capturing the essence of neural processing and structure. The human brain is a creamy coloured, wrinkled object isolated from the rest of the body in its own compartment. It has no moving parts, and weighs, on average, about 1.3 kg. The brain is comprised of many different cells, the majority of which are split into two distinct sets: neurons and glia. Neurons transmit information between themselves, and glia can be viewed as the tissue which surrounds and supports neurons in the central nervous system. There are approximately 10^{12} neurons in the human brain. Due to the soft nature of the material, the Greeks assumed that it was the perfect site for the immortal soul. This changed when Alcmaeon of Croton discovered that there are connections from the eyes to

the brain; thus claiming that it was the seat for thought. This discovery agreed with two Alexandrian physicists, Herophilus and Erasistratus, who had found nerves leading from parts of the body into the brain. The Greek physician Galen (A.D 129–199) then proposed that the soul was to be found in the fluid which bathes the brain and the spinal cord (cerebrospinal fluid). This fluid is constantly circulated (produced at about 0.2 ml/min in humans) and is known to contain salts, sugars and proteins. This is a far cry from being the seat of the soul and has even been called the 'urine of the brain'. People who believe in the immortal soul are now convinced that it cannot be found in the brain, and that the brain's sole purpose is for thought and feeling.

Throughout the ages, neuroscience has attracted the interest of some of the most remarkable people in history including Leonardo Da Vinci, René Descartes and Luigi Galvani. This particular area of science began to increase in momentum in the 18th century when it was revealed that the nervous system was essentially electrical in nature. Experimentation using electricity supported the assertion that different regions of the brain controlled different aspects of physical and emotional abilities. The actual architecture of the brain is extremely complex and many different regions have been categorised for brain function. For example, the hippocampus has become the primary region in the mammalian brain for the study of the synaptic basis of memory and learning [145], and the majority of input to the cortex is relayed through the thalamus [112].

The first person to describe a nerve cell was Johannes Purkinje in 1837, and the large nerve cells in the cerebral cortex bear his name. More recently, Golgi and Ramón y Cajal shared the Nobel prize in medicine in 1906 for their work on the structure of the nervous system. The techniques they developed to distinguish individual neurons are still in use. It was around this time that mathematical neuroscience began, and the seminal paper can be regarded as Lapicque's in 1907 [96]. The mechanisms responsible for the generation of neuronal action potentials were not known at this time, but Lapicque postulated that an action potential would be generated when the membrane capacitor

reached a certain threshold level. The action potential is the response of a neuron to sufficient stimulus. These action potentials (known as spikes) are used to communicate with other neurons in the system. Even though the Lapicque model is a simple caricature, it is extremely useful for modelling purposes.

In the middle of the 20th century, Sir Alan Lloyd Hodgkin and Sir Andrew Fielding Huxley wrote a series of papers which detailed their experiments on the squid giant axon [70, 71, 72]. In [73], they summarised these papers and cast them into mathematical form. The four-dimensional model formulated forms the basis of many mathematical models used today, and the authors won a Nobel prize in medicine in 1963 for their pioneering work. Other popular neural models soon followed. Fitzhugh and Nagumo independently calculated a two-dimensional model which is the most simple model proposed for spike generation [52, 53, 114]. The Morris-Lecar model is used effectively to describe neural dynamics, although it was originally introduced to describe the dynamics of a calcium spike in barnacle muscle (not nerve) fibres [110].

There is a great deal of evidence which suggests that when neurons communicate, it is the actual timing of the spikes which is important. Examples include visual encoding in flies [33], tiger salamander and rabbit [7], sound localisation in the auditory system of animals such as the barn owl [22] and odour encoding in locusts [155]. However, tsetse flies (Glossina spp.) process information in antennal olfactory cells using a rate-coding [152]. The current theory is that rate-coding and temporal-coding are both used in the olfactory system, but at different stages of the encoding process [97]. Recent studies on the rat somatosensory cortex conclude that the timing of the first spike from single neurons in response to a stimulus is the crucial element for coding stimulus location [118, 120]. Hence, more recent work has focussed on using models which support analytical calculations and capture these firing times.

Analysis is difficult to perform on these biophysical multi-variable models. Many biologically realistic models of the single neuron are so complex that they provide little

intuitive insight into the dynamics they simulate. Systematic reduction of the Hodgkin-Huxley model to a single variable model [1, 84] makes more effective analysis possible. A popular reduced model of a neuron is the integrate-and-fire model [96, 149]. This model is nonlinear, and cannot be described by smooth differential equations, since whenever the voltage of an integrate-and-fire neuron crosses a preset threshold, the neuron fires an action potential and the voltage is reset to some value. Threshold models such as this have led to detailed studies at the network level (see Bressloff and Coombes [18] for a recent review), where the properties of dendrites, axons and synapses are described with a biologically realistic delay kernel, and the timing of each action potential is deemed to be most important.

Rhythmic activities of various neural systems (first found in humans in 1929 [6]) can produce oscillations in, for example, locomotion, respiration, and heart beat. A network model with only a few variables was proposed by Wilson and Cowan (1972) [156]. A popular way to model these oscillations is by using coupled oscillators, which have been particularly successful when describing the synchronous flashing within firefly communities (which has much in common with neuronal oscillators since both communicate via pulses of activity) [43, 44, 108]. Indeed, phase-locked oscillators form the basis for virtually all rhythmic motor behaviour: breathing, swimming, running, and chewing for example. The theory developed to describe this natural phenomena is particularly useful when describing other forms of coupled oscillators — in particular, the interaction of neural cells. Oscillations are prevalent within the brain and are associated with, for example, learning [132], arousal [103], and Parkinson's disease [151].

Limit-cycle oscillators are particularly hard to treat analytically, which makes collective behaviour extremely difficult to analyse in general. However, progress can be made by assuming that these oscillators interact *weakly*. One of the first weakly connected systems to be studied was in a pair of pendulum clocks. Christian Huygens in 1665 noticed that the two clocks synchronised when attached to a beam rather than a wall.

The weak vibrations transmitted along the beam ensured that the pendulums swung in phase. Analysis of weakly coupled systems has mainly been made through the application of phase reduction methods to reduce the network dynamics to a system in which the relative phase between oscillators is the relevant dynamical variable [94]. This has been utilised for a number of models including Hodgkin-Huxley, integrate-and-fire and more general descriptions of neural oscillators [41, 48, 49, 60, 61, 62, 75]. Phase-locked states such as synchrony and travelling waves have been studied in terms of this description. These are solutions in which the neurons fire at a fixed common frequency.

However, it has not been established that neurons interact weakly and so one of the main challenges now involves extending this analysis to strongly coupled oscillators. For weak coupling, a ring of neural oscillators with excitatory subpopulations which are locally connected act as a pool of independent oscillators. Increasing the connection strengths leads to complex behaviour such as stochastic oscillations and travelling waves [9, 10]. Mirollo and Strogatz analysed a globally coupled integrate-and-fire network by using a return map argument, and showed that synchronisation almost always occurs in the presence of instantaneous excitatory interactions [108]. Bressloff and Coombes have recently made progress with a novel way of solving systems of strongly coupled neural oscillators [17, 18, 29]. Their analysis showed that some stability results calculated previously are only applicable for weak coupling [150] or for finite networks with slow synapses [54]. Indeed, this work bridges the gap between weakly coupled oscillator models and strongly coupled firing-rate (analog) models, which utilise a slow synapse approximation. Hence, an analytically tractable model which captures many of the features of more biophysical models is produced, without having to succumb to phase reduction techniques or averaging theory to calculate results pertaining to strong coupling and fast synapses.

Recently, experimentalists have been able to record travelling wave structures in various neural tissues. Stimulating regions of, for example, the cortex [55] and tha-

lamus [85] leads to the propagation of electrical activity. Spindle waves are observed at sleep onset [133] and a travelling wave is involved in epilepsy [25]. The functional significance of waves in these systems is not always clear. Elucidating the mechanisms of wave initiation, propagation and bifurcation is therefore directly relevant to determining the functional roles that waves may take on. Indeed, the propagation of synchronous spikes has been proposed by Abeles as a mechanism for generating the precisely timed spike events observed in multielectrode recordings of cortical circuits [3].

To capture the essence of a wave of spiking activity it is natural to work with perhaps the most simple spiking neuron model, namely the integrate-and-fire (IF) model. At the network level analytical and numerical studies have already shown wave behavior consistent with more detailed biophysical models. In particular, Golomb and Ermentrout [56, 57, 58] and Bressloff [14, 15] have developed a mathematical framework that can provide an exhaustive analysis of the speed and stability for solitary traveling pulses. Golomb and Ermentrout have made the fascinating observation that discrete delays arising in synaptic interactions can lead to the formation of non-smooth *lurching waves* of the type observed in numerical simulations of thalamic networks [130]. In a complementary fashion, the work of Bressloff builds upon this treatment, covering general forms of delay kernel often encountered in models of synaptic and dendritic processing. Moreover, away from the long-wavelength limit, the determination of wave stability is shown to be a highly non-trivial mathematical problem, involving the solution of a linear map of infinite order. Hence, almost nothing is known about the stability of periodic waves nor of the actual mechanisms by which periodic waves can lose stability. Previous studies of travelling waves have consisted of numerical studies of more complicated biophysical models [106, 129].

By performing experiments, Jahnsen and Llinàs found that thalamic cells offer two different types of neural firing; a burst and a tonic mode [82, 83]. Bursting occurs if sufficient hyperpolarisation occurs, an additional calcium current is activated upon depo-

larisation and a number of conventional sodium spikes will appear riding on the crest of some broad voltage envelope. tonic firing occurs if the calcium current is not activated. Any stimulus will then either cause a sub-threshold depolarisation, or a sequence of conventional sodium spikes. Many previous mathematical treatments of travelling waves do not take into account cells which rebound and fire an action potential after sufficient hyperpolarisation.

The aim of this thesis is to provide insight into the propagation and bifurcation of travelling waveforms in biologically realistic systems. First, by building upon an existing theory, the effects of synaptic adaptation on small discrete networks of integrate-and-fire neurons is examined. A simple model is used to elucidate any quantitative change in neural function. Then, the effects of dendrites and post-inhibitory rebound on travelling waves in one-dimensional continua are studied. A detailed overview of the thesis follows.

1.1   Overview of the thesis

Chapter 2 - Mathematical tools for neural analysis

Biological data is difficult to analyse and changing parameter values in an experiment can be costly and time consuming. Hence, mathematical models based on experimental data are formulated in order that insight can be gained quickly and effectively. Additionally, salient parameters in the model can be isolated without resorting to experiments. This chapter will discuss the biophysics of the neural models used throughout this thesis. The models illustrated are in current neuroscience literature. Firstly, it is important to capture the essential properties of a single neuron. A discussion on the Hodgkin-Huxley model of a neuron and its reduction to more analytically tractable models is presented. Secondly, neurons communicate with other neurons with action potentials. A biologically realistic mathematical form for this post-synaptic response is generated. Finally, neurons capture information at synaptic terminals on their dendrites (a branched tree-like structure). In this thesis, these are chosen to be modelled with a one-dimensional cable equation.

Sometimes, electrical properties may vary along the length of the dendrites, resulting in a cable with resonant properties. In this quasi-active case, a linearised form of the Hodgkin-Huxley model forms the basis of these electrical properties. Derivation of the dendritic model is presented in both the passive and quasi-active cases.

Chapter 3 - Synaptic adaptation in discrete integrate-and-fire networks

There is a great deal of experimental evidence which shows that the response of some neurons to synaptic input is not constant. As a result, the connection strengths between neurons can be modified and these modifications may persist, thereby forming elementary components of memory storage. A simple model for adapting synapses is incorporated into an existing theory of discrete networks of integrate-and-fire neurons (formulated by Bressloff and Coombes [18]). In this simple model of synaptic adaptation, the strength of the synaptic interaction is strongly dependent on the activity of the pre-synaptic neuron, where the connections between neurons may become stronger (facilitation) or weaker (depression). States in which the network exhibits synchronous behaviour are analysed, and oscillator death, bursting and pattern formation are shown to arise through a discrete Hopf (Neimark-Sacker) bifurcation in the firing times when the coupling strength is increased. The stability borders created in this chapter are qualitatively similar to those in a network without adaptation. By creating stability borders when the level of synaptic adaptation is the bifurcation parameter, depression is seen to have a significant role in neural coding. As the parameter regime changes from one exhibiting synaptic depression to one with facilitation, the firing rates in the system tend to form bursting packets as opposed to a more regular output, and vice-versa. These bursts can be represented effectively by a firing rate formalism, whereas a spike coding is more appropriate for activity with more spread.

Chapter 4 - Synaptic travelling waves in integrate-and-fire systems

A travelling wave is a phase-locked state with a constant phase difference between adjacent units. Many spatially extended dynamical systems support travelling waves. For example, action potentials on axons, spiral waves of electrical activity on hearts, and flame fronts in forest fires. Travelling waves of neural activity have been experimentally observed in many neural systems [5, 34, 122, 128, 157]. They are believed to be the mechanism for epileptic seizures [25], and are found in central pattern generators ([113] and references within), which are neural networks producing rhythmic patterned outputs without rhythmic sensory or central input. Periodic travelling waves and pulses are analysed in a one-dimensional continuum of synaptically-interacting integrate-and-fire neurons. Neurons in the system are considered to be connected with either compact or non-compact support, and with realistic synaptic interactions such as the so-called "α-function", and passive and quasi-active dendrites. For travelling pulse solutions, qualitatively similar shapes for the speed curves were found for all axo-dendritic connections — two branches (one fast, one slow) coalescing in a saddle point at a critical value of the synaptic coupling. The faster (slower) branch is shown to be linearly stable (unstable). For a smooth wave, there is a constant phase difference between each neuron and its neighbours. Axonal delays introduce an instability into the system resulting in the formation of lurching waves [57]. These waves recruit new clusters of oscillators into the wave in a saltatory manner. This travelling pulse work is extended to periodic travelling waves. Dispersion curves relating the speed of a periodic travelling wave to its period are constructed for the various axo-dendritic connections and similar shapes are observed. Two branches (one fast, one slow) meet at a minimum period. However, for quasi-active dendritic membranes, additional stationary points are present in the upper branch of the dispersion curve. A kinematic theory shows that the linear stability of travelling waves depends upon the gradient of the dispersion curve, resulting in a change of stability is predicted at stationary points. Periodic travelling waves with two constant periods are found to emerge from all local maxima in the dispersion curves via a drift in the spike times.

Chapter 5 - Biophysical models

Recent interest in thalamic relay cells has stemmed from the discovery that the thalamus does not serve as a simple relay to the cortex [135]. Thalamocortical relay cells express slow calcium currents which give rise to post-inhibitory rebound [82, 83]. This is a phenomenon whereby a neuron is induced to emit an action potential upon release from sustained inhibition. This so-called T-current could persist and ensure bursts of activity occur. An analytically tractable model of this phenomenon, and a comparison with other models, is presented. Precise mathematical statements show that half-centre oscillators exist only if the external drive to the system takes values in a narrow band. The size of this band decreases with the coupling strength. Similarly, for a travelling pulse in a one-dimensional continuum, only a single branch to the speed curve exists. Simulations of some of the more complex waveforms in a one-dimensional continuum of these neurons are presented.

Chapter 6 - Conclusions and further work

A summary of the major achievements, and possible extensions, of the thesis is presented. The extensions include stochastic systems, inhomogeneous networks and travelling waves in higher spatial dimensional waves.

Chapter 2

Mathematical tools for neural analysis

In this chapter, models will be presented which are used throughout this thesis. It is important to clarify the nature and development of these models in order that the analytical statements are sufficiently biologically realistic. In addition, the salient parameters of the dynamics can be given a useful biological interpretation. The network studies presented in the following chapters all rely on the neural responses described here.

2.1 Neuronal structure and spike generation

A neuron (or nerve cell) is any of the impulse-conducting cells which constitute the brain, spinal column, and nerves, consisting of a nucleated cell body (called a soma) with one or more dendrites and a single axon (see figure 2.1). The dendrites capture action potentials generated by other neurons at chemical junctions called synapses. These signals propagate along the path of least resistance. Injected current can travel long distances along the dendritic core before a significant fraction leaks out across the highly resistive cell membrane. In addition, more distal dendrites are thinner than those nearer the soma. Hence, the current travels towards the soma (usually spherical or pyramidal in shape with
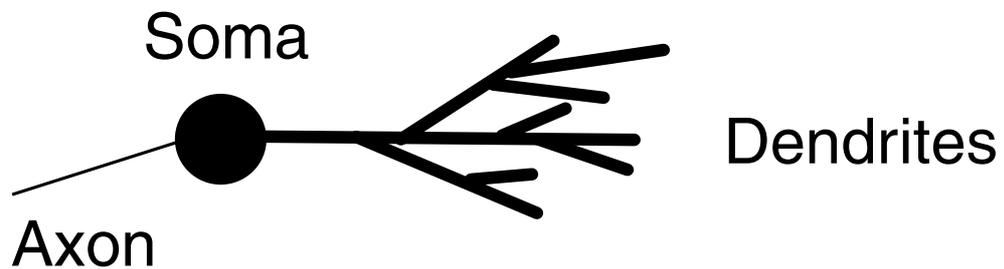
Figure 2.1 A cartoon depiction of a neuron. Action potentials are captured in the dendrites, which then cause electrical activity to travel towards the soma. Here the stimulus is processed and any resulting output (action potential) is passed along the axon. Axons form contacts at synapses with, for example, other axons or dendrites of other neurons.

a nucleus at its centre surrounded by cytoplasmic material and bounded by a membrane). Here the currents are processed, and any resulting output (known as an action potential or "spike") is passed along the axon. The axon is a thin, tube-like structure which extends from the soma. This part of the cell can vary greatly in size and studies have found lengths between several micrometres to one metre and diameters between several micrometres and a millimetre. Axons can make one or many connections with other parts of nerve cells at chemical junctions called synapses. Different types of contact can exist, for example axon with axon, and axon with soma, but by far the most frequent is an axon with the dendritic structure of another neuron. A single neuron may have hundreds of thousands of synapses, but the network is still sparsely connected due to the large number of neurons in the mammalian neocortex.

Sodium (Na^+), potassium (K^+), chlorine (Cl^-) and calcium (Ca^{2+}) ions are all present in the fluid in which the neurons exist. Channels exist in the membrane of the neuron in order that these ions can pass through. Concentrations of these ions are markedly different on either side of the membrane, since these channels are stimulus dependent (either voltage or chemical) and selective. With no stimulus, a nerve membrane typically has a resting potential of approximately -70mV with respect to the exterior and the gated channels are closed. In this equilibrium state, the concentration of the potassium ions in the intra-cellular fluid is ten times that in the extra-cellular fluid, whereas the sodium ions have a ten times greater concentration in the extra-cellular fluid.

For an action potential to be generated, the membrane's potential must be sufficiently depolarised and pass a certain threshold level (approximately -55mV). This then causes the voltage-gated sodium and potassium channels in the nerve membrane to open. Due to the significant difference in the concentration of the sodium ions, and the fact that the membrane potential is negative, the membrane potential surges toward a positive resting potential ($+50$mV) whereupon the sodium gates are closed. The membrane then starts to attract negative ions, thus repelling positive ions, which results in an even greater negative potential (-75mV) than the rest state. At this point, the voltage-dependent potassium channels close and the potential returns to the equilibrium value. Whilst the sodium gates are open, the neuron may not produce another action potential, and this phase is called the absolute refractory period. The neuron membrane has a much higher resistance compared to the intra-cellular fluid and so the action potential propagates down the axon.

The Hodgkin-Huxley model, which captures the method of spike generation in single neural cells, is presented in the following section. This four-dimensional biophysical model is difficult to analyse mathematically, and its reduction to the more readily analysed integrate-and-fire model is illustrated.

2.2   Reduction of the Hodgkin-Huxley model

The standard description of a neuron with spatially constant membrane potential V is based upon the conservation of electric charge (Kirchoff's Current Law[1]), such that

$$C_M \frac{dV}{dt} = -F + I_s + I, \tag{2.1}$$

where V is the displacement of the membrane potential from its resting level (in mV) The function F is the membrane current, and I_s is the sum of external synaptic currents contributed to by other neurons in the network, with I describing any external currents. The membrane capacity per surface unit (in $\mu F/cm^2$), C_M, is taken to be constant since there is only a 2% change during the 100mV depolarization of an action potential [26, 74].

The Hodgkin-Huxley model of a neuron is recognised as one of the most complete models of a neuron. It was initially conceived to deal with the behaviour of the squid (*Loligo*) giant axon, and considerable agreement with experimental data is observed [73]. Currents in the model arise due to the conduction of sodium and potassium voltage dependent channels in the membrane. All other currents are assumed to obey Ohm's law[2].

The Hodgkin-Huxley model of the nerve cell is equation (2.1) with the function F defined as,

$$F(V; m, n, h) = g_{Na} m^3 h (V - V_{Na}) + g_K n^4 (V - V_K) + g_L (V - V_L), \tag{2.2}$$

where the sodium activation, sodium inactivation and potassium activation gating variables are denoted as m, h, n respectively and are bounded by 0 and 1. For $X \in \{m, n, h\}$,

$$\tau_X(V) \frac{dX}{dt} = X_\infty(V) - X, \tag{2.3}$$

with

$$\tau_X(V) = \frac{1}{\alpha_X(V) + \beta_X(V)}, \quad X_\infty(V) = \alpha_X(V) \tau_X(V). \tag{2.4}$$

---

[1]The sum of all currents entering a node is equal to the sum of all currents leaving that node.

[2]The potential difference across an ideal conductor is proportional to the current through it.

Parameter	Value	Unit
Cellular parameters		
V_{Na}	50	mV
V_K	-77	mV
V_L	-54.4	mV
g_{Na}	120	mS/cm^2
g_K	36	mS/cm^2
g_L	0.3	mS/cm^2
C_M	1	μF/cm^2

Table 2.1 Standard cellular parameter values for the Hodgkin-Huxley model of a nerve cell, obtained from fits with experimental data (from the giant axon of the squid *Loligo*). These parameters are considered to be temperature independent [73].

The parameters g_{Na}, g_K and g_L are the conductances to sodium (Na), potassium (K) and leakage capacitance respectively. The terms on the right of equation (2.2) are respectively the current carried by Na ions, the current carried by K ions, and the leak current. Table 2.1 gives typical values for the parameters based on experimental data (at 6.3°C) [73].

The six functions $\tau_m(V), \tau_n(V), \tau_h(V)$ (time constants of the conductance variables) and $m_\infty(V), n_\infty(V), h_\infty(V)$ (asymptotic values of the conductance variables), shown in figure 2.2, are given by the following formulae [73],

$$
\alpha_m = \frac{V+40}{10\left(1-e^{-\frac{V+40}{10}}\right)}, \quad \beta_m = 4e^{-\frac{V+65}{18}},
$$

$$
\alpha_n = \frac{V+55}{100\left(1-e^{-\frac{V+55}{10}}\right)}, \quad \beta_n = \frac{1}{8}e^{-\frac{V+65}{80}}, \tag{2.5}
$$

$$
\alpha_h = \frac{7}{100}e^{-\frac{V+65}{20}}, \quad \beta_h = \frac{1}{1+e^{-\frac{V+35}{10}}}.
$$
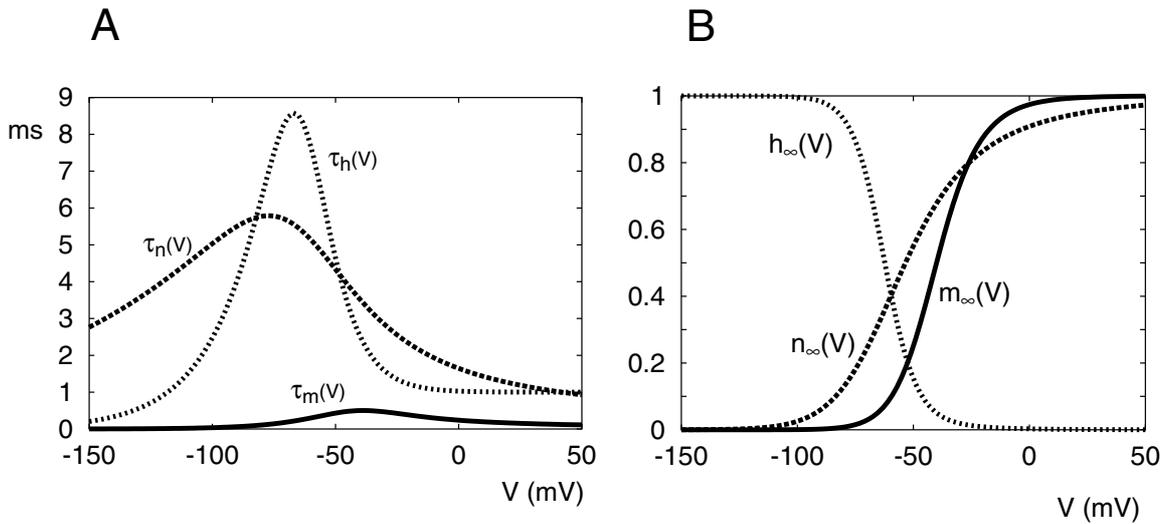
Figure 2.2 A: The time constants of the conductance variables (m, n, h) as functions of the voltage V. B: The asymptotic values of the conductance variables (m_∞, n_∞, h_∞) as functions of the voltage V. The figures are created using the functions given in equations (2.4) and (2.5) with parameter values given in table 2.1.

An example of a Hodgkin-Huxley spike is given in figure 2.3. In the paper by Hodgkin and Huxley [73], the formulae were given relative to the resting potential (approximately -65 mV) and depolarisation was taken to be negative. Throughout this thesis, depolarisation is taken to be positive. It is possible to reduce the Hodgkin-Huxley model of the neuron to more simple models. Indeed, this is necessary in order that analysis can be effectively carried out. Reduction may proceed in a variety of ways. For example Kistler *et al.* [88] consider approximating the dynamics with a Volterra expansion resulting in the spike response model, of which the integrate-and-fire model is a special case. A different approach was undertaken by Destexhe [35] who constructed a pulse-based model. The philosophy behind this description is to approximate the time course
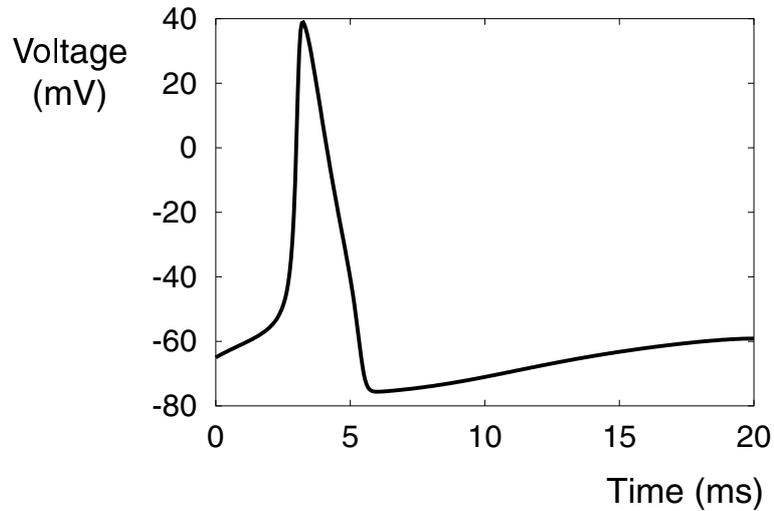
Figure 2.3 An action potential generated by the Hodgkin-Huxley model of nerve membrane. Note that the asymptotic steady state of the potential is approximately -65 mV. The parameter values used are given in table 2.1. A single neuron (equation (2.1) with equation (2.2)) is driven with a constant current $I = 5$ μA/cm^2 ($I_s = 0$ μA/cm^2).

of the rate constants by a pulse, triggered when the membrane potential crosses a given threshold. The variables in equations (2.5) take on different values before, during and after this pulse. During the pulse, $\beta_m, \alpha_h, \beta_n = 0$ and otherwise, $\alpha_m, \beta_h, \alpha_n = 0$. The non-zero values of the other variables at these times are evaluated from the value of the voltage-dependent expressions (equation (2.5)) at hyperpolarised and depolarised potentials (chosen to be -70 mV and $+20$ mV respectively). Both of these reduced models show excellent agreement with the full Hodgkin-Huxley model.

The method chosen to reduce the Hodgkin-Huxley system of equations in this thesis was applied by Abbott *et al.* [1, 84]. It involves the use of equivalent potentials and proceeds as follows. From figure 2.2(A) notice that the time constant governing the

conductance variable m is much smaller than those for n and h. Therefore, since the m dynamics are relatively fast, m can be replaced by its asymptotic value $m_\infty(V)$. The model is now already reduced to three variables from four at the expense of accuracy over very short time intervals. However, the variables n and h cannot be replaced by their asymptotic values because the model would then be unable to generate action potentials, as h and n would counteract the action potential as quickly as m would create it. To demonstrate h and n lagging behind (see figure 2.2(A)), they are slaved to auxilliary voltages U_h and U_n respectively. Then, the slower approach of h and n to their asymptotic values can be mimicked by the replacement

$$X = X_\infty(U_X), \quad X \in \{h, n\},$$

This can always be solved exactly for U_X since the functions X_∞ are monotonic and hence invertible. However, it is found in practice that the two potentials U_h, U_n are remarkably similar and so can be assumed to be identical, and thus, $U_h = U_n = U$. However, the model will only be reduced to two variables if U is chosen appropriately. This is done by ensuring that the time-dependence of U in $f(V, U) = F(V; m_\infty(V), h_\infty(U), n_\infty(U))$ mimics the time-dependence induced in $F(V; m_\infty(V), h, n)$ in the full model. By equating time derivatives of F and f at constant V, the following is imposed,

$$\frac{\partial F}{\partial h}\frac{dh}{dt} + \frac{\partial F}{\partial n}\frac{dn}{dt} = \left(\frac{\partial f}{\partial h_\infty}\frac{dh_\infty(U)}{dU} + \frac{\partial f}{\partial n_\infty}\frac{dn_\infty(U)}{dU} \right)\frac{dU}{dt}.$$

Combining this with equation (2.3), with $X_\infty(U)$ replacing X for $X = h, n$, gives dU/dt in terms of V and U, and the reduced Hodgkin-Huxley model is

$$C_M\frac{dV}{dt} = -f(V, U) + I, \tag{2.6a}$$

$$\frac{dU}{dt} = g(V, U), \tag{2.6b}$$

where

$$g(V, U) = \frac{\frac{\partial F}{\partial h}\left(\frac{h_\infty(V) - h_\infty(U)}{\tau_h(V)} \right) + \frac{\partial F}{\partial n}\left(\frac{n_\infty(V) - n_\infty(U)}{\tau_n(V)} \right)}{\frac{\partial f}{\partial h_\infty}\frac{dh_\infty}{dU} + \frac{\partial f}{\partial n_\infty}\frac{dn_\infty}{dU}},$$

and with the evaluation of $\partial F/\partial X$ being performed at $X = X_\infty(U)$, $X = h, n$.
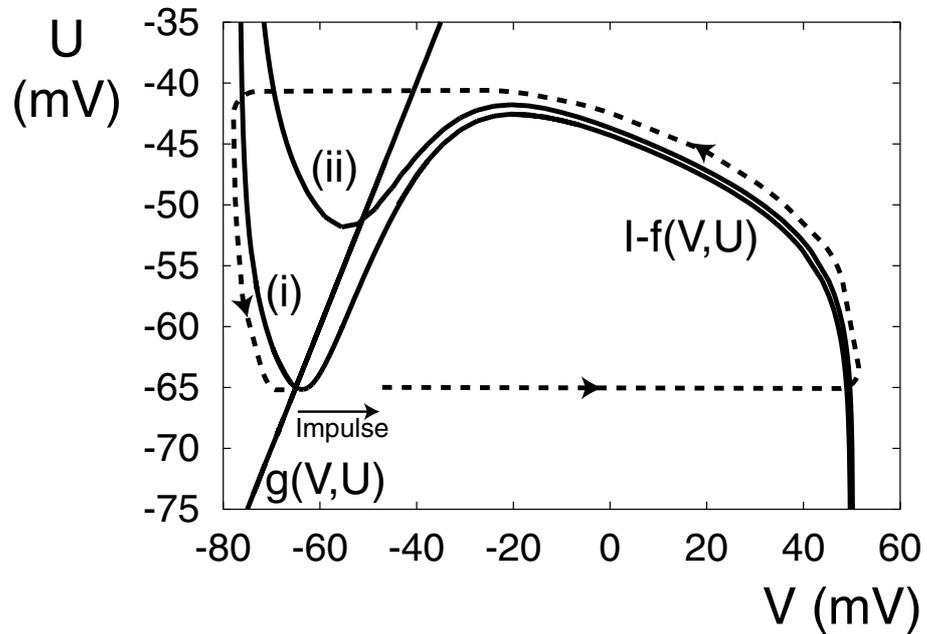
Figure 2.4 U, V nullclines defined by equations (2.6) with (i) $I = 0$ (excitatory regime). The impulse indicates an initial shock to the system due to current injection. As a result of a suitably sized impulse, the U and V variables follow the path indicated by the dashed line. This corresponds to an action potential being formed in the system. Without this initial impulse, the system will remain at the stable steady state defined by the intersection of the nullclines, $(U, V) \approx (-65, -65)$. (ii) $I = 50$ (oscillatory regime). The steady state is no longer stable and so no impulse is required to create the large potential excursion. A limit cycle is created resulting in repetitive firing.

The nullclines ($dV/dt = 0, dU/dt = 0$) of the system in equations (2.6) are shown in figure 2.4 for different values of the input current I. The variable V describes the capacitive nature of the cell and U describes the time-dependence of the membrane conductance. In fact, U may be regarded as a variable for the refractory period of the

neuron in the following way. If the neuron has just fired then the potential V will be on the V nullcline moving towards the steady state. Hence, for the small impulses, the neuron will be unable to fire since there will be insufficient stimulus to cross the positive gradient section of the V nullcline. For small values of input current I, the stable steady state of the system (at the intersection of the nullclines) is to the left of the local minima of the V nullcline. Hence, for small perturbations, the voltage will relax back to the steady state. For larger initial excursions, the refractory variable will take effect and force the voltage to take a large deviation following the path shown. This signifies that an action potential has been created and the neuron has fired. When the external input is large enough, the steady state is unstable and so repetitive firing must occur. It is convenient at this point to define oscillatory and excitatory regimes. When a neuron is in the oscillatory regime, repetitive firing will occur (figure 2.4(ii)). In the excitatory regime (figure 2.4(i)), extra current injections need to be provided to the cell in order that an action potential can be generated. This reduced model (equations (2.6)) is similar to the Fitzhugh-Nagumo model of a nerve cell [52, 53, 114]

$$
\begin{aligned}
\frac{dV}{dt} &= V - \frac{V^3}{3} - U + I, \\
\frac{dW}{dt} &= \phi(V + a - bW),
\end{aligned}
$$

where the parameters a, b and ϕ are dimensionless and positive.

The equations for V incorporate the capacitive and integrative natures of the cell, whilst U represents the refractory period. Further reduction of the Hodgkin-Huxley model to an integrate-and-fire model can be achieved by assuming the refractory process U takes place instantaneously. In this case, time dependence of the membrane conductance is not produced, and the model cannot generate action potentials. To overcome this problem, it is assumed that when the membrane potential exceeds a certain threshold value, an action potential is fired, and the voltage reset to some determined lower level. The potential U can be eliminated in one of two ways; $U = V$ or $U = -65$. In both cases, the parameter values are given by the underlying Hodgkin-Huxley model. First, consider the case where
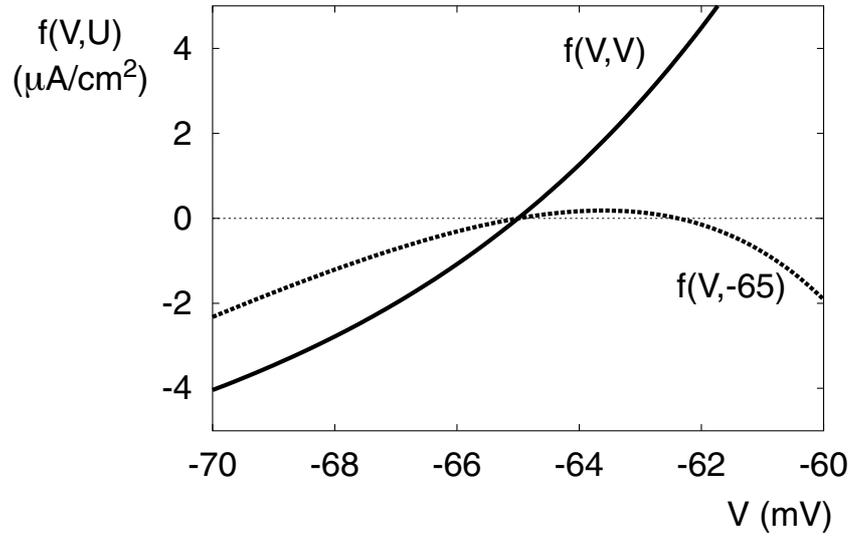
Figure 2.5 The function $f(V, U)$ evaluated for $U = -65$ and for $U = V$. It is clear from the diagram that $f(V, V)$ is approximately linear, whereas $f(V, -65)$ is more nonlinear.

$U = -65$. Then, the Marquardt-Levenberg algorithm can be utilised to fit this curve (see figure 2.5) to a quadratic polynomial $f(V, -65) = a(V - V_A)(V - h)$ where $a \approx -0.1$, $V_A \approx -65.2$ and the threshold for firing is given by $h \approx -63.4$. On the other hand, a linear integrate-and-fire model can be produced by setting $U = V$ and fitting the curve to $f(V, V) = a(V - h)$ with $a \approx 1.1$ and $h \approx -65.4$. The (linear) integrate-and-fire model used throughout this thesis has the form

$$\frac{dV}{dt} = -\frac{V}{\tau} + I,$$

where V represents the membrane potential, τ is the membrane time constant and I represents any current input to the neuron. This equation is supplemented with the reset condition such that whenever the voltage reaches some threshold V_θ with positive gradient in time, the membrane potential is discontinuously reset to a lower predetermined level.

21

This section has illustrated the reduction of the Hodgkin-Huxley system of equations which describe spike generation in single neural cells. The resulting integrate-and-fire model is more suitable for mathematical analysis since it involves a single linear ordinary differential equation with nonlinear reset. Single cells communicate with other cells to form neural networks. Methods by which these signals are transmitted are covered in the following two sections.

2.3   Synaptic interactions

In 1906, Sherrington coined the phrase "synapse" to describe the communication junction between neurons [136].

If there exists any surface or separation at the nexus between neurone and neurone, much of what is characteristic of the conduction exhibited by the reflex-arc might be more easily explicable.... In view, therefore, of the probable importance physiologically of this mode of nexus between neurone and neurone, it is convenient to have a term for it. The term introduced has been synapse.

Synapses can be electrical (gap junctions), but synaptic interactions in this thesis will be assumed to take place at the more common chemical junctions. At a chemical synapse, the axon enlarges to form a terminal bouton, inside which a large number of vesicles exist. Each vesicle is filled with a chemical transmitter. Whenever pre-synaptic firing occurs, these vesicles are released and flow across the gap between the axon and the terminal (called the synaptic cleft; approximately 20 nm wide) and bind onto receptors on the terminal. This causes a change in the membrane conductance of the post-synaptic neuron. For an excellent review of the full mechanics of this process see Thomson [142].

This post-synaptic current (I_s in equation (2.1)) may be written

$$I_s = g_s s (V_s - V),$$

where V is the voltage of the post-synaptic neuron, V_s is the membrane reversal potential and g_s is a constant. The variable s corresponds to the probability that a synaptic receptor channel is in an open conducting state. This probability depends upon the presence and concentration of neurotransmitter released by the pre-synaptic neuron. The sign of V_s relative to the resting potential determines whether the synapse is excitatory ($V_s > V_{rest}$) or inhibitory ($V_s < V_{rest}$). The main neurotransmitter responsible for inhibitory synapses is γ-aminobutyric acid (GABA).

The post-synaptic conductance is regarded as a train of pulses, each one induced by the arrival of a pre-synaptic action potential with specific shape J,

$$(2.7)$$

The arrival times are calculated according to a threshold crossing condition in the pre-synatic neuron (which defines T^m), plus a suitable communication delay, τ_a. The shape of the post-synaptic potential is given by the function $J(t)$ ($J(t) = 0$, $t < 0$), with normalisation chosen such that

$$\int_0^\infty J(s)\,ds = 1.$$

Following Destexhe *et al.* [37], expressions for the post-synaptic firing are developed with the use of Markov kinetics. A simple first order kinetic scheme, obtained by assuming a closed receptor in the presence of a concentration of neurotransmitter [T] equilibriates with the open receptor state, is given by

$$C \underset{r_1(V,[T])}{\overset{r_2(V)}{\rightleftharpoons}} O,$$
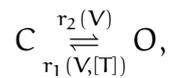
where C and O represent the closed and open states of the channel and $r_1(V,[T])$ and $r_2(V)$ are the associated rate constants. However, in many cases, synaptic channels are found to have time dependent properties that are more accurately modelled with

a second order kinetic scheme [37]. The presence of one or more receptor sites on a channel allows the possibility of transitions to *desensitised states*, as they are called in the receptor kinetics literature, which are equivalent to the *inactivated states* of voltage-dependent channels. Consider the following second-order gating system for the closed forms of the receptor, C and C_1, and the open (conducting) form O:

$$
C \quad \underset{r_2}{\overset{r_1([T])}{\rightleftharpoons}} \quad C_1
$$

$$
\searrow r_4 \qquad \swarrow r_3
$$

$$
O
$$
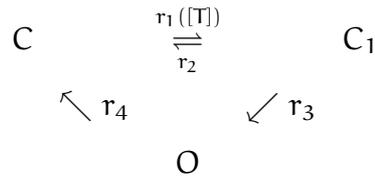
where r_1, r_2, r_3, r_4 are voltage-independent rate constants. Two approximations are made to simplify the mathematics:

- The neurotransmitter concentration [T] occurs as a Dirac δ-function $\delta(t - t_0)$. Thus, for a release event occurring at time $t = t_0$, the rate constant satisfies $r_1([T]) = r_1\delta(t - t_0)$. This means that the pulse is infinitely large and has an infinitely short duration.

- The closed state C occurs in much greater quantites than C_1 and O. Therefore, the fraction of channels in state C is considered to be constant and always approximately unity. This happens if very few receptors bind the neurotransmitter and hence nearly all receptor molecules remain in C form.

With these assumptions, the following equations are derived,

$$
\begin{aligned}
\frac{dx}{dt} &= r_1\delta(t - t_0) - (r_2 + r_3)x, \\
\frac{dy}{dt} &= r_3 x - r_4 y,
\end{aligned}
$$

where x, y represent the fraction of receptors in the forms C_1 and O respectively. To solve these equations, the Laplace transform is employed. This transform and its inverse

is defined for continuous functions $(t > 0)$ by,

$$\bar{f}(p) = \int_0^\infty e^{-pt} f(t) \, dt, \quad f(t) = \frac{1}{2\pi i} \lim_{R \to \infty} \int_{\sigma - iR}^{\sigma + iR} \bar{f}(p) e^{pt} \, dp, \quad (\sigma > c, \operatorname{Re}[p] > c \geq 0),$$

(2.8)

Hereafter, all Laplace transforms in this thesis will be represented with the "bar" notation. The transformed equations (provided $e^{-pt} f(t) \to 0$ as $t \to \infty$) are

$$p\bar{x}(p) - x(0) = r_1 e^{-pt_0} - (r_2 + r_3)\bar{x}(p),$$

$$p\bar{y}(p) - y(0) = r_3 \bar{x}(p) - r_4 \bar{y}(p).$$

Whence, solving simultaneously, $\bar{y}(p)$ is given by

$$\bar{y}(p) = \frac{y(0)}{p + r_4} + \frac{r_3}{(p + r_4)(p + r_2 + r_3)}(r_1 e^{-pt_0} + x(0)).$$

Using the inverse Laplace transform (equation (2.8)), and the fact that initially the fraction of channels in the C_1 and O states is approximately zero,

$$y(t) = r_1 r_3 \frac{e^{-\alpha_1(t-t_0)} - e^{-\alpha_2(t-t_0)}}{\alpha_2 - \alpha_1} \Theta(t - t_0),$$

where $\alpha_1 = r_2 + r_3$ and $\alpha_2 = r_4$, and $\Theta(t)$ is the heaviside step function

$$\Theta(x) = \begin{cases} 0, & x < 0 \\ 1, & x \geq 0 \end{cases}$$

(2.9)

Thus, the response from a single pulse is the difference of two exponentials, where t_0 is the time at which the neuron produces an action potential. A different representation is called the α-function response originally introduced by Rall [126] and will be shown below. Alternatively, a square pulse of synaptic conductance had been used and was adequate for some computations [124]. However, a smooth time course for the synaptic conductance is preferred. Consider the limit $\alpha_2 \to \alpha_1 = \alpha$. Then,

$$y(t) = r_3 r_1 (t - t_0) e^{\alpha(t-t_0)} \Theta(t - t_0).$$

The form of the α-function which is used in this thesis is normalised and given by (replacing y with η)

$$\eta(t) = \alpha^2 t e^{-\alpha t} \Theta(t),$$

(2.10)

25
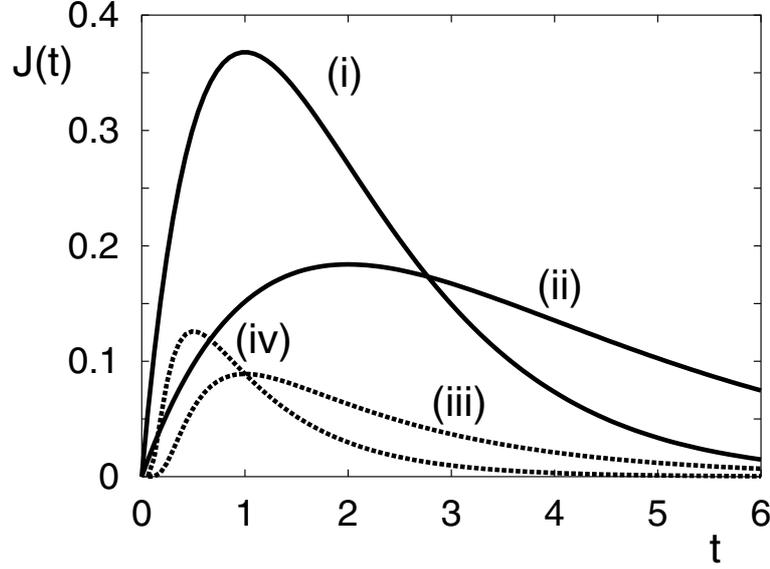
Figure 2.6 Various synaptic responses. The α-function with (i) $\alpha = 1$ and (ii) $\alpha = 0.5$ [solid] (equation (2.10)). The passive dendritic response with (iii) $\tau_D = \xi_0 = 1$ and $D = 0.5$, and (iv) $\tau_D = 2$, $\xi_0 = \sqrt{2}$ and $D = 0.5$ [dashed] (equation (2.16)). See section 2.4 for details of passive dendrites. All of these responses have qualitatively the same shape.

where $1/\alpha$ is the time taken to reach the peak of the function so that α determines the speed of the synapse (shown in figure 2.6). Differentiating equation (2.10) twice leads to a useful representation for the α-function

$$\dot{\eta}_1 = \eta_2, \tag{2.11a}$$

$$\dot{\eta}_2 = -2\alpha\eta_2 - \alpha^2\eta_1 + \alpha^2\sum_m \delta(t - T^m - \tau_a), \tag{2.11b}$$

where $\eta_1 = \eta$ and $\eta_2 = \dot{\eta}$ and with initial conditions $\eta_1(0) = 0$, $\eta_2(0) = \alpha^2$. This form is used in the direct numerical simulation schemes of this thesis (see appendix A).

A different type of synaptic response is fast threshold modulation (FTM) [139]. In spiking models, the post-synaptic responses are instantaneous whilst in bursting models the activity accounts for a significant portion of the overall period of a driven neuron. Hence, it is more suitable to suppose that a post-synaptic neuron feels the effects of a pre-synaptic neuron whilst it is active. This naturally leads to modelling the synaptic interaction as an extra conductance, but with the gating variable dependent upon the voltage of the pre-synaptic neuron: $g_{syn}(v_{pre})(v - v_{syn})$, where v_{pre} denotes the potential of the pre-synaptic neuron and v the post-synaptic neuron. The constants v_{syn} and g_{syn} respectively represent the reversal potential and the conductance associated with the synapse. This expression would be included (in I_s) on the right of equation (2.1).

Voltage-dependent synaptic conductances are another common way to represent synaptic interactions. Consider a system of differential equations based on the pre-synaptic potential v_{pre}. Then the synaptic gating variable $s(t)$ (representing the fraction of open channels) satisfies an ordinary differential equation such as

$$\frac{ds}{dt} = \beta_1(1 - s)H(v_{pre} - v_\theta) - \beta_2 s,$$

or

$$\frac{ds}{dt} = \beta_1(1 - s)H(v_{pre} - v_\theta) - \beta_2 H(v_\theta - v_{pre})s.$$

Here β_1 and β_2 are constants and $H(v)$ is a saturating threshold function such as

$$H(v) = \frac{1}{1 + \exp(-v/v_s)}.$$

As $v_s \to 0$, $H(v)$ approximates a heaviside step function. This model is often referred to as a *direct* synapse since it is activated as soon a membrane potential crosses the threshold v_θ (at least for the case $v_s \to 0$). To better represent the range of synapse dynamics observed biologically it is sometimes necessary to consider models of the form

$$\frac{dx}{dt} = \varpi\alpha_x(1 - x)H(v_{pre} - v_\theta) - \beta_x x,$$
$$\frac{ds}{dt} = \alpha(1 - s)H(x - x_\theta) - \beta s,$$

27

as discussed by Rubin and Terman [131]. The effect of such an *indirect* synapse is to introduce a delay in the onset of response, determined by the time it takes for the x variable to cross x_θ after v_{pre} crosses v_θ. Here x represents the activation level of some G-protein. The constant ϖ determines whether the turn-on in the model is fast or slow. A similar type of an indirect synapse is the phenomenological model of *slow* $GABA_B$ inhibition, where synaptic gating is described by [59]

$$
\begin{aligned}
\frac{dx}{dt} &= \varpi\alpha_x(1-x)H(v_{pre}-v_\theta)-\beta_x H(v_\theta-v_{pre})x, \\
\frac{ds}{dt} &= \alpha(1-s)x^4-\beta s.
\end{aligned}
$$

Given a particular choice of synaptic transmission from those outlined above, it is necessary to include the details of signal propagation along dendritic branches. The next section introduces two primary ways to represent this propagation.

2.4   Dendrites and the cable equation

Dendrites are tube-like extensions of a neuron which branch repeatedly to form a tree-like structure, and significantly influence neural firing patterns [98]. This structure can be large and in some neurons the dendrites can account for over 99% of the neuron surface area. Tiny spines exist along the length of the dendritic tissue, and it is at these points that synaptic junctions are created. To simplify the mathematics, the extensive morphology of the dendritic structure is collapsed onto a single cable, which is typically modelled by the cable equation,

$$
r_D C_D \frac{\partial V}{\partial t}(\xi, t) = -V(\xi, t) + \frac{r_D}{r_a}\frac{\partial^2 V}{\partial \xi^2}(\xi, t),
$$

where $V(\xi, t)$ denotes the membrane potential at time t and position ξ along the cable relative to the resting potential of the membrane. The passive electrical properties are determined by the parameters C_D, r_D and r_a which are the membrane capacitance (in units

of F/cm), the membrane resistance and the internal resistance (both in units of Ω/cm) respectively. This equation is generated by applications of both Kirchoff's Current Law and Ohm's Law [127]. It is useful to reduce the number of parameters in the cable equation, and so it is reformulated as

$$\frac{\partial V}{\partial t}(\xi, t) = -\frac{V(\xi, t)}{\tau_D} + D\frac{\partial^2 V}{\partial \xi^2}(\xi, t) + I(\xi, t), \qquad (2.12)$$

where $\tau_D = r_D C_D$ and $D = 1/(r_a C_D)$, and where in addition a source term $I(\xi, t)$ has been included.

Equation (2.12) is a parabolic partial differential equation and has a unique solution if two boundary conditions and an initial condition are specified. The initial voltage is set to be $V(\xi, 0) = 0$. Treating the soma as one end of the cable means that a semi-infinite cable is considered, imposing the condition

$$\lim_{\xi \to \infty} |V(\xi, t)| < \infty.$$

Other boundary conditions can take many forms, but it is typical to model the $\xi = 0$ end (soma) as sealed. This means that there is no longitudinal current, and hence

$$\left.\frac{\partial V}{\partial \xi}\right|_{\xi=0} = 0.$$

The solution to equation (2.12) is given by,

$$V(\xi, t) = \int_0^\infty \int_0^t G(\xi - \xi', t - t')I(\xi', t')\, dt'\, d\xi',$$

where the Green's function $G(\xi, \xi', t, t')$ satisfies

$$\frac{\partial G}{\partial t} + \frac{G}{\tau_D} - D\frac{\partial^2 G}{\partial \xi^2} = \delta(t)\delta(\xi - \xi'), \qquad (2.13)$$

with the same boundary conditions as V. One of the more simple ways to solve this equation is by use of the Fourier transform. This could be taken with respect to either variable, but perhaps the t variable provides most flexibilty. The Fourier transform, and its inverse, is defined for continuous t by

$$\widehat{J}(\omega) = \int_{-\infty}^\infty e^{-i\omega t}J(t)\, dt, \quad J(t) = \int_{-\infty}^\infty e^{i\omega t}\widehat{J}(\omega)\frac{d\omega}{2\pi}.$$

Hereafter, all Fourier transforms in this thesis will be represented with the "hat" notation. Thus, equation (2.13) becomes

$$\frac{\partial^2 \widehat{G}}{\partial \xi^2} - \left(\frac{1 + i\omega\tau_D}{D\tau_D}\right) \widehat{G} = 0. \tag{2.14}$$

Let the propagation constant $\gamma_{\text{pass}}(\omega)$ be defined as

$$\gamma^2_{\text{pass}}(\omega) = \frac{1 + i\omega\tau_D}{D\tau_D}.$$

Let, z_m denote the linearized, frequency dependent impedance and z_a denote the serial impedance. For a passive dendrite, the membrane consists only of a resistor in parallel with a capacitor (see figure 2.7). Hence, z_m is given by

$$z_m = \frac{r_D}{1 + i\omega\tau_D},$$

The serial impedance is simply given by an ohmic resistor, $z_a = r_a$. The propagation constant is given by Koch in terms of the ratio of these impedances [91],

$$\gamma^2_{\text{pass}}(\omega) = \frac{z_a(\omega)}{z_m(\omega)} = \frac{r_a(1 + i\omega\tau_D)}{r_D}. \tag{2.15}$$

The solution of equation (2.14), using the boundary and initial conditions, is

$$\widehat{G}(\xi, \omega) = \frac{1}{D\gamma_{\text{pass}}(\omega)} e^{-\gamma_{\text{pass}}(\omega)\xi}.$$

The Fourier transform of the Green's function is sometimes referred to as the transfer function or transfer impedance. Suppose $I(\xi, t) = \delta(\xi - \xi_0)I(t)$, then the Green's function is

$$G(\xi_0, t) = \frac{1}{\sqrt{4\pi Dt}} e^{-t/\tau_D} e^{-\frac{\xi_0^2}{4Dt}} \tag{2.16}$$

The form of this response is plotted in figure 2.6.

In reality, dendrites branch repeatedly and the electrical properties may vary along the length of the cable. Dendrites with such electrical properties are known as quasi-active dendrites. Under certain conditions, this type of membrane gives rise to a membrane impedance that displays a prominent maximum at some nonzero resonant

frequency. These dendrites will be addressed in the following section. Multiple branches will not be discussed, although Rall demonstrated that an extensively branched tree may be viewed as an equivalent cylinder if certain conditions are satisfied [127]. Compartmental modelling may be used to model the extensive branching of the dendrite by taking each section as a small cylinder each having its own cable equation.

2.4.1 Linearised quasi-active membranes

For quasi-active dendrites, linear cable theory is inadequate to describe the complicated nonlinear processes involved. However, progress may be made if the membrane's potential is restricted to relatively small deviations around the rest state. The Hodgkin-Huxley system of equations [73] (given as equation (2.1) with equation (2.2) with no synaptic input) is an excellent starting point for modelling truly active membranes. The quasi-active model is generated by linearising each current around some fixed potential [91].

For simplicity, consider the potassium current I_K in equation (2.2). A small perturbation around a fixed potential V_r may be written as

$$\delta I_K = \frac{\delta V}{R_K} + 4g_K n^3 (V - V_K)\delta n, \quad R_K^{-1} = g_K n_\infty^4 (V_r). \tag{2.17}$$

Hence, from equations (2.3) and (2.4),

$$\left(\frac{d}{dt} + \alpha_n + \beta_n\right)\delta n = \left(\frac{d\alpha_n}{dV} - \frac{d}{dV}(\delta\alpha_n + \delta\beta_n)\right)\delta V. \tag{2.18}$$

Combining equations (2.17) and (2.18) leads to the equation for the first-order variation of the potassium current,

$$\delta I_K = \frac{\delta V}{R_K} + \delta I,$$

with δI satisfying

$$\left(\frac{1}{r_n} + L_n\frac{d}{dt}\right)\delta I = \delta V,$$

and

$$
\begin{aligned}
L_n^{-1} &= \left\{ 4g_k n^3(V)(V-V_K)\left[\frac{d\alpha_n}{dV} - \left(\frac{d\alpha_n}{dV} + \frac{d\beta_n}{dV}\right)n\right]\right\}\Bigg|_{V=V_r}, \\
r_n &= \frac{L_n}{\alpha_n + \beta_n}\Bigg|_{V=V_r}.
\end{aligned}
$$

Thus, for a small perturbation δV around V_r, the potassium current responds as though the resistance R_K is in parallel with a resistance r_n that is itself in series with an inductance L_n. Figure 2.7 shows a circuit diagram representing a dendritic cable in both the passive and active cases. This inductive term can lead to an oscillitory overshoot in the potential after the generation of an action potential. The sodium and leak currents may be linearised in the same manner, and the linearisation of the full set of Hodgkin-Huxley equations can be represented in Fourier space as

$$
\widehat{\delta V}(\omega) = K(\omega)\left[\widehat{\delta I_K}(\omega) + \widehat{\delta I_{Na}}(\omega) + \widehat{\delta I_L}(\omega)\right],
$$

where $K(\omega)$ is the complex impedance of the linearised Hodgkin-Huxley membrane. This impedance has the form [91]

$$
K(\omega) = \frac{\beta_0 + \beta_1\omega + \beta_2\omega^2 + \beta_3\omega^3}{\alpha_0 + \alpha_1\omega + \alpha_2\omega^2 + \alpha_3\omega^3 + \alpha_4\omega^4}.
$$

The α_i's and β_i's are complex constants which depend upon the values of the electrical components.

Hence, in order to model quasi-active dendrites, the passive cable equation (2.12) is supplemented by an equation describing the current through the inductive branch of the equivalent system $I_D(\xi, t)$ as follows,

$$
\begin{aligned}
\frac{\partial V}{\partial t}(\xi, t) &= -\frac{V(\xi, t)}{\tau_D} + D\frac{\partial^2 V}{\partial \xi^2}(\xi, t) + \frac{I_D(\xi, t)}{C_D} + I(\xi, t), & \text{(2.19a)} \\
l\frac{\partial I}{\partial t}(\xi, t) &= -r_l I(\xi, t) + V(\xi, t), & \text{(2.19b)}
\end{aligned}
$$

where l and r_l are the inductance and the resistor in series. Note that this system can switch between the quasi-active (r_l finite) and passive ($r_l \to \infty$) with different values
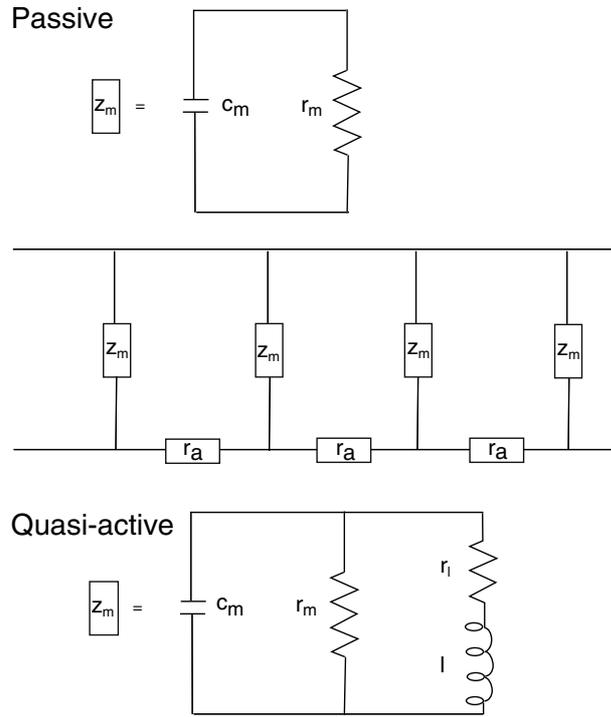
Figure 2.7 A schematic description of passive and quasi-active membranes in terms of electrical circuit diagrams. The passive dendrite can be viewed as a capacitor c_m in parallel with a resistance r_m. A quasi-active dendrite has an additional inductive branch with a resistance r_l in series with an inductance l.

of the parameter r_l. This system can be solved in exactly the same way as the passive dendrite case. The Fourier transform of both equations in (2.19) is taken with respect to the time variable, and $\widehat{I_D}(\xi, \omega)$, eliminated to get

$$\frac{d^2\widehat{V}}{d\xi^2}(\xi, \omega) = \gamma_{act}^2(\omega)\widehat{V}(\xi, \omega),$$

where the propagation constant is now

$$\gamma_{act}^2(\omega) = \frac{r_a}{z_m(\omega)},$$

33

with

$$z_m(\omega) = \frac{r_D(r_l + i\omega l)}{r_D + r_l - \omega^2 l\tau_D + i\omega(l + r_l\tau_D)},$$

resulting in the Fourier transform of the Green's function given by

$$\widehat{G}(\omega) = \frac{1}{D\gamma_{act}(\omega)} e^{-\gamma_{act}(\omega)\xi}.$$

This useful form is employed in the analysis of travelling waves in chapter 4 rather than equations (2.19). Note that the passive dendritic case is recovered in the limit $r_l \to \infty$ (equation (2.15)) with $D\tau_D = r_D/r_a$.

2.5   Recapitulation

This chapter has presented the derivation of some of the mathematical models used for describing neural oscillators and spike propagation which are popular in current neuroscience literature. All of these models have biophysical motivation and are presented in a reduced form. The integrate-and-fire model of a neuron is particularly useful since it is a linear differential equation (with discontinuous reset), thus enabling robust mathematical analysis. The integrate-and-fire model, in combination with the different synaptic responses, forms the basis of the neural networks studied throughout this thesis.

Chapter 3

Synaptic adaptation in discrete integrate-and-fire networks

An important property of single neurons currently being studied at the network level is that of synaptic adaptation (sometimes called synaptic plasticity or phasic neurons). Experimental evidence shows that the amplitude of the response of a neuron to some synaptic input is not constant, but depends upon the previous firing history of the neuron [2]. It is thought that the synaptic connections between those neurons mediating behaviour can be modified and that these modifications may persist, serving as elementary components of memory storage. Synaptic connections could be modified differently depending on the specific learning process. For example, the synaptic strength of a single synaptic connection could be increased (decreased) with sensitisation (habituation) [107], and references within. Other hypotheses exist which concern memory storage. For instance, long-term information storage could be due to the selective addressing of synaptic contacts onto active dendritic subunits [121]. Another type of synaptic adaptation is the formation of new synaptic terminals (boutons) on dendrites. This phenomena is particularly difficult to model and subsequently analyse and will not be considered further.

Synaptic depression causes the amplitude of the response to a spike input to decrease with repetitive stimulus, whereas the amplitude of the response is increased for facilitation. The effects of synaptic adaptation in large networks of neural oscillators with adapting synapses have been addressed in various systems. Some analytical progress has been made using mean field theory in large discrete networks [12]. For integrate-and-fire oscillators, with the simple model of synaptic adaptation described by Abbott [2], it was shown that synaptic depression can decrease (increase) the collective period of oscillation in an inhibitory (excitatory) network and that the opposite occurs for facilitation. Moreover, synaptic facilitation can enhance the stability of a frequency locked state, whilst depression can have a destabilising effect.

Other properties within the synaptic adaptation framework have been addressed. Within a Wilson-Cowan firing rate formalism, and using a more complex description of synaptic adaptation, Tsodyks *et al.* [147] have shown that large networks with excitatory coupling can support regular and irregular network activity. Short-term effects, such as synchronised bursting, have been associated with the dynamics of adapting synapses in an integrate-and-fire network [148]. Pattern formation has been shown to exist in small discrete networks exhibiting synaptic adaptation [102].

Kistler and van Hemmen [90] developed a minimal time-continuous model. Using the spike response model of a neuron, they found that short-term depression did not affect the stability properties of neurons firing in a synchronous state. However, in the case of short-term facilitation, their theory predicts that the stability of the steady state is dependent upon the relative values of the asymptotic value of the facilitation and the synaptic coupling strength. However, after an extensive parameter search, no realistic parameter setting was found which would destabilise a solution which was synchronous in the non-adapting case.

Complex computational [95] and mathematical [38, 51] models of synaptic adaptation based on experimental data exist, but are difficult to analyse. The following simple

mathematical model was suggested by Abbott and Marder [2]. The post-synaptic potential caused by a single action potential is typically modelled as an α-function or the difference of two exponentials (see section 2.3). If the shape of the post-synaptic response is labelled J, and a pre-synaptic spike occurs at time T^m, then the post-synaptic response at time t is given by $J(t - T^m)$. Thus, for numerous pre-synaptic spikes, the post-synaptic response function is given by

$$P(t) = \sum_{T^m < t} J(t - T^m).$$

However, since synaptic facilitation and short-term depression cause the amplitude of the response to depend on the previous history of *pre-synaptic* firing, a more accurate description of post-synaptic responses may be achieved by incorporating these history dependent events as an amplitude factor to adjust the magnitude of the spike response J. Hence, take

$$P(t) = \sum_{t > T^m} A(T^m) J(t - T^m).$$

where the function $A(t)$ scales the response evoked by a single spike at the mth firing time T^m by an amount that depends on the timing of the spike relative to others in the train. A simple way to model this phenomenon [2] is for each spike to modify $A(t)$, but between spikes, $A(t)$ exponentially returns to its equilibrium value of unity. Hence, including a time constant τ_γ, $A(t)$ is represented by,

$$\tau_\gamma \frac{dA}{dt} = 1 - A \quad \text{for } T^m < t < T^{m+1}. \tag{3.1}$$

Synapses typically adapt on a time scale of between 100ms and a few seconds [92], and on a time scale longer than that of the membrane. Other phenomena, such as LTP (long-term potentiation), can be modelled with dependence on both pre- and post-synaptic activity. For facilitation (depression), a pre-synaptic spike causes an increase (decrease) in the amplitude of the post-synaptic potentials. This can be modelled as follows,

$$A(T^m+) = \begin{cases} \gamma A(T^m), & \text{multiplicative,} \\ A(T^m) + \gamma - 1, & \text{additive,} \end{cases} \tag{3.2}$$

37

where $A(t+) = \lim_{\delta \to 0^+} A(t+\delta)$. Thus, $\gamma > 1$ ($\gamma < 1$) signifies facilitation (depression). The effects of synaptic adaptation on discrete networks of integrate-and-fire neurons is included in an existing framework in the following section.

3.1 Adaptation in discrete integrate-and-fire networks

Consider a network of N synaptically-coupled integrate-and-fire neurons, with spike train outputs. Let $V_i(t)$ denote the state of the ith neuron at time t, $i = 1, \ldots, N$. Suppose that the neurons evolve according to the following dynamics

$$\frac{dV_i(t)}{dt} = -\frac{V_i(t)}{\tau} + I_i + S_i(t), \qquad (3.3)$$

for $T_i^m < t < T_i^{m+1}$ where T_i^m represents the mth firing of a neuron at position i, I_i is a constant external bias, τ is the membrane time constant, and $S_i(t)$ is the total synaptic current into the cell. A reset condition is also required, such that whenever $V_i(t) = V_\theta = 1$, then $V_i(t^+) = V_{\text{reset}} = 0$. The condition $I_i\tau > 1$ is introduced so that all neurons fire in the absence of coupling (the oscillatory regime). The excitable regime ($I_i\tau < 1$) will not be considered here. The time constant of the membrane, τ, has typical values in the range 5-20msec, and in this chapter the units of time will be fixed by setting τ equal to unity.

Including synaptic adaptation into the synaptic input,

$$S_i(t) = \epsilon \sum_{j=1}^{N} W_{ij} \sum_{m \in \mathbb{Z}} A_j(T_j^m) J(t - T_j^m). \qquad (3.4)$$

Elements in this expression are defined as follows: $\epsilon > 0$ is the global coupling strength, W_{ij} is the coupling weight of the connection from the jth to the ith neuron, $J(t)$ is the post-synaptic response of a single spike with $J(t) = 0$ for $t < 0$, and T_j^m are the firing times of the jth neuron (m runs through the integers). Note that there is no restriction on the size of the positive coupling ϵ. Hence the theory presented will be applicable for strong coupling. A biologically motivated choice for this response is a unit normalised α-function, $J(t) = \eta(t) = \alpha^2 t e^{-\alpha t} \Theta(t)$, where Θ is the unit step function (see section 2.3).

Integrating equation (3.1) between the firing times T_j^m leads to the following difference equation for $A_j(T_j^m)$,

$$A_j(T_j^{m+1}-) = 1 + [A_j(T_j^m) - 1]e^{-(T_j^{m+1}-T_j^m)/\tau_\gamma},$$

where $A(t-) = \lim_{\delta \to 0^+} A(t-\delta)$, and after dropping transients this gives the asymptotic solution,

$$A_j^\ddagger(T_j^{m+1}-) = 1 + (\gamma - 1) \sum_{k=0}^{\infty} \gamma^{\ddagger k} e^{-(T_j^{m+1}-T_j^{m-k})/\tau_\gamma}, \tag{3.5}$$

in the additive ($\ddagger = 0$) and multiplicative ($\ddagger = 1$) cases.

The firing times T_j^m evolve according to an infinite-order nonlinear difference equation defined by $T_i^m = \inf\{t \mid V_i(t) \geq V_\theta, t > T_i^{m-1}\}$. Suppose $T_j^n = (n - \phi_j)\Delta$ for a self-consistent period Δ and some constant phases ϕ_j. This mean that the oscillators are all firing with the same period, but at different times (phase-locked). By integrating (3.3) over the region $t \in (T_i^n, T_i^{n+1})$ and using (3.4), the dynamics reduce to the N equations,

$$1 = (1 - e^{-\Delta})I_i + \epsilon \sum_{j=1}^{N} W_{ij} K_\Delta^\ddagger(\phi_j - \phi_i), \tag{3.6}$$

for $i = 1, \ldots, N$, where the convolution of the integrate-and-fire response and the periodic input is given by,

$$K_\Delta^\ddagger(\phi) = A_\infty^\ddagger(\Delta) K_\Delta(\phi),$$

and

$$\begin{aligned} K_\Delta(\phi) &= e^{-\Delta} \int_0^\Delta e^\tau P_\Delta\left(\phi + \frac{\tau}{\Delta}\right) d\tau, \\ P_\Delta(\theta) &= \sum_{m \in \mathbb{Z}} J((\theta + m)\Delta), \\ &= \frac{\alpha^2 e^{-\alpha\theta\Delta}}{1 - e^{-\alpha\Delta}}\left(\theta\Delta + \frac{\Delta e^{-\alpha\Delta}}{1 - e^{-\alpha\Delta}}\right), \end{aligned}$$

for $\theta \in [0, 1)$ and periodic extension $P(\theta) = P(\theta + m)$. Using the ansatz for T_j^m, the asymptotic steady state of $A(t)$ is given by,

$$A_\infty^\ddagger(\Delta) = 1 + \frac{(\gamma - 1)e^{-\Delta/\tau_\gamma}}{1 - \gamma^\ddagger e^{-\Delta/\tau_\gamma}},$$

where $\ddagger = 0$ or 1 depending on whether the additive or multiplicative case is respectively being considered. In order that the sum converges it is required that $|\gamma^{\ddagger} e^{-\Delta/\tau_{\gamma}}| < 1$. The index j is dropped since the asymptotic value is the same for all $A_j(t)$. This is appropriate because, after transients, all synapses see the same frequency of spike train. This value for $A_{\infty}^{\ddagger}(\Delta)$ diverges if $\gamma > 1$ and $\ddagger = 1$, and $A_{\infty}^{\ddagger}(\Delta)$ becomes negative for a range of values of Δ when $\ddagger = 0$ and $\gamma < 1$. Thus, the multiplicative case is taken when $\gamma < 1$ (depression) and the additive case taken when $\gamma > 1$ (facilitation) in order to be realistically plausible.

Consider the synchronous case $\phi_i = \phi$, $\forall i \in \mathbb{Z}$. Solutions are ensured to exist by imposing the *balance condition*

$$I_i = I \left[1 - \epsilon K_{\Delta}^{\ddagger}(0) \Gamma_i \right], \tag{3.7}$$

for $i = 1, \ldots, N$ and where $\Gamma_i = \sum_{j=1}^{N} W_{ij}$. This is derived from (3.6) by decomposing I_i as $\widetilde{I}_i + I$ and balancing the synaptic current with $\widetilde{I}_i$ so that we get an effectively isolated neuron with constant drive. Then all neurons will fire at the same time (no phase lag) with time period $\Delta = \ln \left[I/(I-1) \right]$. Perturbations of the firing times of the form $T_k^n \to T_k^n + \zeta_k^n$ are considered. Substitution of these perturbed firing times into the firing condition $V_k(T_k^n) = 1$ and linearising around the synchronous solution $T_k^n = n\Delta$ yields a linearised firing map. In this case, substitution into (3.5) gives,

$$A_j^{\ddagger}(T_j^m) = A_{\infty}^{\ddagger}(\Delta) - (A_{\infty}^{\ddagger}(\Delta) - 1)\frac{\zeta_j^m}{\tau_{\gamma}} + B_j^{\ddagger}(m-1, \Delta),$$

where

$$B_j^{\ddagger}(m, \Delta) = \frac{\gamma - 1}{\tau_{\gamma}} \sum_{k=0}^{\infty} \gamma^{k\ddagger} e^{-(k+1)\Delta/\tau_{\gamma}} \zeta_j^{m-k}.$$

Integrating (3.3) for $t \in (T_j^m, T_j^{m+1}]$ and expanding to first order in the perturbations leads to the following linear difference equation,

$$\left[\zeta_i^{n+1} - \zeta_i^n \right] \left\{ I_i - 1 + \epsilon \sum_{j=1}^{N} W_{ij} P_\Delta(0) A_\infty^{\ddagger}(\Delta) \right\} =$$
$$\epsilon \sum_{j=1}^{N} W_{ij} \sum_{m \in \mathbb{Z}} \left\{ M_m(0, \Delta) A_\infty^{\ddagger}(\Delta) \left[\zeta_j^{n-m} - \zeta_i^n \right] - L_m(0, \Delta) L_j^{\ddagger}(n - m, \Delta) \right\},$$

(3.8)

where, using the notation $J'(s) = dJ/ds$,

$$M_m(\phi, \Delta) = \int_0^\Delta e^u e^{-\Delta} J'(u + (m + \phi)\Delta) \, du,$$
$$L_m(\phi, \Delta) = e^{-\Delta} \int_0^\Delta e^u J(u + (m + \phi)\Delta) \, du,$$
$$\tau_\gamma L_j^{\ddagger}(x, \Delta) = [1 - A_\infty^{\ddagger}(\Delta)] \zeta_j^x + \tau_\gamma B_j(x - 1, \Delta).$$

The asymptotic behaviour of the perturbations is then determined by solutions of an eigenvalue equation, evaluated by substituting $\zeta_j^n = e^{n\lambda} \zeta_j$ into difference equation (3.8). Incorporating balance condition (3.7) into eigenvalue equation (3.8),

$$\Omega_i^{\ddagger}(0, \Delta, \lambda) \zeta_i = \epsilon \sum_{j=1}^{N} W_{ij} \zeta_j \Lambda^{\ddagger}(0, \Delta, \lambda),$$

(3.9)

where

$$\Omega_i^{\ddagger}(\phi, \Delta, \lambda) = \left[e^\lambda - 1 \right] \left(I - 1 + \frac{\epsilon I A_\infty^{\ddagger}(\Delta) \Gamma_i}{\Delta} \frac{dK_\Delta(\phi)}{d\phi} \right) + \frac{\epsilon A_\infty^{\ddagger}(\Delta) \Gamma_i}{\Delta} \frac{dK_\Delta(\phi)}{d\phi},$$
$$\Lambda^{\ddagger}(\phi, \Delta, \lambda) = \sum_{m \in \mathbb{Z}} \{ A_\infty^{\ddagger}(\Delta) M_m(\phi, \Delta) - L_\infty^{\ddagger}(\lambda, \Delta) L_m(\phi, \Delta) \} e^{-m\lambda},$$

and where

$$\tau_\gamma L_\infty^{\ddagger}(\lambda, \Delta) = 1 - A_\infty^{\ddagger}(\Delta) + \frac{(\gamma - 1) e^{-\Delta/\tau_\gamma} e^{-\lambda}}{1 - \gamma^{\ddagger} e^{-\Delta/\tau_\gamma} e^{-\lambda}},$$

with

$$P_\Delta(\phi) - IK_\Delta(\phi) = \frac{I}{\Delta} \frac{dK_\Delta(\phi)}{d\phi} = \sum_{m \in \mathbb{Z}} M_m(\phi, \Delta),$$
$$\sum_{m \in \mathbb{Z}} L_m(\phi, \Delta) = K_\Delta(\phi).$$

For sufficiently small coupling strength ϵ, equation (3.9) shows that the local asymptotic stability condition of the synchronous state is given by (modified from the theorem in [17])

$$\epsilon \frac{dK_\Delta^\ddagger}{dt}(0)\mathrm{Re}[\kappa_p] > 0, \quad p = 1, \ldots, N-1, \tag{3.10}$$

where κ_p, $p = 1, \ldots, N-1$ are the non-zero eigenvalues of $\widetilde{W}$ defined by

$$\widetilde{W_{ij}} = W_{ij} - \delta_{ij} \sum_{k=1}^{N} W_{ik},$$

and where δ_{ij} is the Kronecker delta (unity when $i = j$ and zero otherwise). As ϵ is increased, destabilisation of the synchronous state can occur by one or more complex conjugate pairs of eigenvalues crossing the imaginary axis in the complex λ-plane from left to right. This defines a discrete Hopf bifurcation (sometimes called a Neimark-Sacker or secondary Andronov-Hopf bifurcation) in the firing times. By substituting $\lambda = 0$ into equation (3.9), it is clear to see that the system is invariant to uniform phase shifts in the firing times. Using the above linear stability analysis, the Hopf bifurcation point is established by finding the minimum value of the global coupling strength, ϵ, for which the solution becomes unstable. This is the fundamental mechanism for the generation of complex firing patterns. The substitution $\lambda = i\beta$ is performed in the eigenvalue equation (3.9). By comparing real and imaginary parts, two simultaneous equations are produced. Solving these for β and ϵ derives solution curves (eigenmodes) for the two variables. [In the special case that Γ_i does not depend upon i, ζ_i can be chosen to lie along one of the eigenvectors of the weight matrix $\mathbf{W}$ to greatly simplify the analysis.] Performing an expansion of λ in the coupling strength, shows that either λ is close to 0 or is a pole of the function $\Lambda(\phi, \Delta, \lambda)$. Define a matrix $H = (H_{ij})$ by $H_{ij} = \epsilon W_{ij}\Lambda(0, \Delta, \lambda) - \Omega_i\delta_{ij}$. Then $H\zeta = 0$, where $\zeta = (\zeta_1, \zeta_2, \ldots, \zeta_N)$. The curve of Hopf bifurcation points is determined by solving $\det H = 0$ with $\lambda = i\beta$. The system for two neurons can be represented as a pair of simultaneous equations

$$\mathrm{Re}[\det H](\epsilon, \beta) = 0, \quad \mathrm{Im}[\det H](\epsilon, \beta) = 0. \tag{3.11}$$

These results can be expressed in the following theorem.

Consider a network of N *integrate-and-fire oscillators evolving according to equations (3.3) and (3.4) with reset condition such that* $V_i(t^+) = 0$ *whenever* $V_i(t) = 1$. *Suppose that the weights* W_{ij} *and external inputs* I_i *satisfy equation (3.7) so that equation (3.6) has a synchronous solution with collective period of oscillation* $\Delta = \ln[I/(I-1)]$. *Then the synchronous state destabilises via a discrete Hopf bifurcation in the firing times at synaptic coupling strength* ϵ_{Hopf} *with period* β, *where* ϵ_{Hopf} *and* β *are the simultaneous solution of equations (3.11).*

In the following examples of this linear stability theory, oscillator death (in which one neuron suppresses the activity of all others), bursting (a periodic temporal variation is seen in the short term averaged firing rate), and pattern formation occur by increasing the coupling strength. The adaptation time constant will be set to $\tau_\gamma = 1$. It has been found that the primary result of increasing τ_γ is to shift the curves in parameter space. For weak coupling, the synchronous state is always stable (subject to equation (3.10)).

3.1.1 Oscillator death in an inhibitory network

As a first example, consider two identical integrate-and-fire oscillators with all-to-all inhibitory coupling and no self-interactions. This network has synaptic weight matrix $\mathbf{W}$ given by $W_{11} = W_{22} = 0, W_{12} = W_{21} = -1$. Then, $\Gamma_i = \sum_{j=1}^{2} W_{ij} = -1$ for $i = 1, 2$. By solving the simultaneous equations (3.11) for the variables ϵ and β with these parameter values, linear stability boundaries of the synchronous state are determined.

Figure 3.1 shows the coupling strength bifurcation curves for two neurons which are inhibitorily coupled. For each value of adaptation γ, the parameter space below the curve represents linearly stable synchronous states. Simulations show that as the coupling strength is increased and crosses the stability boundary, the synchronous state ceases to be
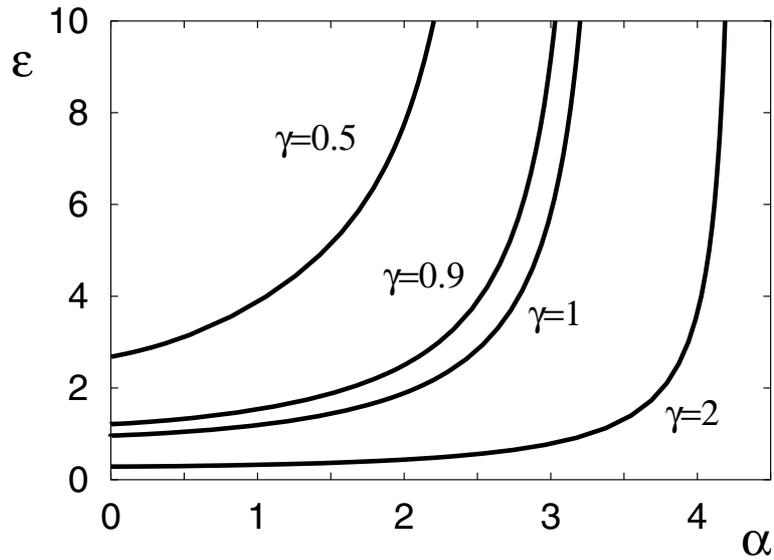
Figure 3.1 Symmetric inhibitory coupling in a pair of integrate-and-fire oscillators. Parameter values $I = 2$, $\gamma = 0.5$ (depression), 0.9 (depression), $1, 2$ (facilitation). These bifurcation curves correspond to the self consistent ϵ solution of equation (3.11) with $\tau_\gamma = 1$. Upon crossing these curves from below, a linearly stable synchronous rhythm destabilises and oscillator death occurs. This means that one oscillator continues to fire, but suppresses the activity of the other. Thus causing the cessation of rhythmic oscillations in that neuron.

stable. Slight differences in the initial conditions mean that one neuron will suppress the activity of the other, resulting in oscillator death. Synchrony persists for greater values of the synaptic coupling when synaptic depression is apparent than for synaptic facilitation. A critical rise time exists for all values of γ. That is, there is a value of α such that the network always has a stable synchronous solution, independent of the coupling strength. Hence, networks with fast synaptic interactions, or high depression, promote synchronous

behaviour. It can also be shown that the critical rise time is a decreasing function of N. This means that synchrony is more likely to occur in large networks. For a discussion in the non-adapting case, see [17].

McMillen *et al.* [104] have considered a simple model of synaptic adaptation which adapts the firing threshold of the neuron. Each equation describing a neural oscillator is augmented with an additional equation which governs the value of the firing threshold: $\dot{V}_\theta = k(V - V_\theta)$ for some constant k, and where the dot signifies differentiation with respect to time. A separate description of an adapting threshold will be given in section 4.4.2. McMillen *et al.* found that mutual inhibition can lead to oscillatory behaviour in a pair of neurons provided that inhibitory effect is of limited duration. This results in the production of a half-centre oscillator. A definition and explanation of such models will be presented in chapter 5.

3.1.2 Bursting in an excitatory-inhibitory pair of neurons

An excitatory-inhibitory pair of integrate-and-fire neurons with self-connections leads to the production of bursting patterns. The synaptic weights are given by

$$\mathbf{W} = \begin{bmatrix} -1 & -2 \\ 1 & -1 \end{bmatrix}.$$

The excitatory and inhibitory synaptic coupling of the second neuron can be thought of as having an excitatory neuron with self-connection mediated by an inhibitory interneuron. According to Dale's Principle and subsequent mathematical definitions [75] individual synapses of a neuron are allowed to have different actions, but the "averaged synapses" from one neuron to another must have the same action.

The bifurcation curves generated by the self-consistent solution of equations (3.11) with this weight matrix are shown in figure 3.2. Once again, a critical rise time in α ex-
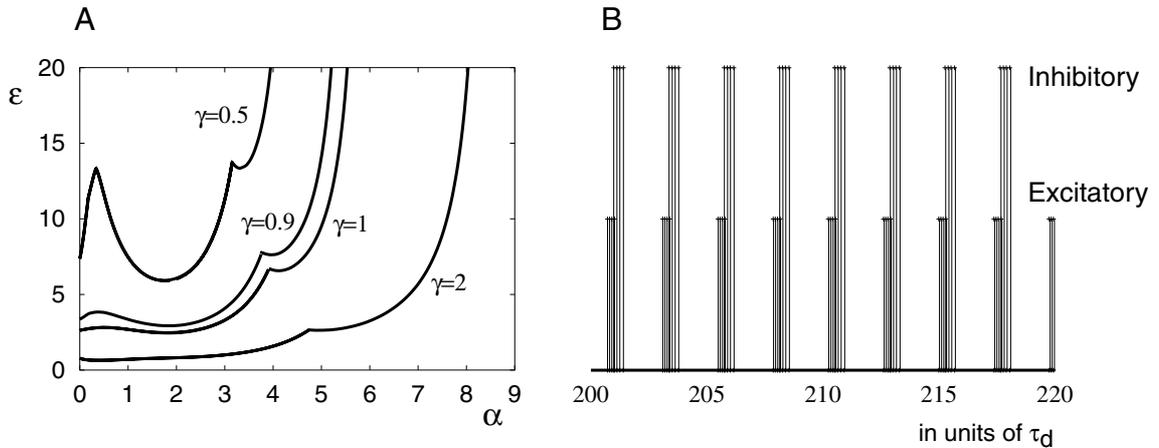
Figure 3.2 A: Excitatory-inhibitory coupling in a pair of integrate-and-fire oscillators with inhibitory self interactions. Parameter values are $I = 2$ with $W_{11} = -1, W_{12} = -2, W_{21} = 1$ and $W_{22} = -1$. The solution to equations (3.11) in this situation produces these bifurcation curves which correspond to the border between synchronous stability and bursting. Upon crossing these bifurcation curves from below, the stable synchronous state destabilises into a bursting state, where both neurons have periods of high activity separated by periods of no activity. The cusp halfway along the stability borders is created by the intersection of two distinct eigenmodes. B: Numerical simulation of a burst train in this network. The shorter spike train represents the excitatory neuron, whilst the taller represents the inhibitory neuron. Parameter values are $\gamma = 1$ (no adaptation), $\alpha = 2$ and $\epsilon = 4$.

ists. Direct numerical simulation shows that when this stability boundary is crossed from below, bursting becomes the stable state in regions close to the stability border. This means that for each neuron there is a period of high activity and a period of no activity. The dependence on γ of the bifurcations is shown to be similar using an analog model

(section 3.2). This activity is interesting because no extra currents are needed to create this behaviour — it is purely a network effect.

3.1.3 Pattern formation in a one-dimensional network

Certain networks of integrate-and-fire neurons support pattern formation. This will be shown in this final section. For example, consider a ring of $N = 2n + 1$ integrate-and-fire neurons defined by (3.3) and (3.4), with weight matrix defined as $W_{ij} = W(|i - j|)$ where

$$W(k) = A_1 \exp\left(-\frac{k^2}{2\sigma_1^2}\right) - A_2 \exp\left(-\frac{k^2}{2\sigma_2^2}\right), \quad 0 < |k| \le n, \tag{3.12}$$

with $W(k) = 0$ for $|k| > n$ and $W(0) = 0$ (no self-interactions). Choosing $A_1 > A_2$ and $\sigma_1 < \sigma_2$ produces a Mexican hat interaction function, in which there is short-range excitation and long-range inhibition. For convenience, $I_i = I$ and A_1, A_2 are chosen so that $\Gamma_i = \sum_{k=-n}^{n} W(k) = 0$ for all i. Thus excitation and inhibition are balanced. With this weight matrix, the collective period of oscillation is $T = \log\left[I/(I-1)\right]$. The n eigenvalues of equation (3.12) are given by

$$\kappa(p) = 2 \sum_{k=1}^{n} W(k) \cos(pk), \quad p = 0, \frac{2\pi}{N}, \dots, \frac{2\pi(N-1)}{N}.$$

The corresponding eigenvectors are given by $v_k = e^{ikp}$ for $p = 0, \frac{2\pi}{N}, \dots, \frac{2\pi(N-1)}{N}$. To investigate the linear stability of this system, substitute in equation (3.9) the following: $\zeta_k = e^{ikp}$, $I_i = I$, $\Gamma_i = 0$ and $\lambda = i\beta$. The resulting equations are,

$$(I - 1)(\cos\beta - 1) = \tilde{\epsilon}\,\text{Re}[\Lambda(0, \Delta, i\beta)], \tag{3.13a}$$

$$(I - 1)\sin\beta = \tilde{\epsilon}\,\text{Im}[\Lambda(0, \Delta, i\beta)], \tag{3.13b}$$

where $\tilde{\epsilon} = \epsilon\kappa(p_{max})$, and $\kappa(p_{max})$ is the first wave to cross the boundary.

Solving these simultaneous equations produces the curves shown in figure 3.3(A). There are non-trivial solutions of equations (3.13) for all values of α. The information is
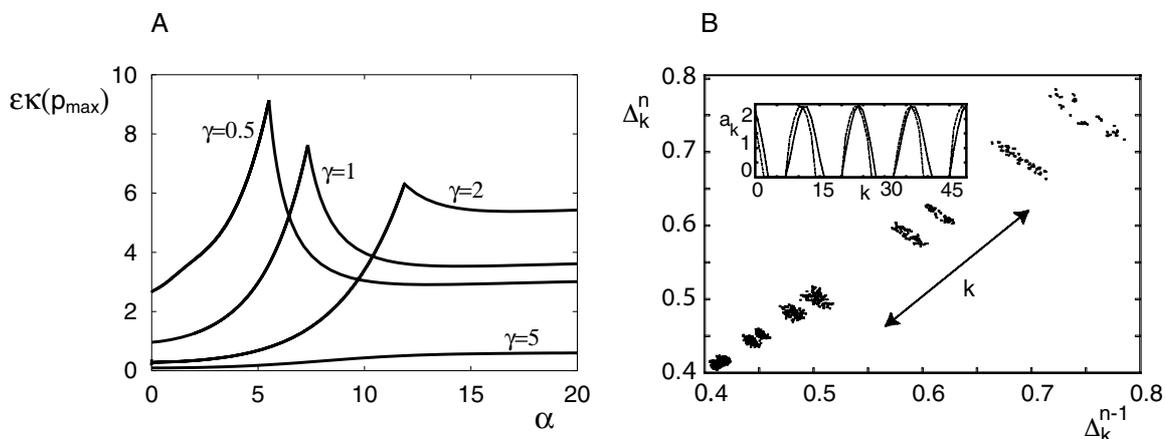
Figure 3.3 A:"Mexican hat" coupling in a ring of integrate-and-fire oscillators. Parameter values $I = 2$, $\gamma = 0.5$ (depression), 1, 2, 5 (facilitation). The solution of equations (3.13) for a given set of parameter values produces a curve which separates the linearly stable parameter regime (below) from the one which produces patterns (above). The cusp is created by the intersection of two distinct eigenmodes. B: Separation of the inter-spike interval orbits in phase-space for a ring of $N = 51$ integrate-and-fire neurons. The attractor of the embedded inter-spike interval with coordinates $(\Delta_k^{n-1}, \Delta_k^n)$ is shown for all N neurons. (Inset) Regular spatial variations in the long-term average firing rate a_k (dashed curve) are in good agreement with the corresponding activity pattern (solid curve) found in the analog version of the network. Parameter values are $\alpha = 2$, $\epsilon = 0.4$, $\sigma_1 = 2.1$, $\sigma_2 = 3.5$, $A_1 = 1.77$ and $\sum_k W(k) = 0$. [Reproduced with kind permission from Coombes [18]]. An analog model is described in section 3.2.

qualitatively the same in all cases. When adaptation reaches a critical value γ_{crit}, the bifurcation structure changes. For $\gamma < \gamma_{crit}$. two eigenmodes intersect to produce the stability boundary. A single eigenmode produces the stability boundary for $\gamma > \gamma_{crit}$. Since previous results concerning oscillator death (section 3.1.1) and bursting (section 3.1.2) show

only qualitative differences (stability boundaries are shifted), little quantitative change is expected here. Hence, direct numerical simulations of this network are not pursued. Examples of patterns in the non-adapting network are given in figure 3.3(B) [18].

3.2 The analog model

One way to approximate integrate-and-fire networks is to assume that synaptic interactions are slow. Then, the output of the neuron can be characterised by a mean (time-averaged) firing rate. Consider the α-function where the synaptic rise time α^{-1} is significantly longer than all of the other timescales in the dynamics. Then, the total external stimulus is slowly varying, and the spike train dynamics $(\sum_{m \in \mathbb{Z}} \delta(t - T_j^m))$ can be replaced with a smooth firing rate function $\Psi(V_i(t))$. This is done in the synchronous case, $\phi_i = \phi$ (for all i), where each synaptic adaptation factor $A_j(T_j^m)$ can be replaced by its asymptotic value $A_\infty^\ddagger(\Delta)$. Decomposing I_i as $I_i = I + \widetilde{I_i}$, where $I > 1$ and absorbing $\widetilde{I_i}$ into the synaptic input S_i (3.4), gives

$$S_i(t) = \widetilde{I_i} + \epsilon \sum_{j=1}^{N} W_{ij} \int_{-\infty}^{\infty} A_\infty^\ddagger(\Delta) J(\tau) \Psi(S_j(t - \tau)) \, d\tau,$$

with firing rate function

$$\Psi(S_i) = \left\{ \ln \left[\frac{I + S_i}{I + S_i - 1} \right] \right\}^{-1} \Theta(I + S_i - 1).$$

Hence, for an α-function, the total synaptic input satisfies the following system of equations, for $i = 1, \ldots, N$,

$$\frac{1}{\alpha} \frac{dS_i(t)}{dt} = -S_i(t) + S_i'(t), \tag{3.14a}$$

$$\frac{1}{\alpha} \frac{dS_i'(t)}{dt} = -S_i'(t) + \epsilon \sum_{j=1}^{N} W_{ij} A_\infty^\ddagger(\Delta) \Psi(S_j(t)) + \widetilde{I_i}. \tag{3.14b}$$

This set of coupled ordinary differential equation generates the α-function response, and has fixed point defined by $S_i(t) = S_i'(t) = \epsilon \sum_{j=1}^{N} W_{ij} A_\infty^\ddagger(\Delta) \Psi(S_j(t)) + \widetilde{I_i}$. Linearising

equation (3.14) about the fixed point (assumed to lie at the origin for simplicity), leads to the equations

$$\frac{1}{\alpha}\frac{ds_i}{dt} = -s_i + s_i', \quad \frac{1}{\alpha}\frac{ds_i'}{dt} = -s_i' + \epsilon \sum_{j=1}^{N} W_{ij}A_\infty^\ddagger(\Delta)\Psi'(0)s_j, \tag{3.15}$$

where s_i and s_i' are perturbations from the steady state, and the balance condition is given by

$$0 = \epsilon \sum_{j=1}^{N} W_{ij}A_\infty^\ddagger(\Delta)\Psi(0) + \widetilde{I}_i. \tag{3.16}$$

Substituting a solution of the form $(s_i(t), s_i'(t)) = (s_i, s_i')e^{\lambda t}$ and supposing $\mathbf{W}$ has eigenvalues κ_p for $p = 1, \ldots, N$, leads to the eigenvalue equation

$$\lambda_p^\pm = -\alpha \pm \alpha\sqrt{\epsilon\kappa_p A_\infty^\ddagger(\Delta)\Psi'(0)} \quad \text{for } p = 1, \ldots, N.$$

A number of different bifurcation scenarios present themselves when the global coupling constant ϵ is treated as the bifurcation parameter.

- All eigenvalues κ_p are real and negative.

  The eigenvalue equation can be reduced to

  $$\lambda_p^\pm = -\alpha \pm i\alpha\sqrt{\epsilon|\kappa_p|A^\ddagger(T)\Psi'(0)} \quad \text{for } p = 1, \ldots, N.$$

  Then the fixed point at the origin is stable for all $\epsilon > 0$.

- A single real eigenvalue crossing the imaginary axis.

  There exists an eigenvalue of $\mathbf{W}$, κ_{max}, which is positive and has the greatest real part. Then, the origin will undergo a static bifurcation at a critical value of the coupling strength given by

  $$1 = \sqrt{\epsilon_{stat}\kappa_{max}A_\infty^\ddagger(\Delta)\Psi'(0)}.$$

  Additional fixed-point solutions which correspond to an inhomogeneous firing rate will emerge.

- A pair of complex conjugate eigenvalues crossing the imaginary axis.

  Suppose there exists a complex conjugate pair κ, κ^* of $\mathbf{W}$ such that $\kappa = re^{i\theta}$ and $\frac{\pi}{2} \leq \theta \leq \frac{3\pi}{2}$ and that all other eigenvalues have negative real part. Then,

  $$\lambda_2^{\pm} = -\alpha \pm \alpha e^{i\theta/2}\sqrt{\epsilon A_{\infty}^{\ddagger}(\Delta)\Psi'(0)r}.$$

  A Hopf bifurcation will occur when $\text{Re}[\lambda_2] = 0$ at the critical value of the coupling strength, $\epsilon_t extHopf$ given by

  $$1 = \cos\frac{\theta}{2}\sqrt{\epsilon_{\text{Hopf}}A_{\infty}^{\ddagger}(\Delta)\Psi'(0)r}.$$

  Periodic solutions (time-dependent firing rates) are formed. Numerical examples indicate that this is a subcritical Hopf bifurcation.

These solutions are illustrated in figure 3.4. The effect of adaptation (either facilitation or depression) merely seems to shift the curves with respect to the unadapted state ($\gamma = 1$). In this rate model the dependence on γ of the bifurcations shows similar trends to those in sections 3.1.1 and 3.1.2 for small α (cf figure 3.4 to figures 3.1 and 3.2).

3.3 Rate-coding vs Spikes

Tsodyks and Markram [146] have considered synaptic adaptation in the context of neural coding. A model of depression was formulated, in which parameters were determined experimentally. The dynamics of the effective, inactive and recovered fractions of resources in the synaptic connection were described using a pair of coupled ordinary differential equations supplemented with the constraint that the three fractions sum to unity. Each pre-synaptic action potential arriving at a neuron activates a fraction of resources in the recovered state. This then inactivates and recovers on two separate time scales. Experimental traces for both regular and irregular trains of pre-synaptic action potentials could
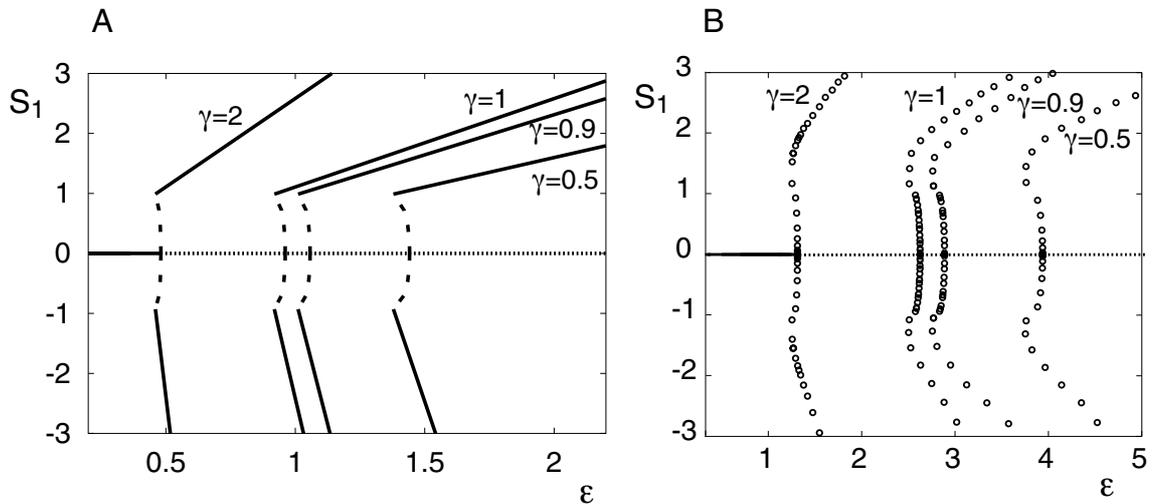
Figure 3.4 Examples of two bifurcation states in the analog model of two coupled integrate-and-fire neurons using equations (3.15) with balance condition (3.16). Parameter values are $N = 2$, $I = 2$, $\alpha = 0.5$ and various values for the strength of adaptation are chosen. A: Symmetric inhibitory coupling (given in section 3.1.1). Solid (dashed) lines denote linearly stable (unstable) solutions. B: A subcritical Hopf bifurcation for a pair of analog oscillators with self-interactions (parameter values given in section 3.1.2). Open circles denote the amplitude of the resulting limit cycle from the Hopf bifurcation point. In both diagrams, the dotted lines need special consideration. To the left of the relevant bifurcation point (in terms of γ), this dotted line is linearly stable, and unstable to the right. These figures are created using XPPAUT (see appendix A for more details).

be produced using this model. Predictions regarding the coding of information through spike timing in physiological neurons were made. By performing experiments on a single neuron in slices of the rat neocortex, and monitoring its response to an input spike train, the predictions were verified. Tsodyks and Markram concluded that the rate of depression
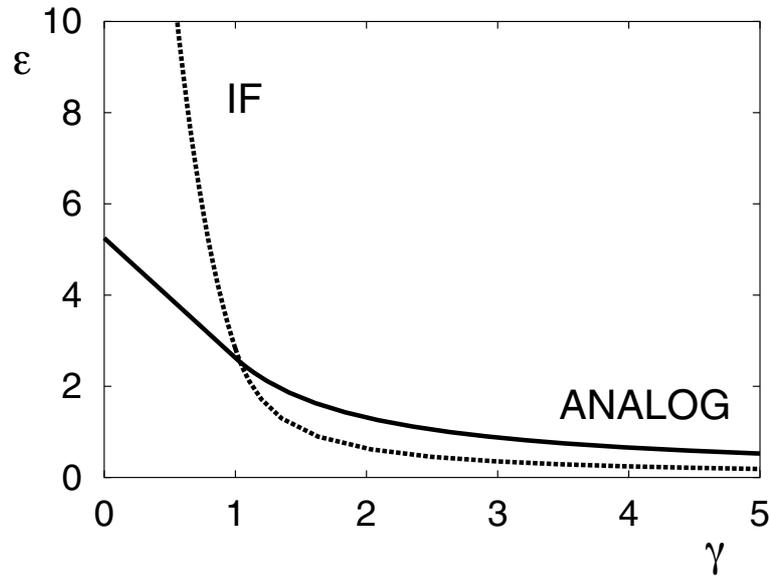
Figure 3.5 Comparison of the integrate-and-fire (IF) dynamics and the analog model in the bursting regime. Parameter values $\alpha = 0.5$, $I = 2$, and $\tau_\gamma = 1$. The curves are created from equations (3.11) and (3.15).

has a marked effect on the neural code. When depression is fast the oscillators tend to have temporal coherence, ie synchrony (all oscillators firing at the same time), but, as depression is reduced, the neural output tends to have alternating regions of high and low activity. A more useful description would therefore be given by using a rate coding, where the activity of the neuron can be appropriately represented by the average firing frequency over some time period.

Throughout this section, the network consisting of two coupled integrate-and-fire neurons with self-interactions presented in section 3.1.2 will be considered. Once again the stability boundary is calculated from equations (3.11). However, instead of treating the global coupling constant ϵ as the variable parameter, the strength of adaptation γ

and the time constant of adaptation τ_γ are chosen. Figure 3.5 would seem to support the claims of Markram and Tsodyks. The figure shows the stability boundary for fixed $\alpha = 0.5$, with γ as the adaptable parameter. The system is in a synchronous state below these curves, and then switches to a bursting state once the integrate-and-fire curves are crossed. If a point is picked above the boundary curve, then by keeping the synaptic coupling strength constant and increasing the amount of depression ($\gamma \to 0$), the system would eventually cross the stability border and be underneath the integrate-and-fire curve, and hence lie in the synchronous region of parameter space. The onset of bursting is described well by the analog model for low levels of depression and also for the facilitation case (see figure 3.6(B)), but begins to fail as the level of depression is increased.

Figure 3.6 shows the comparison of the integrate-and-fire and analog models with τ_γ as the variable parameter for $\gamma = 0.5$ (depression) and $\gamma > 1$ (facilitation). For small values of τ_γ (fast dynamics), both the analog and integrate-and-fire models have stability borders which remain close, but as τ_γ increases (slower dynamics) these curves diverge in the case of depression. As α decreases, or γ increases, this region becomes larger. This is similar to the claim of Tsodyk's and Markram [146] because bursting occurs for fast dynamics, but by keeping the same level of adaptation and reducing the speed of adaptation dynamics ($\tau_\gamma \to \infty$), the system displays synchronous behaviour. Figure 3.6(B) shows that in the facilitation regime, both models show qualitative agreement for all values of the time constant τ_γ. This means that a rate coding is appropriate for the network activity, suggesting smooth variation in the firing rate. As a comparison, figure 3.7 shows these stability boundaries in a region where the analog model is not defined (large α). It is clear that the analog model does not represent the data well anywhere in this parameter regime.

To show that the integrate-and-fire and analog models do not always agree, the output of the integrate-and-fire and analog models are numerically compared. In figure 3.8
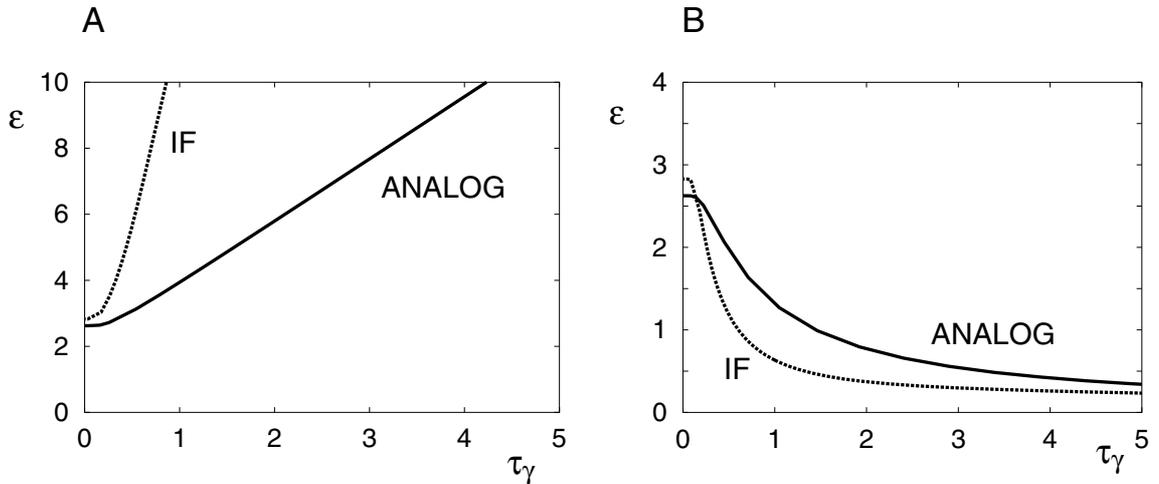
Figure 3.6 Comparison of the stability boundaries for the integrate-and-fire (IF) and analog models with a change in the time constant of adaptation using the self-consistent solution of equations (3.11) and (3.15). Both have parameter values $\alpha = 0.5$ and $I = 2$. A: Depression is set at $\gamma = 0.5$. It can be seen that for small values of τ_γ, the integrate-and-fire dynamics and the analog model produce stability boundaries which are very close, and that as τ_γ is increased these curves diverge. This suggests that for large values of τ_γ, the analog model no longer produces results which are comparable with the integrate-and-fire model. B: The facilitation regime $\gamma = 2$. The curves are very close throughout indicating that the analog model gives comparable results in all parameter regimes.

bursting patterns are plotted for the integrate-and-fire model (the spikes) along with the equivalent data from the analog model (the envelopes). As γ is decreased (A→C), the envelopes of the analog model do not overlap the integrate-and-fire spikes quite so well and exhibit drift. As τ_γ is decreased (B→C), it can be seen that these envelopes become a much better fit. As τ_γ is increased, the drift will become more pronounced. In hindsight this seems an obvious conclusion since for fast dynamics, the synaptic adaptation will
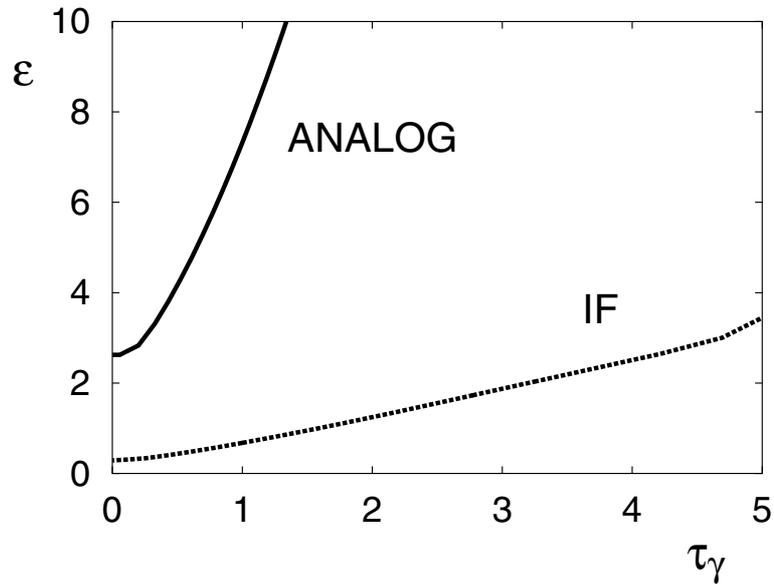
Figure 3.7 Comparison of the integrate-and-fire (IF) dynamics and the analog model with a change in the time constant of adaptation using the self-consistent solution of equations (3.11) and (3.15). Parameter values $\alpha = 20$, $I = 2$, $\gamma = 0.5$. Nowhere in the figure is the analog model close to the integrate-and-fire model. This means that the analog model is totally unsuitable for representing data with large values of α.

evolve very quickly and relax to unity. However, neurons adapt their synaptic connections on timescales much longer than the nerve membrane (in this thesis equal to unity). In conclusion, both τ_γ and γ play an important role in the coding of neural information. Rate-coded models give a good approximation to the integrate-and-fire model when there is little or no depression and also when the depression has fast dynamics.
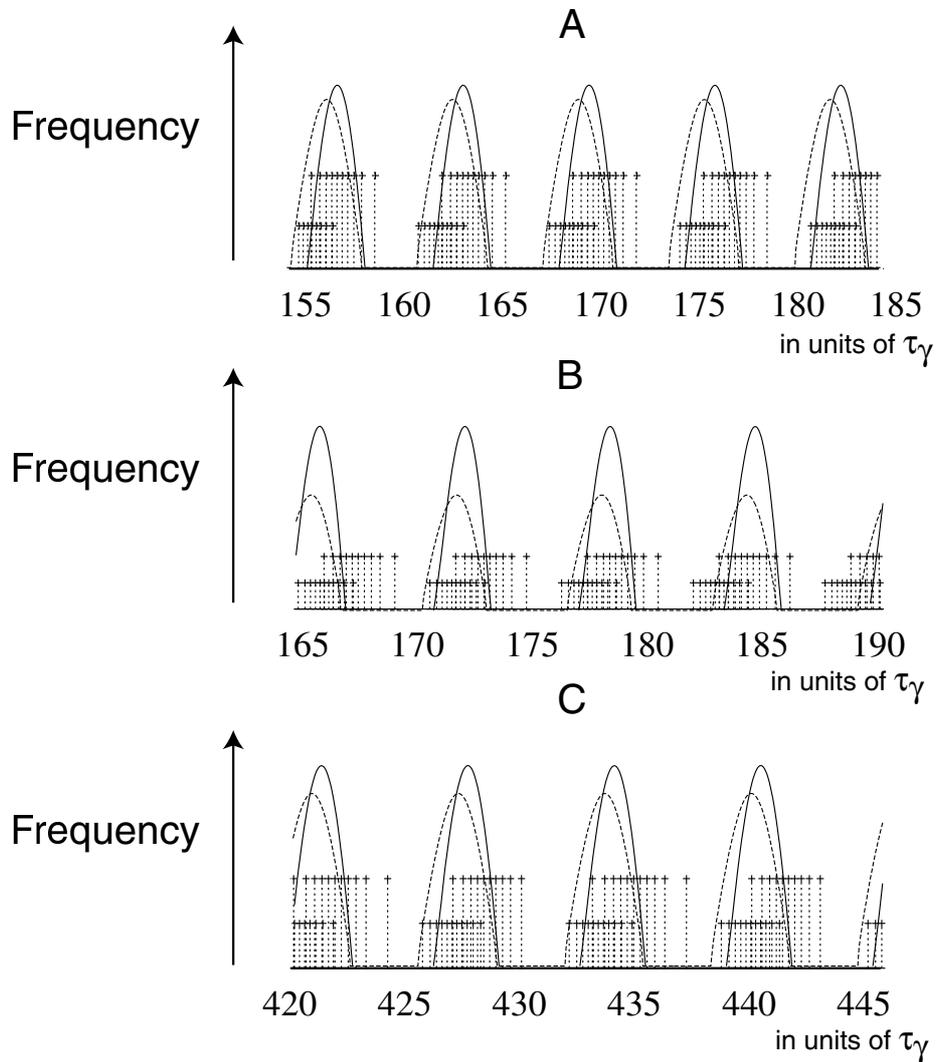
Figure 3.8 Comparison of the integrate-and-fire dynamics and the analog model in the bursting regime. Output is created by cimparing direct numerical simulation of equation (3.3) and (3.4) (with balance equation (3.7)) with that of equations (3.15). Parameter values $\alpha = 0.5$, $I = 2$, A: $\gamma = 0.99$, $\tau = 5.0$, $\epsilon = 3.5$, B: $\gamma = 0.9$, $\tau_\gamma = 5.0$, $\epsilon = 8.0$, C: $\gamma = 0.9$, $\tau = 0.2$, $\epsilon = 3.5$. See the text for a description of the dynamics.

3.4   Recapitulation

A simple model to describe synaptic adaptation (the modification of inter-neural connection strengths in response to persistent stimulation) has been used in a discrete network of integrate-and-fire neurons. This modification of current theory has shown that the qualitative nature of the bifurcations remain the same, but the stability borders shift in parameter space. One attribute of synaptic adaptation is that it can produce a switch in the behaviour of the network. As the level of synaptic depression is increased ($\gamma \rightarrow 0$), a network exhibiting synchrony evolves into one in exhibiting bursting. However, since the primary effect of the inclusion of synaptic adaptation in these networks leads to little quantitative change, emphasis will henceforth be placed on studying travelling waves without adaptation.

Chapter 4

Synaptic travelling waves in integrate-and-fire systems

In the preceding chapter, small networks were considered in order to demonstrate the different phenomena which integrate-and-fire neurons can produce. It was shown that synaptic adaptation has little effect on the quantitative mechanisms of neural interaction. Hence, synaptic adaptation will not be considered further. Even though the brain may be viewed as a network of discrete cells, there are billions of cells and it seems prudent to approximate this system as a continuum. Then, established calculus techniques can be used to analyse the systems.

Travelling waves have been experimentally observed in many neural systems, for example thalamocortical regions of humans [128], the retina of developing rabbits [157] and mice [5], the visual cortex of the turtle [122] and the olfactory system of the mollusc [34]. Travelling waves are present in central pattern generators in the locomotion system of fish ([113] and references within). Hippocrates in the 4th century BC discussed epilepsy as a disturbance of the brain. The actual mechanism for epilepsy is that a collec-

tion of neurons begin to fire synchronously [27] and then this activity propagates across the neural media [25]. Here, and throughout the thesis, the term travelling wave means that a phase difference exists between the activity of neighbouring neurons rather than the propagation of axonal voltage waves.

The cortex is often considered to be a thin sheet about 0.2 m^2 in area and 2–3 mm thick. Here, to simplifiy the mathematics, a one-dimensional continuum of integrate-and-fire neurons will be examined. Studying this reduced system will give insight into ways in which progress can be made in higher spatial dimensions. The integrate-and-fire model is a reasonable model of travelling waves in the cortex since Ermentrout showed that the velocity of a travelling pulse is independent of the ionic details irrespective of the membrane model selected, and depends only on the effective rise time of the synapse [45]. Boundary conditions are neglected in this model, but this is a suitable assumption since cortical interactions between neurons take place on distances of order $100\mu\text{m}$-$500\mu\text{m}$ and cortical nets are of the order of centimetres [42]. Taking the spatial extension of equations (3.3) and (3.4), the dynamic equation for the membrane potential $V(x, t)$ is given by

$$\frac{\partial V(x, t)}{\partial t} = I_0 - \frac{V(x, t)}{\tau} + S(x, t), \tag{4.1}$$

where I_0 is the external drive, τ is the membrane time constant (set to unity, thereby fixing the units of time), and $S(x, t)$ is the synaptic input. Equation (4.1) is supplemented by the reset condition such that, whenever $V(x, t) = V_\theta$ with positive gradient in time, then $V(x, t^+) = V_{\text{reset}}$, where V_θ is the threshold value, and V_{reset} is the reset level. The notation $V(x, t^+) = \lim_{\delta \to 0^+} V(x, t + \delta)$ is used.

The synaptic input current has the form

$$S(x, t) = \epsilon \int_{-\infty}^{\infty} \int_{-\infty}^{\infty} W(x, x')J(\tau)\Psi(x', t - \tau) \, d\tau \, dx', \tag{4.2}$$

where $\epsilon > 0$ is the global coupling strength, and $W(x, x')$ is the weight kernel between neurons at positions x and x'. The delay kernel $J(t)$ determines the shape of the post-synaptic potential and can contain axonal delays, dendritic delays and synaptic adaptation.

The general shape of such a response is given in figure 2.6. Finally, $\Psi(x, t)$ is the output spike train of the neuron at position x in the one-dimensional continuum. In the oscillatory regime $(I_0 > V_\theta)$, the neurons fire independently in the absence of coupling with period $\Delta_0 = \log\left(\frac{I_0 - V_{reset}}{I_0 - V_\theta}\right)$. In the excitable regime $(I_0 < V_\theta)$, the neurons cannot fire without coupling.

Let the mth firing time of the neuron at position x be given by $T^m(x)$. Neglecting the shape of an individual pulse, the output spike train of each neuron is represented as a sequence of Dirac delta functions

$$\Psi(x, t) = \sum_{m \in \mathbb{Z}} \delta(t - T^m(x)).$$

The weight kernel is taken to be a function of the separation of the neurons. Hence, $W(x, x') = W(x - x')$. Two different types of weight function are considered in this chapter. The normalised square wave synaptic footprint is defined as

$$W(x) = \frac{1}{2\sigma}\Theta(x + \sigma)\Theta(\sigma - x), \tag{4.3}$$

where $\Theta(x)$ is the heaviside step function defined in equation (2.9) and, in addition, a spatial scaling σ has been included. The weight kernel $W(x)$ has compact support limiting the range of communication between neurons. The connection strength is independent of distance (provided the neurons are close enough). As a contrast, the normalised exponential synaptic footprint

$$W(x) = \frac{1}{2\sigma}e^{-\frac{|x|}{\sigma}},$$

is considered. Each neuron communicates with every other neuron, and the interaction strength decreases the greater the separation between the neurons.

Chapter 3 dealt with the emergence of various network states when the synchronous state was destabilised. A transition can occur between an oscillatory regime and one in which a periodic travelling wave propagates. Consider a firing time of the form $T(x) = \Delta_1 + \beta x$. For $\beta = 0$, synchronous behaviour will be apparent and when

the spatial term is switched on ($\beta \neq 0$) a travelling wave will be defined. Bifurcations in this system have been calculated and the transition was found to be partially due to the properties of the axonal coupling [32, 47]. For a periodic travelling wave, the firing time ansatz is

$$T^m(x) = (m + kx)\Delta_1, \tag{4.4}$$

for some fundamental period Δ_1 and wavenumber k. This defines a wave of speed $c = 1/(k\Delta_1)$ in the travelling wave framework. It is implicitly assumed throughout the analysis that the system has already settled into some asymptotic steady state. Osan *et al.* have examined the onset and evolution of travelling waves in integrate-and-fire and theta neuron networks [116, 117]. It was found that for sufficiently large coupling strengths, two smoothly propagating travelling wave solutions exist.

Integrating equation (4.1) between successive firing times gives,

$$V_\theta - V_{\text{reset}}e^{-\Delta_1} = I_0\left(1 - e^{-\Delta_1}\right) + \epsilon \int_{-\infty}^{\infty} W(x)K_{\Delta_1}(kx)\,dx, \tag{4.5}$$

where

$$K_{\Delta_1}(x) = \int_0^{\Delta_1} e^{-\Delta_1}e^u \sum_{m \in \mathbb{Z}} J(u + (m + x)\Delta_1)\,du. \tag{4.6}$$

In the limit $\Delta_1 \to \infty$, the travelling pulse solution is found. It is useful to consider this scenario since simulations of conductance-based models predict that the propagation velocity of neural activity is determined primarily by the response of the post-synaptic neuron to the first one or two spikes of the pre-synaptic neuron [45, 55]. In this situation, equation (4.5) obviously only has a solution if and only if the system is in the excitable regime ($I_0 < V_\theta$). The large Δ_1 limit of equation (4.6) is

$$K_{\Delta_1}(kx) \approx \int_{-\Delta_1}^{0} e^\tau J(\tau + kx\Delta_1)\,d\tau, \tag{4.7}$$

since $J(t) \to 0$ as $\Delta_1 \to \infty$, the sum is dominated by the $m = 0$ term, and $K_{\Delta_1}(kx) \to 0$ as $\Delta_1 \to \infty$ unless $k\Delta_1 = 1/c$ is independent of the size of Δ_1, ie $c(\Delta_1) \to c_\infty$. Then, the large Δ_1 limit of equation (4.5) is given by

$$V_\theta = I_0 + \epsilon \int_0^\infty W(x)e^{-\frac{x}{c}} \int_0^{\frac{x}{c}} e^t J(t)\,dt\,dx, \tag{4.8}$$

since $J(t) = 0$ for $t \leq 0$. This expression can be obtained directly by simply integrating equation (4.1) over the interval $(-\infty, T^0(x)]$. It is sometimes useful to represent the formulae in terms of the travelling wave coordinate $\chi = ct - x$, where c is the self-consistent speed of the wave. Firing times occur when $\chi = 0$, and thus integrating equation (4.1) over the range $(-\infty, \chi]$

$$V(\chi) = I_0 + \frac{e^{-\chi/c}}{c} \int_{-\infty}^{\chi} S(\chi')e^{\chi'/c} \, d\chi'. \tag{4.9}$$

A number of different synaptic responses are going to be addressed in the context of this travelling pulse set-up, and comparisons between the compact and non-compact synaptic support will be made. Firstly, however, theory regarding the linear stability of these solutions will be presented.

4.1 Linear stability of a travelling pulse

Consider a single pulse propagating in the excitable regime $(I_0 < V_\theta)$ with firing times $T(x) = x/c$. Linear stability is determined by studying the dynamics of a perturbation of the firing times. Let $T(x) \to T(x) + \zeta(x)$. Equation (4.1) is integrated over $(-\infty, T(x)]$ to produce

$$e^{T(x)+\zeta(x)}(1 - I_0) = \varepsilon \int_{-\infty}^{T(x)+\zeta(x)} \int_{-\infty}^{\infty} e^t W(x, x')J(t - T(x') - \zeta(x')) \, dx' \, dt.$$

Expanding to order 1 leads to the original result for a pulse (equation (4.8)). Expanding to first order in the perturbations and substituting a solution of the form $\zeta(x) = e^{\lambda x}$ gives,

$$\int_{-\infty}^{0} e^t \int_{0}^{\infty} W(x)J'(t - x/c)[e^{\lambda x} - 1] \, dx \, dt = 0. \tag{4.10}$$

Solutions are asymptotically stable if all non-zero solutions λ of equation (4.10) have negative real part. These solutions depend upon the speed c which is given by equation (4.8). Let $\lambda = a + ib$ in equation (4.10) and separate into real and imaginary parts to obtain

the simultaneous equations

$$H(a, b) = \int_0^\infty (e^{ax} \cos(bx) - 1) W(x) f(x/c) \, dx = 0, \tag{4.11a}$$

$$G(a, b) = \int_0^\infty \sin(bx) W(x) f(x/c) \, dx = 0, \tag{4.11b}$$

where $f(s) = \int_0^{-s} e^{(s+u)} J'(u) \, du$. Solving these simultaneous equations for a and b leads to the stability of the travelling pulse for the given architecture.

Other types of bifurcation may occur in this neural system since the firing times are defined by a harsh nonlinearity. Type I and Type II grazing bifurcations (shown in figure 4.1) are common in impact oscillators (such as a ship bumping against a harbour wall, bouncing balls and vibrating beams) ([8, 20, 115] give an introduction to a number of articles on this subject). Type I bifurcations occur when there is a loss of solution via a local maxima decreasing through threshold. Type II is categorised by the creation of a solution as a local maxima increases through threshold. The existence of grazing bifurcations in strongly-coupled integrate-and-fire networks can have a marked effect on the possible solutions [30]. This is easiest to check in the travelling wave framework $(\chi = c - x)$, where grazing bifurcations are categorised by

$$\frac{dV}{d\chi}(0) = 0, V(0) = V_\theta \quad \text{(Type I)} \tag{4.12a}$$

$$V(0) = V_\theta, \frac{dV}{d\chi}(\beta) = 0, V(\beta) = V_\theta \quad \text{(Type II)} \tag{4.12b}$$

with $\beta < 0$ and $V(\chi)$ given by equation (4.9).

Having established equations which define the speed and stability of travelling pulses in the one-dimensional continuum, solutions for the qualitatively different square and exponential synaptic weight kernels will be given. After these examples, the extension of the theory to cover periodic travelling waves will be developed.
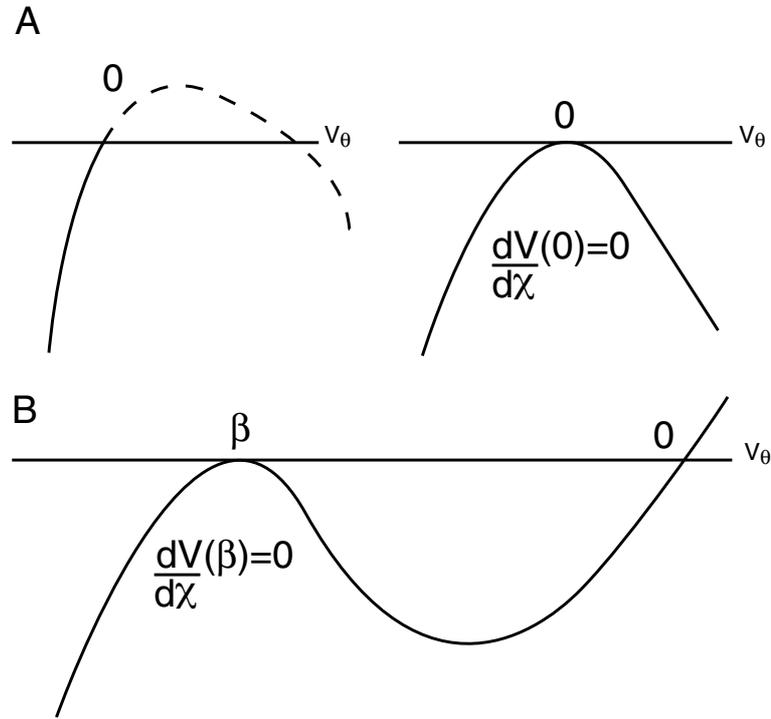
Figure 4.1 Depictions of A: Type I and B: Type II grazing bifurcations. Type I grazing bifurcations result in the loss of a firing solution as the local maxima decreases through the threshold V_θ. Type II grazing bifurcations result in the creation of an earlier firing event as a local maxima increases through threshold V_θ.

4.2 Travelling pulses (square synaptic footprint)

Using the Fourier transform of the delay kernel $J(t)$, equation (4.8) becomes,

$$V_\theta = I_0 + \frac{\epsilon c}{4\pi\sigma} \left\{ \int_{-\infty}^{\infty} \frac{\widehat{J}(\omega)e^{i\omega\sigma/c}}{(1+i\omega)i\omega} - \frac{\widehat{J}(\omega)}{(1+i\omega)i\omega} + \frac{\widehat{J}(\omega)}{1+i\omega}(e^{-\sigma/c}-1)\,d\omega \right\}.$$

This integral is evaluated by using contour integration (see figure 4.2). Causality of the delay kernel and Jordan's lemma impose that the first part of the integral must be
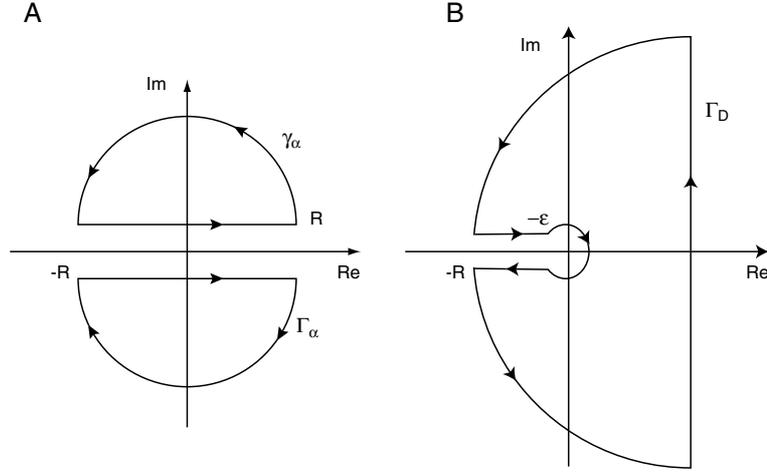
Figure 4.2 A: Contours used in integrations involving α-function responses. The limit of the contour integral as $R \to \infty$ of semicircles in the complex plane are taken. B: The "keyhole" contour is used when evaluating the synaptic input in the passive dendritic case in section 4.2.2. The limit of the contour integral as $\epsilon \to 0$ and $R \to \infty$ is taken.

evaluated in the upper complex plane (contour γ). The latter parts will be evaluated in the lower half plane (contour Γ). This is easily applicable in the case of α-functions since the poles of $\widehat{\eta}(\omega)$ are solely in the upper half plane. More care needs to be taken when considering dendritic kernels since branch points must be taken. Suppose $\widehat{J}(\omega)$ has poles at $\omega = \omega_k$, k=1,...,n (and $\omega_k \neq 0, i$). Then,

$$V_\theta = I_0 + \frac{\epsilon c}{2\sigma} \left[\widehat{J}(0) - \widehat{J}(i)e^{-\sigma/c} - \sum_{k=1}^{n} \text{res} \left\{ \frac{\widehat{J}(\omega)e^{i\omega\sigma/c}}{(1 + i\omega)\omega}; \omega_k \right\} \right]. \quad (4.13)$$

The stability is determined from the simultaneous solution for a, b of equations (4.11). For a general solution $\lambda = a + ib$, solutions are linearly stable if $a < 0$. In the Fourier

transform representation, the linear stability condition is defined by

$$
\begin{aligned}
0 \;=\;& \frac{c^2 \lambda \widehat{J}(-ic\lambda)}{(1+c\lambda)} + \frac{\widehat{J}(i)e^{-\sigma(\lambda+1/c)}}{(\lambda+1/c)} - ce^{-\sigma/c}\widehat{J}(i) \\
& + \operatorname{res}\left\{ \frac{c\widehat{J}(\omega)e^{i\omega\sigma/c}i}{1+i\omega}; \omega_k \right\} + \operatorname{res}\left\{ \frac{\omega\widehat{J}(\omega)e^{-\sigma(\lambda-i\omega/c)}}{(1+i\omega)(\lambda-i\omega/c)}; \omega_k \right\}. \quad (4.14)
\end{aligned}
$$

This equation is then split into real and imaginary parts and solved simultaneously for a and b. Solutions to equations (4.13) and (4.14) will be presented in the next two section in the cases of α-function and passive dendritic delay kernels.

4.2.1 α-**function**

Temporal delay

First consider the α-function $J(t) = \eta(t-\tau_a)$, where an axonal delay τ_a has been included in equation (2.10), as the shape of the post-synaptic response. Both the speed and the stability equations need the value of $\widehat{J}(\omega)$. In this case,

$$
\widehat{J}(\omega) = \frac{\alpha^2 e^{-i\omega\tau_a}}{(\alpha+i\omega)^2}.
$$

Evaluation of equation (4.13) gives,

$$
V_\theta = I_0 + \frac{\epsilon e^{\alpha\tau_a}c}{2\sigma(1-\alpha)^2}\left\{ \kappa e^{-\alpha\sigma/c} + (1-2\alpha)e^{-\alpha\tau_a} - \alpha^2 e^{(1-\alpha)\tau_a}(e^{-\sigma/c} - e^{-\tau_a}) \right\},
$$

$$
(4.15)
$$

where $\kappa = \alpha - (1-\alpha)(\alpha\sigma/c - \alpha\tau_a + 1)$. Solutions of equation (4.15) are shown in figure 4.3 for different values of the axonal delay, and shows the variation of the speed of the pulse with the coupling strength. A critical coupling ϵ_{crit} exists such that there are no travelling pulse solutions for $\epsilon < \epsilon_{\text{crit}}$ and two solutions exist for $\epsilon > \epsilon_{\text{crit}}$. For this value of the critical coupling, sufficient synaptic currents are transmitted to other neurons in the continuum in order that a travelling pulse can propagate. These solutions coalesce in a saddle-node bifurcation.
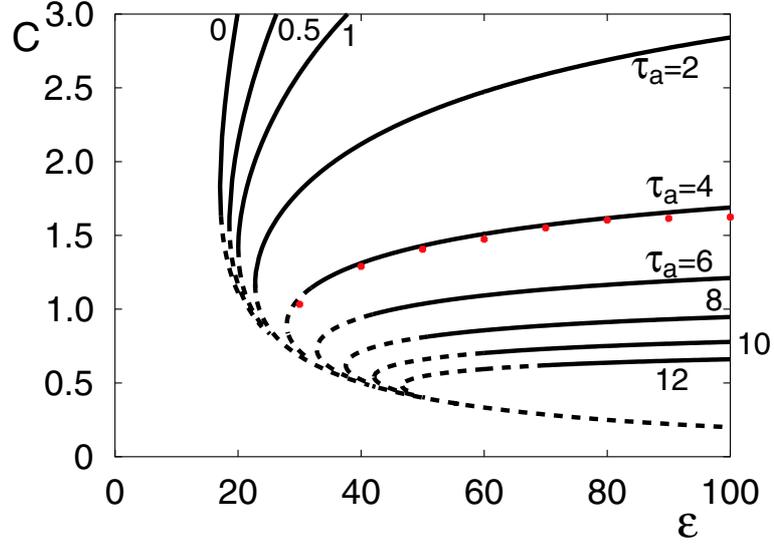
Figure 4.3 The variation of speed c of a travelling pulse in a network with square foot-print interactions with α-function delay kernel as a function of the global coupling strength ϵ for different values of the axonal delay τ_a (the value of τ_a is given next to the curve). The curves are generated using equation (4.15) with linear stability determined by equation (4.14). Dashed lines signify unstable branches. Parameter values: $\alpha = 0.5$, $\sigma = 10$, $I_0 = 0$, $V_\theta = 1$, $V_{reset} = 0$. The red dots next to the curve $\tau_a = 4$ indicate the values found for the speed using numerical simulations of an integrate-and-fire network. For details on the numerical simulations see appendix A.

The bifurcation points determined from equation (4.14) are shown in figure 4.3. Dashed lines correspond to unstable branches of the speed curve. As τ_a is increased, the critical instability point moves away from the limit point and along the upper (stable) branch. This introduction of an axonal delay creates a new type of bifurcation. As with a discrete Hopf (Neimark-Sacker) bifurcation, a pair of complex conjugate eigenvalues cross the imaginary axis from left to right. However, since space is also included in the

description of stability, this name seems inappropriate. Bressloff stated and proved the following theorem for a pulse propagating via α-function post-synaptic responses with axonal delays included [15]:

Let C_+ and C_- denote, respectively, the fast and slow solution branches $c_0 = c_\pm(\epsilon)$, $\epsilon \geq \epsilon_{crit}$, of the self-consistency condition (4.8) for the velocity of a solitary pulse with synaptic delay kernel $J(t) = \eta(t - \tau_a)$ where $\eta(t)$ is given by equation (2.10). Here ϵ_{crit} is the critical coupling for the existence of a solitary wave. Then we have the following stability results: (i) The branch C_- is unstable for all τ_a and α. (ii) The branch C_+ is stable for all α in the case of zero axonal delays ($\tau_a = 0$). (iii) For non-zero delays and sufficiently fast synapses (large α), there exists a Hopf bifurcation point ϵ_{hopf} such that $c_+(\epsilon)$ is stable (unstable for $\epsilon > \epsilon_{hopf}$, ($\epsilon_s \leq \epsilon < \epsilon_{hopf}$)).

Part (iii) of this theorem is particularly interesting because instabilities are shown to occur on the upper (fast) branch. This is unusual in excitable systems.

The spatial scaling σ does not affect the position of the instability. It has been found analytically that in order for this new bifurcation to travel along the upper branch of the speed curve, the axonal delay must be larger than some critical value of axonal delay τ_a^{crit}. Simulations of the network for $\tau_a > \tau_a^{crit}$ produce lurching waves (see figure 4.6 for an example of this waveform), and these will be analysed in more detail later. No solutions were found to equations (4.12) and hence there are no grazing bifurcations in this system.

By considering limit points in bifurcation diagrams (for example the speed-coupling plot in figure 4.3), it is possible to track out boundary curves for parameters such that a travelling pulse solution exists. These are presented in Figure 4.4. A different critical value of the axonal delay τ_a exists to that which governs the emergence of lurching phenomena (figure 4.4(C)). If the delay is greater than this value then no travelling pulse
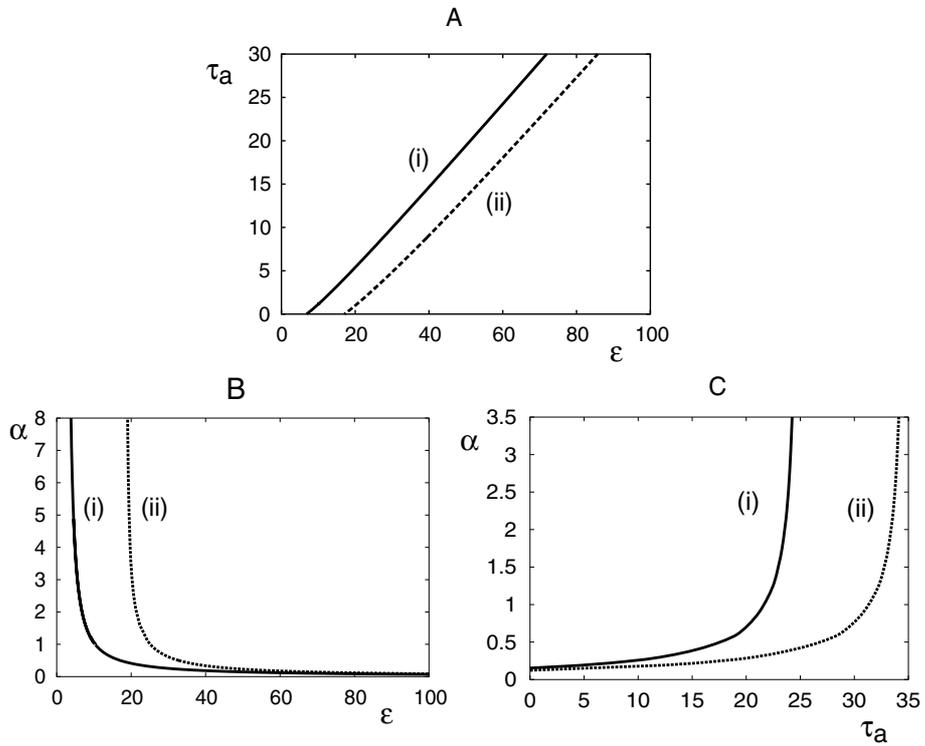
Figure 4.4 Boundary curves to show the existence of a travelling pulse solution for different parameter pairs in a one-dimensional continuum of integrate-and-fire neurons with square synaptic weight kernel and α-function delay kernel. A: (i) $\alpha = 2$, (ii) $\alpha = 0.5$. Solutions exist in the area to the right of the respective curve. B: (i) $\tau_a = 0$, (ii) $\tau_a = 6$. Solutions exist to the right of the respective curve. C: (i) $\epsilon = 60$, (ii) $\epsilon = 80$. Solutions exist to the left of the respective curve.

solutions exist for any parameter values. From figure 4.4(B), the speed of the synapse must be larger than some value for a given coupling strength ϵ in order that travelling pulse solutions exist. However, providing the coupling strength is large enough, any non-zero value for the synapse speed can produce a solution. If grazing bifurcations were
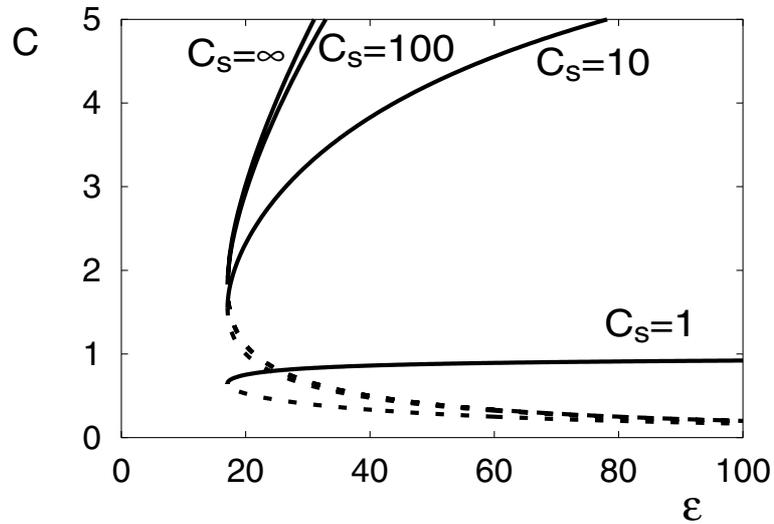
Figure 4.5 Speed curves for a travelling pulse in a network of neurons with square synaptic weight kernel and the α-function delay kernel. The synaptic response includes spatial delay and synaptic connections are with a square synaptic weight kernel. Parameter values are $\alpha = 0.5$, $\sigma = 10$, and $\tau_a = 0$. The $c_s = \infty$ is equivalent to the $\tau_a = 0$ curve in figure 4.3. The other curves are scaled versions of this. As before , dashed lines indicate unstable pulse speeds whereas solid lines represent linearly stable speeds.

present in the system then these existence boundaries would be transformed or shifted. This is because extra solutions would be introduced into the wave train.

α-function with spatial delay

The spatial delay depends upon the separation of the neurons and the speed of the action potential, c_s, and is introduced in the response kernel of the neuron. Thus,

$J(t) = J\left(t - \frac{|x|}{c_s}\right)$ where x is the separation of the neurons. Following the analysis as before only leads to the modification $\frac{1}{c} \to \frac{1}{c} - \frac{1}{c_s}$, and so all results carry through as before, except the speed is scaled (see figure 4.5).

Lurching

Lurching waves propagate such that cells are recruited into the wave in a non-smooth fashion, and are defined by $T(x+L) = T(x) + T_{per}$ where L is the spatial period length, and T_{per} is the time period of the lurching cycle (see figure 4.6). Lurching is evident in models of a structured network model of γ-aminobutyric acid-containing (GABAergic) neurons exhibiting post-inhibitory rebound [59, 130]. However, it is not known at present whether lurching waves exist in a slice of cortex since spatial measurements of the membrane are not sufficiently fine to discriminate variations in the velocity due to heterogeneities from actual dynamic lurching. Spindle waves occur in the thalamus and are a form of synchronised oscillation that typically appear in the electroencephalogram (EEG) as a brief (1–2 s) period of oscillation (6–14 Hz) during slow wave sleep or drowsiness and are made up of waxing and waning activity [4, 133]. Experiments have suggested that these oscillations propagate by progressive recruitment of neighbouring neurons into the oscillation [85]. Numerical simulations of conductance-based models can reproduce spindle and slow bicuculline induced oscillations observed *in vitro* [36]. In this case, *in vitro* means that a very thin slice of the brain is removed from the animal and bathed in nutrient solution. These simulations show that these discharges propagate in a *lurching* (or saltatory) manner. Suppose the lurching period starts at $x = 0$ and $T(0) = 0$, then

$$T(x) = \left\lfloor \frac{x}{L} \right\rfloor T_{per} + f(\widehat{x}),$$

where f describes the shape of the "lurch" and is defined on the interval $[0, L]$ such that $f(0) = 0$, and $\widehat{x} = x - \left\lfloor \frac{x}{L} \right\rfloor L$.
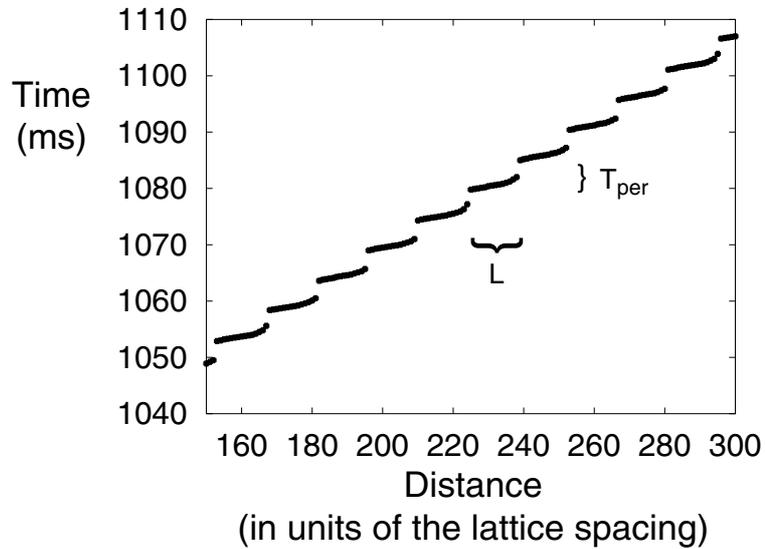
Figure 4.6 An example of a lurching wave in a one-dimensional integrate-and-fire continuum (4.1) with (4.2). The delay and weight kernels are given by equations (4.3) and (2.10). The firing times are shown for 150 grid points in a 500 grid point simulation of the network with square synaptic footprint and α-function delay kernel. System parameter values are given by $\alpha = 0.5$, $V_\theta = 1$, $\epsilon = 30$, $\sigma = 10$, $\tau_a = 4$. A description of the direct numerical simulation scheme is given in appendix A.

Analysis is followed along the same lines as Golomb and Ermentrout in order to find the velocity of lurching pulses [57]. Through simulations they deduced that neurons only fire during a time period which is small in comparison to the delay, and that L is almost unaffected by the axonal delay period (provided the axonal delay is large enough). Hence, the pulse velocity is given by $c_{\text{lurch}} = L/\tau_a$.

Since the system which exhibits lurching waves requires a large axonal delay, a neuron is not affected by other neurons contained within its own lurching period. The

axonal delay causes the neuron to be affected only by those in the previous lurching period since other contributions have already decayed to a negligible level. Now, suppose the lurching wave is initiated for large negative x, and that a lurching period starts at $x = 0$. Consider neurons in the range $0 \leq x < L$. Hence, equation (4.5) becomes,

$$V_\theta = I_0 + \epsilon \int_{-L}^{0} W(x - x') \int_{-\widetilde{T}}^{0} \alpha^2 (u + \widetilde{T}) e^u e^{-\alpha(u + \widetilde{T})} \, du \, dx', \qquad (4.16)$$

where $\widetilde{T} = T_{per} - \tau_a > 0$ (shown in simulations by Golomb and Ermentrout [57]). It has been assumed that $f(x) \approx f(v)$ for $x, v \in [0, L)$. Golomb and Ermentrout showed that as α increases, $\alpha f(x)$ tends towards a constant function (see figure 6 in [57]). Hence, α must be taken to be large. Thus the analysis for lurching pulses is only correct in the limit $\tau_a \gg 1 \gg 1/\alpha$. Evaluating the integral in equation (4.16), and using the condition that $x \in [0, L)$, the following conditions are found in the large α limit,

$$V_\theta = \begin{cases} I_0 + \frac{\epsilon e^{-\widehat{T}}}{2\sigma}(\sigma - L), & \frac{\sigma}{2} < L \leq \sigma, \\ I_0 + \frac{\epsilon e^{-\widehat{T}}}{2\sigma}L, & 0 \leq L < \frac{\sigma}{2}. \end{cases}$$

Taking the limit for small $\widetilde{T}$ (simulations in Golomb and Ermentrout [57] show that $\widetilde{T}$ scales as $1/\alpha$), identical expressions to those calculated by Golomb and Ermentrout are recovered.

4.2.2 Passive dendrites

In the case of passive dendrites, equation (4.2) describing the synaptic input current has the form,

$$S(x, t) = \epsilon \int_{-\infty}^{t} G(\xi, t - t') \int_{-\infty}^{\infty} W(x - x') \Psi(x', t') \, dx' \, dt',$$

assuming the dendritic contact point is at ξ. Rall first demonstrated that a passive dendritic branch can act as a spatiotemporal filter which selects specific temporal sequences of synaptic inputs [125]. This is because it depends upon which part of the dendrite is

stimulated at which time. To evaluate this integral it is best to use the Laplace transform (equation (2.8) on the time variable, with p as the Laplace variable. This leads to

$$\overline{S}(\xi, p) = \frac{\epsilon c}{2\sigma} \frac{\overline{G}(\xi, p) e^{-px/c}(e^{p\sigma/c} - e^{-p\sigma/c})}{p(1 - e^{-p\Delta_1})},$$

where the firing time ansatz for a periodic travelling wave (4.4) has been substituted and $k\Delta_1 = 1/c$. Hence, upon inverting and introducing the travelling wave coordinate $\chi = ct - x$,

$$S(\chi) - S(\chi - c\Delta_1) = \widetilde{A}(\xi, (\chi + \sigma)/c) - \widetilde{A}(\xi, (\chi - \sigma)/c), \qquad (4.17)$$

where

$$\widetilde{A}(\xi, t) = \frac{\epsilon c}{4\pi\sigma i} \int_{e-i\infty}^{e+i\infty} \frac{\overline{G}(\xi, p) e^{pt}}{p} \, dp,$$

and the Laplace transform of the Green's function is given by

$$\overline{G}(\xi, p) = \frac{e^{-\gamma_{\text{pass}}(-ip)|\xi|}}{2\gamma_{\text{pass}}(-ip)D},$$

with $\gamma_{\text{pass}}(x)$ is given by equation (2.15). In the case of a travelling pulse, the second term on the left-hand side of equation (4.17) is omitted. Calculating the inverse Laplace transform along the lines of Coombes in [28],

$$\widetilde{A}(\xi, t) = \frac{\epsilon c e^{-t/\tau_D} \sqrt{D\tau_D}}{4\sigma D} \left[R(\xi, t) - Q(\xi, t)\right] \Theta(t),$$

where

$$
\begin{aligned}
R(\xi, t) &= e^{-|\xi|/\sqrt{D\tau_D}} e^{t/\tau_D}, \\
Q(\xi, t) &= \frac{e^{t/\tau_D}}{2} \left\{ e^{-|\xi|/\sqrt{D\tau_D}} \text{erfc}\left(-|\xi|/\sqrt{4Dt} + \sqrt{t/\tau_D}\right) \right. \\
&\quad \left. + e^{|\xi|/\sqrt{D\tau_D}} \text{erfc}\left(|\xi|/\sqrt{4Dt} + \sqrt{t/\tau_D}\right) \right\}.
\end{aligned}
$$

Hence,

$$S(x, t) = \begin{cases} \widetilde{A}(\xi, (\chi + \sigma)/c) - \widetilde{A}(\xi, (\chi - \sigma)/c), & \text{pulse,} \\ \sum_{n=0}^{\infty} \left\{ \widetilde{A}(\xi, (\chi + \sigma)/c - n\Delta_1) - \widetilde{A}(\xi, (\chi - \sigma)/c - n\Delta_1) \right\}, & \text{periodic.} \end{cases}$$
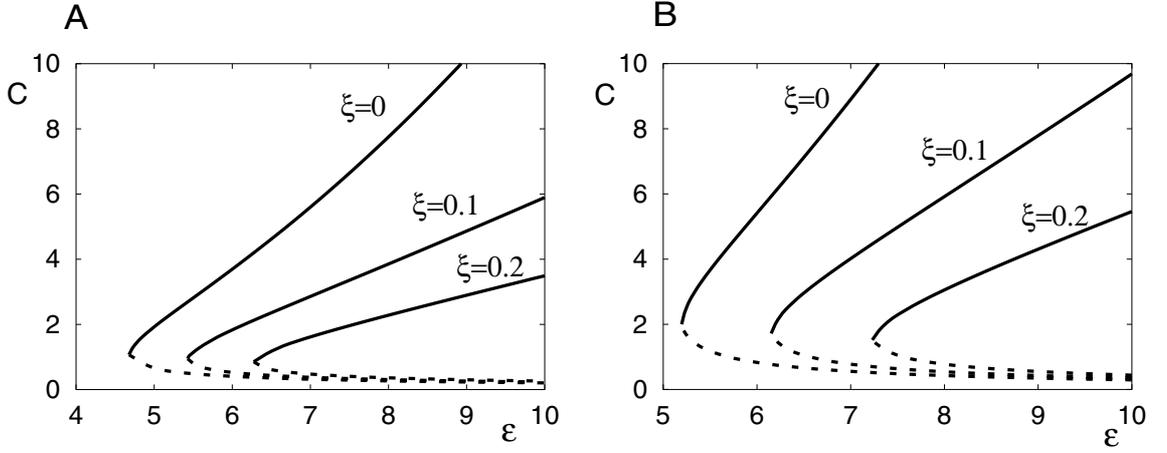
Figure 4.7 A: The speed curves for the passive dendrite calculated using the square weight kernel. B: The speed curves for the passive dendrite calculated using the exponential synaptic weight kernel (equation (4.18)). Parameter values $D = \tau_D = \sigma = 1$. Solid (dashed) lines represent linearly stable (unstable) solutions. Qualitatively similar results are produced for both synaptic weight kernels.

To evaluate the threshold condition, $V(0) = V_\theta$ in the travelling wave framework (equation (4.9)) the trapezium rule was employed. The curves generated in figure 4.7A are qualitatively the same (except for scaling) as those derived using the exponential weight kernel (figure 4.7B) (the equations are given in the next section where $\widehat{J}(\omega) = \widehat{G}(\omega)$ with $\widehat{G}(\omega)$ given by equation (2.16)). There is no further bifurcation in the upper branch. Hence, to ease calculations in the much more complex case of quasi-active dendrites, the exponential synaptic footprint will be used.

4.3 Travelling pulses (exponential synaptic footprint)

In the case of the exponential footprint, equation (4.13) is replaced with the more simple [15]

$$V_\theta = I_0 + \frac{\epsilon c}{2\sigma} \frac{\widehat{J}(-\frac{ic}{\sigma})}{\left(1 + \frac{c}{\sigma}\right)}. \tag{4.18}$$

This is considerably more succinct than in the compact support case since poles in the upper half plane are not considered. The linear stability condition (equation (4.14)) is also simplified. In terms of a pair of simultaneous equations, it is given by (see section 4.1)

$$H(a, b) = \mathrm{ReP}\left(\frac{c}{\sigma} + a + ib\right) - P\left(\frac{c}{\sigma}\right), \tag{4.19a}$$

$$G(a, b) = -\mathrm{ImP}\left(\frac{c}{\sigma} + a + ib\right), \tag{4.19b}$$

where,

$$P(z) = \frac{z}{1 + z}\widehat{J}(-iz),$$

and solutions are stable if the solution for λ has $\mathrm{Re}[\lambda] < 0$.

4.3.1 Quasi-active dendrites

So far, this discussion on dendrites has been focussed on passive cables. The speed curves generated by passive dendrites with an exponential synaptic weight kernel (for fixed ξ) are given in figure 4.7. However, the presence of voltage-dependent gated channels along the dendritic membrane enables the dendrite to perform a number of different functions. There are many possible information processing activities which active membranes could support such as amplification and linearisation of action potentials, and decomposition of the dendrites into a number of distant multiplicative subunits [92, 134]. It has been suggested that local computations could be performed on clusters of synapses [105]. Resonant elements (bandpass filters) have been located in the amphibian cochlea where they are used for electrical tuning [92]. Linearising the Hodgkin-Huxley equations (equations (2.1) and (2.2)) leads to a simple model of an active linearised membrane as an

electrical circuit consisting of a passive component in parallel with an inductive branch containing an inductance l in series with a resistance r_l (see section 2.4.1). At a phenomological level this represents the electrical behaviour of a specific type of active channel for small variations in the membrane potential [91]. For such a circuit, $\widehat{J}(\omega) = \widehat{G}(\omega)$ is given in equation (2.20).

The effects of quasi-active dendrites on phase-locked neurons has been addressed by Bressloff [13]. It was found that when the collective frequency of a group of oscillators is close to the resonant frequency, then weak excitatory coupling leads to a form of resonantlike synchronisation. Quasi-active dendrites were shown to destabilise a pair of phase-locked solutions in the presence of strong coupling. This led to periodic bursting patterns and multistability.

The speed curves calculated from equation (4.18) in this case are plotted in figure 4.8. Once again the same shape is present and an instability occurs at the limit point, so that the faster wave is stable. However, there is no Hopf-like bifurcation present in the upper branch for any parameter values.

4.4   Extension to periodic travelling waves

The theory will now be extended to include periodic travelling waves. Previous analytical treatments have focussed on travelling pulse solutions [15, 57, 58] and travelling wave solutions have been considered numerically [106, 129]. A dispersion curve is the wave speed c as a function of the period Δ_1. Since $K_{\Delta_1}(x)$ (equation (4.6)) is a real periodic function of x, Fourier transforms are used to calculate the dispersion curves. The Fourier series of the function $K_{\Delta_1}(x)$ is calculated to be

$$K_{\Delta_1}(x) = \frac{(1 - e^{-\Delta_1})}{\Delta_1} \sum_{m \in \mathbb{Z}} \left(a\left(\frac{2\pi m}{\Delta_1}\right) \cos(2\pi m x) + b\left(\frac{2\pi m}{\Delta_1}\right) \sin(2\pi m x) \right), \quad (4.20)$$
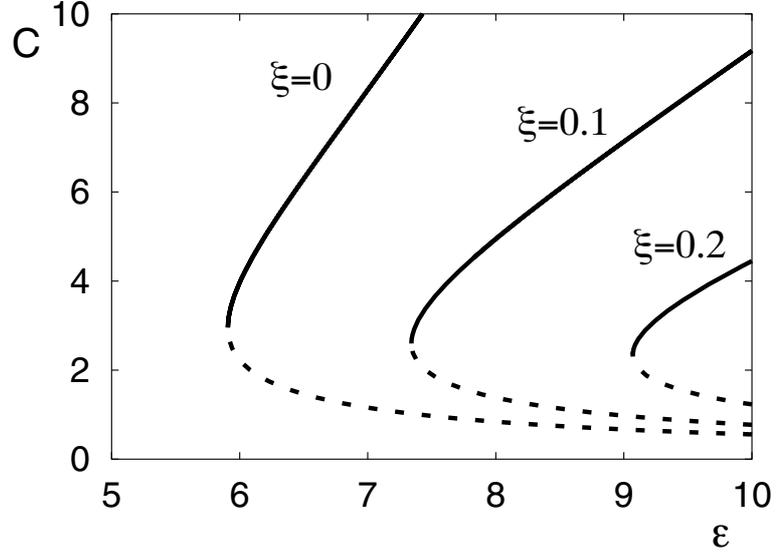
Figure 4.8 The variation of speed c of a travelling pulse as a function of the coupling strength ϵ for different values of the dendritic coordinate ξ, generated using (4.18) with speed determined by (4.19). In this figure, $l = 0.2$ and $r_l = 0.5$ to give a quasi-active dendrite using (2.20). If r_l decreases then the curves shift to the right and if r_l increases, the curves shift to the left. All other parameter values (σ, r_a, r, D, τ_D) are unity. Solid (dashed) lines represent linearly stable (unstable) solutions.

where

$$a(\omega) = \text{Re}\left[\frac{\widehat{J}(\omega)}{1 + i\omega}\right], \quad b(\omega) = \text{Im}\left[\frac{\widehat{J}(\omega)}{1 + i\omega}\right]. \tag{4.21}$$

Since $W(x)$ is symmetric, equation (4.5) simplifies to

$$V_\theta - V_{\text{reset}}e^{-\Delta_1} = (1 - e^{-\Delta_1})I_0 + \epsilon\frac{(1 - e^{-\Delta_1})}{\Delta_1}\sum_{m\in\mathbb{Z}}a\left(\frac{2\pi m}{\Delta_1}\right)\widehat{W}(2\pi mk). \tag{4.22}$$

79

4.4.1 Stability of periodic travelling waves - kinematic formalism

Bressloff formulated a theory to analyse the stability of travelling waves [15].

Consider a travelling wave solution of wavenumber k and collective period Δ_1 satisfying the phase-locking equation (4.5). Suppose that the set of firing times T of an integrate-and-fire network is decomposed according to $T^\pm = \{T_m(x), (x, m) \in D_\pm\}$ where $D_+ = \{(x, m), x \in \mathbb{R}, m \in \mathbb{Z} | m + kx > 0\}$ and $D_- = \{(x, m), x \in \mathbb{R}, m \in \mathbb{Z} | m + kx \leq 0\}$. Let T^+ represent the solution to the Cauchy problem specified by the initial data T^-. Set $\phi_m(x) = T_m(x) - (m + kx)\Delta_1$. The travelling wave solution is (locally) stable if and only if for all $\epsilon > 0$ there exists $\Delta_1 > 0$ such that if $\sup\{|\phi_m(x)|, (x, m) \in D_-\} < \Delta_1$ then $\sup\{|\phi_m(x)|, (x, m) \in D_+\} < \epsilon$. The solution is said to be asymptotically stable if it is locally stable and there exists $\Delta_1 > 0$. (Uniform initial data with respect to which a solution is always neutrally stable is excluded). Whence, the following stability result: a travelling wave solution is (locally) asymptotically stable if the solutions of the characteristic equation

$$(z - 1)[I_0 - 1 + \epsilon A] = \epsilon[\widetilde{B}(z, p) - \widetilde{B}(1, 0)],$$

satisfy $|z| < 1$ for all $p \in \mathbb{R}$ (except for one solution $z = 1$ at $p = 0$), and

$$A = \int_{-\infty}^{\infty} W(x) \sum_{M \in \mathbb{Z}} J([m + kx]\Delta_1) \, dx,$$

$$\widetilde{B}(z, p) = \sum_{n \in \mathbb{Z}} \int_{-\infty}^{\infty} e^{-ipx} z^{-(n+kx)} B_n(x) \, dx,$$

$$B_m(x) = = W(x) e^{-\Delta_1} \int_0^{\Delta_1} e^t J'(t + [m + kx]\Delta_1) \, dt.$$

There are an infinite number of solutions to the characteristic equation. A more simple way to analyse these wave trains is by looking at a kinematic theory. The

kinematic formalism has been introduced to follow the evolution of the spike train at the expense of a detailed description of the pulse shape. The shape of the dispersion curve is sufficient to describe the evolution of impulse propagation in the system. Changing interspike intervals during impulse propagation for the Hodgkin-Huxley [40] and Fitzhugh-Nagumo [129] models have been considered, along with propagating trains in a reaction-diffusion system [106]. By differentiating the firing time ansatz for a periodic traveling wave with respect to the spatial variable,

$$\frac{dT^n(x)}{dx} = \frac{1}{c(\Delta_1)}, \tag{4.23}$$

where $c(\Delta)$ is the dispersion curve. The kinematic formalism assumes that there is a description of irregular spike trains in this form such that the differential equation is dependent upon all spike times in the system. By further assuming that the most recent spike has the strongest influence, equation (4.23) is reproduced only if $c(\Delta_1)$ is replaced by $c(T^n(x) - T^{n-1}(x))$, where $T^n(x) - T^{n-1}(x)$ is the instantaneous period of the wave train at position x. The power of the kinematic theory is demonstrated in its simplicity and the following shows the main result.

Suppose there are two pulses and that the first has speed θ_f. Then,

$$\frac{dt_1}{dx} = \frac{1}{\theta_f}, \quad \frac{dt_2}{dx} = \frac{1}{\theta(t_2 - t_1)},$$

where t_1, t_2 are the arrival times of the pulses. Thus, the differential equation for the interspike interval $\Delta_1(x)$ is given by

$$\frac{d\Delta_1}{dx} = \frac{1}{\theta(\Delta_1)} - \frac{1}{\theta_f}. \tag{4.24}$$

Any interspike interval, Δ_f for which the dispersion relation $\theta(\Delta_f) = \theta_f$ is a possible equilibrium solution to equation (4.24). Linear stability of this solution is considered by perturbing Δ_f. Let $\Delta_1(x) = \Delta_f + \zeta(x)$. Then,

$$\frac{d\zeta}{dx} = -\frac{\theta'(\Delta_f)}{\theta_f^2}\zeta.$$

Hence, the solution is unstable if $\theta'(\Delta_f) < 0$ and stable if $\theta'(\Delta_f) > 0$. This result is put into practice in the following sections, but first an application of the theory will be presented showing that non-periodic waves may also be described in this formalism [76].

Applications of the kinematic formalism

The "derivation" of the kinematic theory ensures that a periodic solution exists for the ordinary differential equations (4.23), but other more complex solutions may exist. The exact shape of $c = c(\Delta_1)$ is found by calculating the dispersion curve (shown for the integrate-and-fire model in sections 4.4.3—4.4.5). Consider a linear approximation (reasonable in the large Δ_1 limit) for $c(\Delta_1)$ (see figures 4.10–4.13 as $\Delta_1 \to \infty$). Then,

$$\frac{1}{c(\Delta_1)} = \frac{1}{c_0} - \frac{c_0'}{c_0^2}\Delta_1,$$

and the interspike intervals satisfy

$$\frac{d\Delta_1^n}{dx} = -\rho[\Delta_1^n - \Delta_1^{n-1}], \tag{4.25}$$

where $\rho = c_0'/c_0^2$. The general solution of the above equation is given by

$$\Delta_1^n(x) = \sum_m G_{nm}(x)\Delta_1^m(0),$$

where

$$G_{nm}(x) = e^{-\rho x}\left[e^{Kx}\right]_{nm}, \quad K_{nm} = \rho\delta_{n,m+1}.$$

Using the series expansion for $\left[e^{Kx}\right]_{nm}$ and noting that $\left[K^j\right]_{nm} = \rho^j\delta_{n,m+j}$ write

$$G_{nm}(x) = e^{-\rho x}\frac{(\rho x)^{n-m}}{(n-m)!}.$$

Thus,

$$\Delta_1^n(x) = e^{-\rho x}\sum_{j=0}^{n}\frac{(\rho x)^j}{j!}\Delta_1^{n-j}(0).$$

For uniform initial data $\Delta_1^n(0) = \Delta_1$ for all n,

$$\lim_{n \to \infty} \Delta_1^n(x) = \Delta_1,$$

since the sum converges to $e^{\gamma x}$ as $n \to \infty$. Now, consider an initial spike train with a step. That is, $\Delta_1^n(0) = \Delta_1$ for $n \le n^*$ and $\Delta_1^n(0) = \Delta_2$ for $n > n^*$. Then,

$$\Delta_1^n(x) = \Delta_1 + (\Delta_2 - \Delta_1)e^{-\rho x} \sum_{j=0}^{n-n^*-1} \frac{(\rho x)^j}{j!},$$

for large n. So, if n^* is close to n then the system at x will fire repetitively with period Δ_1, but as n^* and n become more separated, the system will switch to firing with a period Δ_2.

Now, consider the approximation

$$\frac{1}{c(\Delta_1)} = \frac{1}{c} + Ae^{-B\Delta_1}.$$

for the dispersion curve. Later sections will suggest that this is a more suitable shape than the linear approximation (see figures 4.10 and 4.12 near the limit point/local maxima respectively). However, similar results are possible. Introduce a set of reference firing times of the form $T_r^n(x) = n\Delta_r + x/c(\Delta_r)$ for some arbitrary Δ_r, and re-scale the firing times according to $T^n(x) \to B(T^n(x) - T_r^n(x))$. Then,

$$\frac{dT^n(x)}{dx} = -ABe^{-B\Delta_r}(1 - e^{-T^n(x)}e^{T^{n-1}(x)}). \tag{4.26}$$

Re-scaling x such that $x \to ABe^{-B\Delta_r}x$ and introducing a further transformaton $z_n(x) = e^{T^n(x)}$ leads to an equation similar to equation (4.25) with $\gamma = 1$. It is then trivial to generate the general solution of the firing time map. Following Horikawa, the solution for an initial spike train with a step difference in the interspike intervals is [76],

$$T^n(0) = \begin{cases} n\Delta_1, & n \le n^* \\ n^*\Delta_1 + (n-n^*)\Delta_2, & n > n^* \end{cases}$$

$$T^n(x) = \begin{cases} n\Delta_1 + x(e^{-\Delta_1} - 1), & n \le n^*, \\ -x + \log\left\{\sum_{j=0}^{n-n^*-1} \frac{x^j e^{n^*\Delta_1 + (n-n^*-j)\Delta_2}}{j!} + \sum_{j=n-n^*}^{n} \frac{x^j e^{(n-j)\Delta_1}}{j!}\right\}, & n > n^*. \end{cases}$$
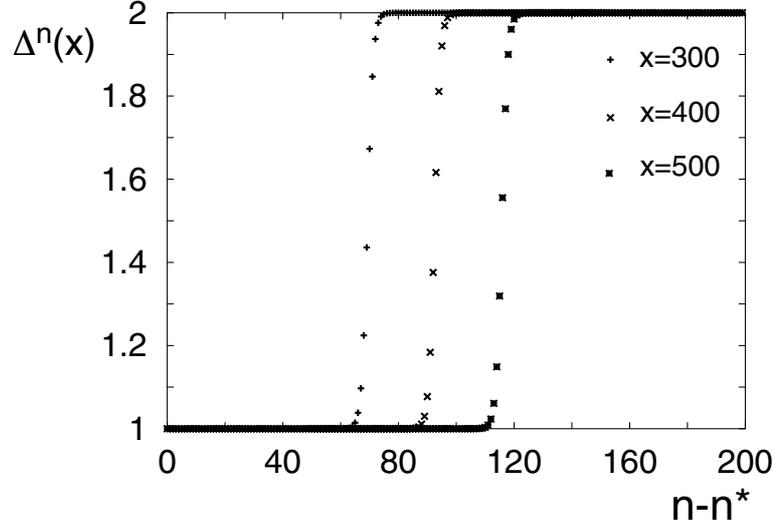
Figure 4.9 Values for the interspike intervals generated from equation (4.27) for different values of the spatial variable x. The initial data at $x = 0$ is such that there is a step interval in the sequence of interspike intervals with $\Delta_1 = 1$ and $\Delta_2 = 2$. The kinematic description used to generate such firing times is given by equation (4.26).

The interspike intervals of the spike times, $\Delta^n(x) = T^n(x) - T^{n-1}(x)$, may be constructed from this solution. By taking the large $n - n^*$ limit, and introducing the functions $\omega = \Delta_1 - \Delta_2$ and $\theta = \exp(-\Delta_2) - \exp(-\Delta_1)$,

$$\Delta^n(x) = -\log\left[e^{-\Delta_1} - \frac{(e^{-\Delta_1} - e^{-\Delta_2})}{1 - e^{(n-n^*)\omega - \theta x}}\right]. \qquad (4.27)$$

Note that this is a function of $z = (n - n^*)\omega - \theta x$, and that $\Delta^n(x) \to e^{-\Delta_1}$ ($e^{-\Delta_2}$) as $z \to \infty$ ($-\infty$). Substitution clarifies that this solution does indeed satisfy the ordinary differential equation derived from equation (4.26). The sequence of interspike intervals given by equation (4.27) is plotted in figure 4.9. The position of the front connecting the two periodic orbits moves with constant velocity $d(n - n^*)/dx = \theta/\omega$. Hence, the front moves backwards in the spike train for $\Delta_2 > \Delta_1$.
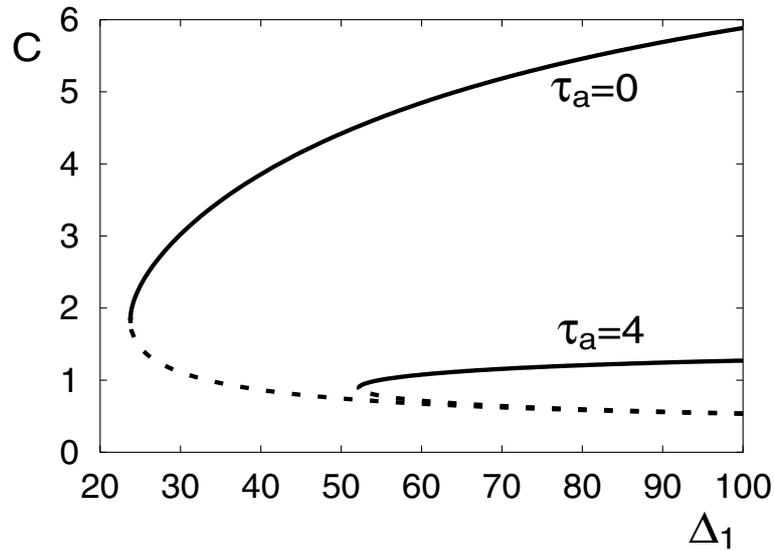
Figure 4.10 Dispersion curves for the square synaptic footprint and α-function response kernel generated from equations (4.21) and (4.22). Parameter values are $\alpha = 0.5$, $\epsilon = 60$, $\sigma = 10$, $I_0 = 0$ and $\tau_R = 0$. Solid (dashed) lines correspond to linearly stable (unstable) travelling waves according to the kinematic theory.

4.4.2 A question of re-excitation

In figure 4.10, dispersion curves for the α-function delay kernel with square synaptic footprint created using equation (4.22) are plotted. When axonal delays, τ_a, are introduced, the basic shape of the dispersion curve remains unchanged. However, bifurcations are known to take place for the α-function with the introduction of delays. The gradient of the dispersion curve does not change under these circumstances and so it is highlighted that the kinematic formalism does not pick up instabilities in the presence of delays.

Now, the shape of the dispersion curve is considered for the exponential footprint. Figure 4.11 (which will be discussed in more detail in the next section) shows the dispersion curve for the exponential footprint and the α-function generated from equation (4.22). Since, the integrate-and-fire model has no notion of a refractory period, arbitrarily high firing rates are possible and thus divergent speeds. Pulse-based models highlight this fact [35]. It may be possible that sufficient synaptic current is present at the location of the neuron *after* firing such that the neuron is able to fire again, and possibly repeatedly. Bressloff and Ermentrout have both presented a discussions on this topic [15, 45]. Possible ways to introduce a refractory period are given below.

- **Adapting threshold**

  An adapting threshold can be described by the following differential equation (reminiscent of the adaptation in chapter 3),

  $$\frac{dV_\theta}{dt} = \frac{V_\theta^c - V_\theta}{\tau_\theta},$$

  where V_θ^c is the level to which the threshold decays and τ_θ is the adaptation time constant, and is larger than all other time constants in the system. In conjunction with this, at the firing times, $V_\theta \to \gamma V_\theta$ where $\gamma > 1$.

  For a periodic wave,

  $$V_\theta^{eq} = \frac{V_\theta^c(1 - e^{-\Delta_1/\tau_\theta})}{1 - \gamma e^{-\Delta_1/\tau_\theta}},$$

  where V_θ^{eq} is the periodic steady state value of the threshold. When $\Delta_1 \to \infty$, $V_\theta^{eq} \to V_\theta^c$ (a constant). Thus in the case of a pulse, the adapting threshold has no effect on the analysis. In a periodic wave, the time taken for the threshold to relax to its steady state is given by the transcendental equation,

  $$\Delta_1 = \tau_\theta \ln\left[\frac{V_\theta^c - 1 + e^{\Delta_1/\tau_\theta}}{V_\theta^c}\right]$$

  However, bounds need to be placed on the new parameter τ_θ. The duration of a spike is typically 1–2 ms, and the membrane time constant varies between 1–2 ms

in neurons specialised in processing high-fidelity temporal information to 100 ms or longer for cortical neurons recorded under slice conditions. A typical range for τ recorded from cortical pyramidal cells in the living animal is between 10 and 20 ms. Hence, it is appropriate to take $\tau_\theta = \tau$. In the case of an adapting threshold, the equations which determine the dispersion relation are identical to equation (4.22).

- **Infinitely negative reset**

This method of correction is exactly the same as using an adapting threshold with unit time constant τ_θ. If the reset level is considered to be negative (in the integrate-and-fire model it is typical to take the level of reset to be zero with the firing threshold given by unity), it takes longer for the neuron to equilibriate. Hence the potential difference between the neuron and the firing threshold remains large for some time. A small negative reset has no effect on the dynamics of the system because the exponential term on the left-hand side of equation (4.22) is very small, even for the smallest existing periodic solution. Hence, to make a suitable contribution, it is typical to take the reset value to be negative infinity. Even in this case, identical results to those generated using an adapting threshold are produced.

- **"Dead time" refractory period**

A more definite way is to introduce a "dead time" style refractory period τ_R in which a neuron cannot fire again and is held at V_{reset}. The result of this is to integrate equation (4.1) over the range $(T^n(x) + \tau_R, T^{n+1}(x)]$. Then, instead of equation (4.20), the speed equation for periodic travelling waves involves the term

$$K_{\Delta_1}(x) = \sum_{m \in \mathbb{Z}} \left(a^{[1]}\left(\frac{2\pi m}{\Delta}\right) \cos(2\pi m x) + b^{[1]}\left(\frac{2\pi m}{\Delta}\right) \sin(2\pi m x) \right),$$

where

$$a^{[1]}(\omega) = \frac{e^{-\Delta_1}}{\Delta} \left[(ec(\Delta_1) - ec(\tau_R)) \, a(\omega) - (es(\Delta_1) - es(\tau_R)) \, b(\omega) \right], \quad (4.28a)$$

$$b^{[1]}(\omega) = \frac{e^{-\Delta_1}}{\Delta} \left[(es(\Delta_1) - es(\tau_R)) \, a(\omega) + (ec(\Delta_1) - ec(\tau_R)) \, b(\omega) \right], \quad (4.28b)$$

where $a(\omega)$ and $b(\omega)$ given in equation (4.21) and

$$ec(x) = e^x \cos(\omega x), \quad es(x) = e^x \sin(\omega x),$$

and, $\Delta = \Delta_1$ in this case. Section 4.4.5 examines waves with multiple periods where Δ is the sum of all periods in the system. The superscript [1] is used here because this coefficient is applicable for waves with a single period.

All three ways of constructing a refractory period result in qualitatively similar dispersion curves for suitable parameter regimes. However, it is easier to create extra stationary points in the dispersion curve with the "dead time" refractory period, as will be demonstrated in the following sections. Henceforth, only the dead time refractory periodwill be considered in the analysis. It has been found that the square synaptic footprint is relatively unaffected by the introduction of a refractory period. This is because compact support means that only a finite region is considered for the synaptic input and hence the input can never become too large. However, when an exponential weight kernel is considered, *all* neurons contributes to a synaptic current leading to large synaptic input currents and possible multiple repetitive firings.

4.4.3 Periodic travelling waves (α-function)

Using the refractory mechanism, dispersion curves shown in figure 4.11 are obtained for the case of the exponential synaptic weight kernel and α-function delay kernel. However, note that if the refractory mechanism is not included in the model, divergent speeds may occur (compare with figure 4.10). If τ_R is greater than some critical value, the lower branch, which is seen for large periods, joins with the upper branch and forms a dispersion curve which is qualitatively the same shape as in the square synaptic weight kernel case. However, once this critical value has been passed, the stationary point which is present in the upper branch for smaller values of the refractory period disappears. This stationary
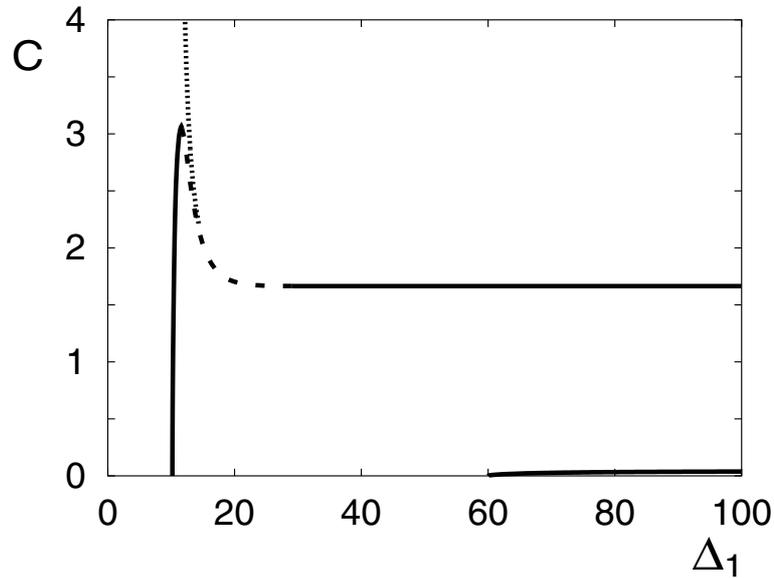
Figure 4.11 Dispersion curves for the exponential footprint and α-function response kernel generated from equations (4.21) and (4.22) and (4.28). Parameter values are $\alpha = 0.5$, $\epsilon = 60$, $\sigma = 1$, $\tau_a = 0$, $I_0 = 0$ and $\tau_R = 10$. Solid (dashed) lines correspond to stable (unstable) travelling waves according to the kinematic theory. The key difference between this figure and the one generated using the square synaptic footprint (figure 4.10) is that (unrealistic) divergent speeds (dotted line) are apparent when there is no refractory mechanism included in the model.

point of "supernormal" wave speeds exists for periodic travelling waves with small periods (using the nomenclature of Rinzel), and will be shown to be critical for the generation of multi-periodic solutions in section 4.4.5. As with the travelling pulse, the introduction of a spatial delay in the synaptic response kernel mostly serves to scale the dispersion curve with zero spatial delay (see figure 4.12).
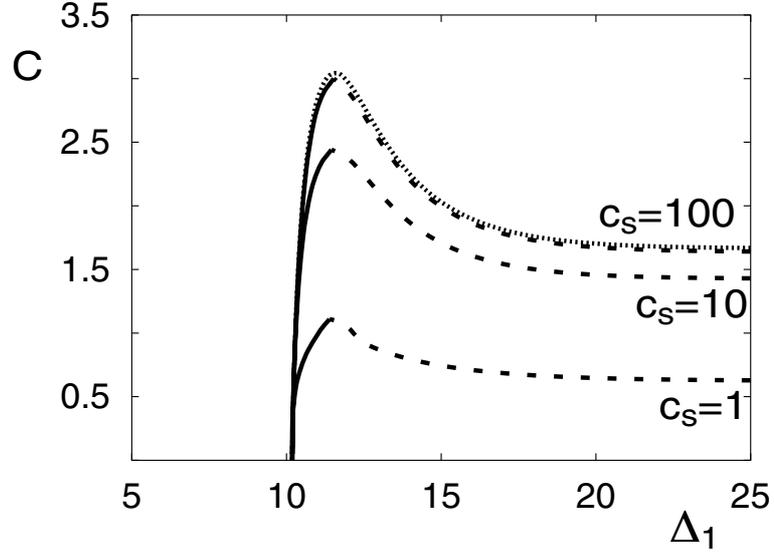
Figure 4.12 Dispersion curves for the exponential footprint with α-function delay kernel including spatial delay using equations (4.22) and (4.28). Parameter values are $\alpha = 0.5$, $\epsilon = 60$, $\sigma = 1$, $\tau_a = 0$, $\tau_R = 10$ and (a) $c_s = \infty$, (b) $c_s = 100$, (c) $c_s = 10$, (d) $c_s = 1$. The dotted line represents the dispersion curve when there is no spatial delay present in the system. Solid (dashed) lines correspond to linearly stable (unstable) travelling waves according to the kinematic theory. The upper branches become stable for large Δ_1.

4.4.4   Periodic travelling waves (dendrites)

Evaluating $a^{[1]}(\omega)$ and $b^{[1]}(\omega)$ using equation (4.28) in the dendritic regime (with real ω) gives

$$a^{[1]}(\omega) = \frac{[\gamma_R(\omega) - \omega_R\gamma_I(\omega)]\cos(\gamma_I(\omega)\xi) - [\omega_R\gamma_R(\omega) + \gamma_I(\omega)]\sin(\gamma_I(\omega)\xi)}{D((1 - \omega_I)^2 + \omega_R^2)(\gamma_R(\omega)^2 + \gamma_I(\omega)^2)e^{\gamma_R(\omega)\xi}},$$

$$-b^{[1]}(\omega) = \frac{[\gamma_R(\omega) - \omega_R\gamma_I(\omega)]\sin(\gamma_I(\omega)\xi) + [\omega_R\gamma_R(\omega) + \gamma_I(\omega)]\cos(\gamma_I(\omega)\xi)}{D((1 - \omega_I)^2 + \omega_R^2)(\gamma_R(\omega)^2 + \gamma_I(\omega)^2)e^{\gamma_R(\omega)\xi}},$$

with

$$\gamma_R(\omega) = \sqrt{\frac{A + \sqrt{A^2 + B^2}}{2}},$$

$$\gamma_I(\omega) = \text{sign}(\omega_R)\sqrt{\frac{-A + \sqrt{A^2 + B^2}}{2}},$$

where

$$A = \begin{cases} \frac{1}{D\tau_D}, & \text{for passive dendrites} \\ \frac{r_a\left[(r+r_l-\omega_R^2 l\tau_D)r_l + (l+r_l\tau_D)\omega_R^2 l\right]}{r(r_l^2 + \omega_R^2 l^2)}, & \text{for quasi-active dendrites} \end{cases}$$

$$B = \begin{cases} \frac{\omega_R}{D}, & \text{for passive dendrites} \\ \frac{r_a\left[(l+r_l\tau_D)\omega_R r_l - (r+r_l-\omega_R^2 l\tau_D)\omega_R l\right]}{r(r_l^2 + \omega_R^2 l^2)}, & \text{for quasi-active dendrites} \end{cases}$$

In both the passive and quasi-active cases, the dispersion curves created look qualitatively the same as those shown in figure 4.10, where a stable upper branch meets an unstable lower branch at a minimum critical period, for all parameter regimes (for large τ_R). More interesting behaviour occurs when τ_R is just big enough to ensure no re-excitation in the system. Using the exponential synaptic weight kernel in equation (4.22) in this case, figure 4.13 shows oscillatory behaviour in the upper branch of the dispersion curve for quasi-active dendrites. Due to the bandpass nature of the membrane, the Green's function develops an oscillatory tail, which in turn leads to oscillatory phenomena in the dispersion curves. This behaviour becomes more pronounced as $r_l \to 0$, where r_l is the resistance in series with the inductance term l (see section 2.4.1). The linear stability of the travelling wave solutions in this dispersion curve is determined using the kinematic theory. As τ_R is decreased, this oscillatory behaviour is accentuated. However, when the refractory period becomes too small, the problem of divergent speeds is encountered again. The oscillations seen in the shape of the dispersion curve for quasi-active dendrites is apparent in dispersion curves generated by many excitable systems [106, 129]. Since some of the periodic travelling wave solutions in the upper branch of the dispersion curve are unstable, it can be postulated that the quasi-active elements of the membrane are tuning the travelling wave to specific frequencies.
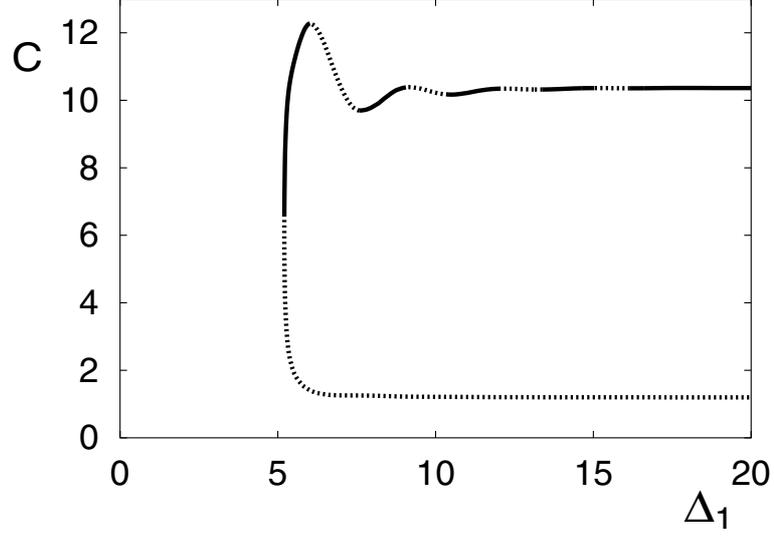
Figure 4.13 Dispersion curves for the exponential footprint in a system with quasi-active dendritic connections using equations (4.22) and (4.28). Parameter values are $\epsilon = 15$, $\xi = 0.2$, $r_l = 0.01$, $I_0 = 0$ and $\tau_R = 5$. All other parameter values $(D, \tau_D, r, r_a, \sigma)$ are unity. Solid (dotted) lines correspond to linearly stable (unstable) travelling waves according to the kinematic theory. Regions of instability appear along the upper branch due to the bandpass nature of the Green's function for quasi-active cables.

4.4.5 Multi-periodic travelling wave trains

Multiply periodic waves may be constructed in an analogous fashion to singly periodic ones with an appropriate choice of firing times. Instead of a wave train with a single period, consider a wave train with periods (interspike intervals) Δ_j, $j = 1, \ldots, n$. The set of n firing times for $T^m(x) \le t \le T^{m+n}(x)$ is defined by $T^m(x) = (m+kx)\Delta$, $T^{m+j}(x) = T^m(x) + d_j$ where $d_j = \sum_{i=1}^{j} \Delta_i$, $\Delta = \sum_{i=1}^{n} \Delta_i$, such that $T^m(x + \Delta) = T^m(x) + \Delta$. The speed of this wave is given by $c = 1/(k\Delta)$. For later convenience a traveling wave

with n distinct periods will be denoted by P_n. A generalisation of the previous analysis leads to a system of n equations (cf equation (4.5)).

$$V_\theta - V_{\text{reset}} e^{-\Delta_j} e^{\tau_R} = I_0 (1 - e^{-\Delta_j} e^{\tau_R}) + \epsilon \sum_{m \in \mathbb{Z}} a_j^{[n]} \left(\frac{2\pi m}{\Delta} \right) \widehat{W}(2\pi m k), \quad j = 1, \ldots, n,$$

(4.29)

where

$$a_j^{[n]}(\omega) = \sum_{l=1}^{n} \cos(\omega[d_j - d_l]) a^{[1]}(\omega) + \sum_{l=1}^{n} \sin(\omega[d_j - d_l]) b^{[1]}(\omega)$$

where $a^{[1]}(\omega)$, $b^{[1]}(\omega)$ are given in equations (4.28). A travelling wave with n distinct periods (which occur cyclically in the train) will be denoted by P_n. The stability of P_n is determined once again by a kinematic theory. For stability, it is required that $c'(\Delta_j) > 0$ for $j = 1, \ldots, n$.

As a first example consider a doubly-periodic travelling wave (periods Δ_1, Δ_2) in a continuum with α-function delay kernel and exponential synaptic delay kernel. The P_1 curve is scaled since $\Delta = \Delta_1 + \Delta_2$. Additionally, another curve is introduced which emerges from the "supernormal" stationary point in the P_1 curve. Note that the kinematic theory predicts a change in stability there (see figure 4.14). However, when τ_R is increased, these waves of supernormal speed are no longer possible since this "supernormal" stationary point disappears as discussed in section 4.4.3. In this system, the stability of the P_2 branch still depends upon the gradient because one of the two periods always remains on the section of the P_1 curve for $\Delta < \Delta_{\text{sup}}$, where Δ_{sup} denotes the period corresponding to the maximum of the "supernormal" speed stationary point in the P_1 curve. The other period moves along the upper branch for increasing $\Delta > \Delta_{\text{sup}}$. The travelling wave with two distinct periods bifurcates from a regular travelling wave by the drift of a spike time.

Doubly periodic travelling waves in the quasi-active dendrite case is more interesting. As with the case of α-functions, extra P_2 curves emerge from the local maxima in the P_1 curve, and the P_1 curve is scaled accordingly. This is plotted in figure 4.15. The stability of the P_2 branches is determined by its gradient as in the α-function case. In this
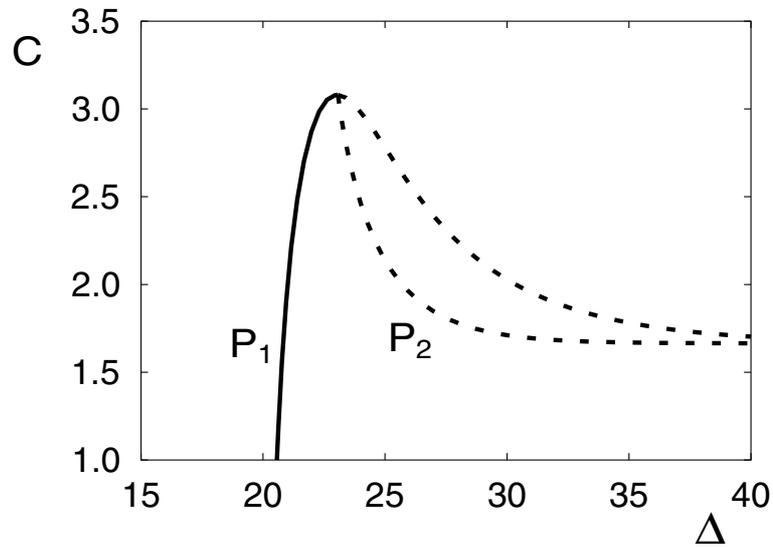
Figure 4.14 Equations (4.29) are solved to give P_1 and P_2 dispersion curves for a continuum of integrate-and-fire neurons interacting via α-functions and the exponential synaptic weight kernel. Parameter values are $\alpha = 0.5$, $\epsilon = 60$, $\sigma = 1$ and $I_0 = 0$. Solid (dashed) lines correspond to linearly stable (unstable) travelling waves according to the kinematic theory. Both the P_1 and P_2 upper branches become stable for large Δ.

system, higher order P_n travelling waves are possible, and must occur wherever there is a change in stability because the new solutions are bifurcations from previous solutions. It is already known that resonant behavior can subserve specific neuronal function. For example, hair cells of a vertebrate cochlear exhibit their maximal sensitivity at some non-zero frequency that depends on their location along the cochlear [31]. Moreover, rod photoreceptors of lower vertebrates have a receptive field that increases with the temporal frequency of the stimulus [144]. The analysis presented here further suggests that quasi-active membrane can have an important role to play in shaping the firing patterns of travelling waves.
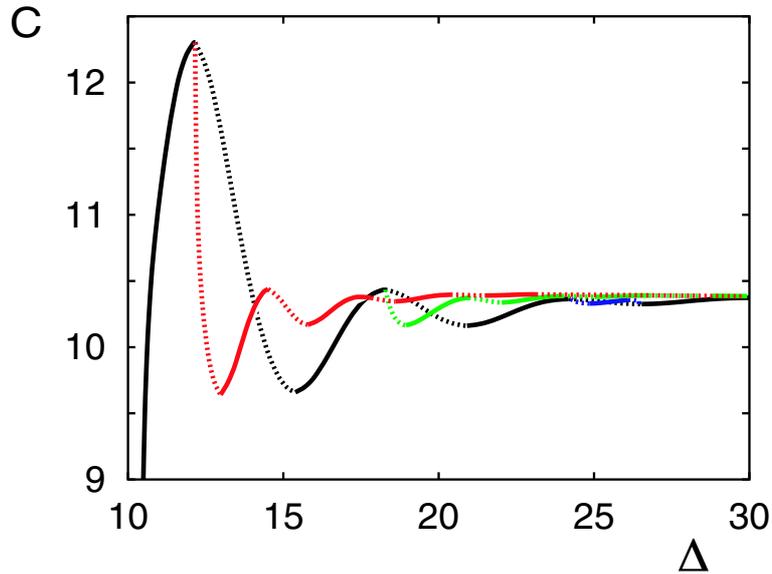
Figure 4.15 The dispersion curve for P_1 and P_2 travelling waves in the case of quasi-active dendrites with the exponential synaptic footprint generated using equations (4.29). The P_1 curve is black and the P_2 curves are given in the various colours. Parameter values for this diagram are identical to figure 4.13. Solid (dotted) lines correspond to stable (unstable) travelling waves according to the kinematic theory. Each local maximum produces an extra P_2 branch which exhibits oscillatory behaviour. The $P_1 \rightarrow P_2$ bifurcation occurs through the drift of the firing times of Δ_1-periodic firing neurons.

Rinzel and Maginu [129] suggested that solution forms composed of periods taken from the kinematically stable parts of the dispersion relation are stable (including combinations of different stable periods). If any combination of periods includes an unstable period, the resulting travelling wave will be unstable.

4.5   Recapitulation

Within a one-dimensional continuum of integrate-and-fire neurons, travelling wave solutions have been analysed. Using a variety of axo-dendritic connections, speed curves for a travelling pulse have been demonstrated to have qualitatively the same shape consisting of two coalescing branches with the uppermost (faster) being linearly stable. In the case of α-function delays, an extra bifurcation exists on the upper speed branch for sufficient axonal delays. Here, a smooth travelling pulse bifurcates into a lurching wave which recruits neurons into the wave in a saltatory manner. The extension of this material to cover periodic travelling waves elucidated the fact that an additional refractory variable needs to be introduced into the integrate-and-fire model in order that divergent speeds are not possible. The addition of this new parameter enabled the existence of periodic waves with "supernormal" speeds. A kinematic theory has been used to deduce the stability of these periodic waveforms, and a change of stability is predicted at the turning point of these "supernormal" stationary points. Here, bifurcations take place such that multi-periodic waves bifurcate from the P_1 curves by the drift of firing times.

Chapter 5

Biophysical models

Two currents have been explicitly considered so far in this thesis, namely sodium and potassium whose dynamics describe spike production. However, neural membrane dynamics are strongly dependent upon calcium ion (Ca^{2+}) conduction. These calcium currents are always activated by depolarisation and always act inwardly, with inactivation taking place on a much slower time-scale than that of the sodium current. It is unclear how many different types of calcium current exist throughout the dendritic structure and cell body, but calcium currents considered in this chapter will be of the low-threshold transient calcium current type; otherwise known as a T-type calcium current [92].

Intracellular recordings from thalamic cells *in vivo* and *in vitro* have indicated different types of firing which depend upon the activation of the T-type calcium current [82, 83]. Experiments performed on live animals are termed *in vivo*. All sensory systems pass information to the cortex by first going through the thalamus, and so this T-type calcium current may play an important part in information transmission [82, 83]. If sufficient hyperpolarisation occurs, the calcium current is activated upon depolarisation and a number of conventional sodium spikes will appear riding on the crest of some broad

voltage envelope for a suitable amount of input. This type of firing is called the *bursting mode*. It has been demonstrated that this mode of firing is a particularly effective means by which perigeniculate and thalamocortical neurons may influence each other [86]. If the calcium current is not activated, then any stimulus will either cause a sub-threshold depolarisation, or a sequence of conventional sodium spikes; known as the *tonic mode*. Recent interest in thalamic relay cells has increased since it became clear that the thalamus does not serve as a simple relay to the cortex [135].

As mentioned in section 2.2, the integrate-and-fire model of a neuron is quite a harsh reduction of the Hodgkin-Huxley model but still captures many of the essential elements of the experimental results. However, many neurons typically emit bursts of activity (a packet of spikes), instead of a single action potential, in response to some stimulus (similar to the bursts produced in section 3.1.2). There are a variety of different types of bursting phenomena in neural cells and Wang and Rinzel have presented a classification based upon geometrical analysis [154]. Many models have been developed to deal with bursting dynamics in neural cells, for example Hindmarsh-Rose [64, 65, 66, 67], Mulloney-Perkel [111, 119], Fan-Chay [50] and Wang-Rinzel [153] models to name a few. In many such models, a so-called T-current exists which provides a slow activation variable and its activation is dependent upon a certain voltage threshold. A neuron exhibits post-inhibitory rebound if it depolarises and fires an action potential when released from sustained inhibition. Many of these models share the same characteristics, and provide qualitatively similar results. However, as with most neural models, analytical progress for networks of these models can be cumbersome and unwieldy.

As demonstrated in the previous chapter, the integrate-and-fire model provides a solid basis for mathematical analysis. It will be convenient to take this model and somehow extend it to incorporate this slow-acting T-current. An approach along these lines has already been developed by Smith *et al.* [137, 138] and will be used throughout this chapter. This integrate-and-fire-or-burst model was analysed by Coombes *et al.* in

the case of a sinusoidally stimulated single neuron [30]. Travelling waves have not yet been studied with this model.

5.1 The integrate-and-fire-or-burst model

The integrate-and-fire-or-burst (IFB) model may be regarded as an integrate-and-fire model with the addition of a slow variable [137]. The cell can operate in either the tonic or bursting regime. In the tonic regime, a single spike response is evoked, whereas in the bursting regime a packet of spikes is emitted indicating that post-inhibitory rebound is having an effect. The current balance equation for the model is

$$C\frac{dV}{dt} = I_{app} - I_L - I_T, \tag{5.1}$$

where I_{app} represents an applied current and $I_L = g_L(V - V_L)$ is a leakage current with constant conductance g_L and leakage reversal potential V_L. The low-threshold Ca^{2+} current is given by $I_T = g_T h(V - V_T)\Theta(V - V_h)$ and the slow variable h has dynamics:

$$\frac{dh}{dt} = \begin{cases} -h/\tau_h^-, & V \geq V_h, \\ (1-h)/\tau_h^+, & V < V_h. \end{cases} \tag{5.2}$$

The slow variable h represents the de-inactivation of the low-threshold Ca^{2+} conductance, which involves T-type Ca^{2+} channels and produces the transmembrane current, I_T. Cells that are hyperpolarised and then released from inhibition can fire a burst of action potentials if there is a slow T-type Ca^{2+} current present. The heaviside step function in the I_T dynamics indicates this release from inhibition, and the slow dynamics of h ensure that this extra current persists and hence possible bursting phenomena may occur. This model exhibits excellent agreement with experimental results relating to sinusoidal stimulation ($I_{app} = I_0 + I_1 \cos(2\pi ft)$) and mode-locking (shown in figures 5.1 and 5.2 which are taken from Smith *et al.* [137]). The experimental results were obtained from intracellular recordings of thalamic relay cells of young cats (5–8 weeks old). For more details of the experimental preparation see Smith *et al.* [137].
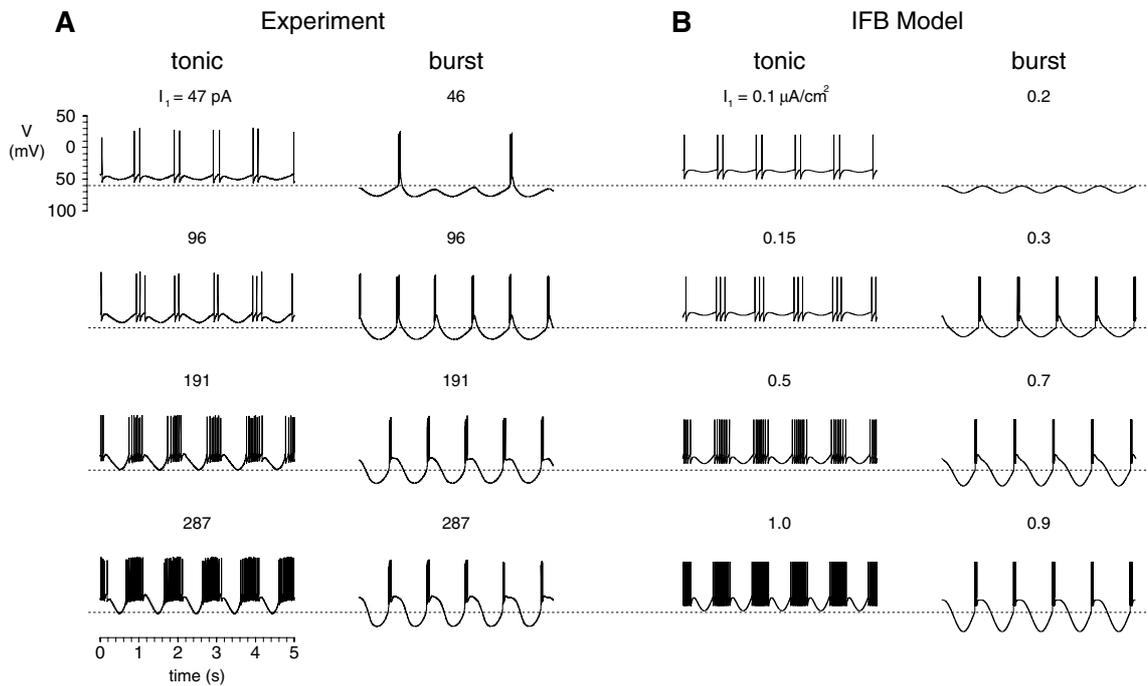
Figure 5.1 A: Whole cell recordings of a single relay neuron showing representative firing patterns during 1 Hz sinusoidal current injection over a range of modulation amplitudes (I_1). Tonic or burst responses are evoked depending on the value of the mean applied current (I_0), which is 335–498 pA for tonic firing and -4 to -136 pA for burst firing. During tonic responses, the average number of spikes/cycle increases as I_1 is increased for successive rows. Subharmonic burst responses are observed for low I_1, but otherwise 1 burst/cycle is observed. B: Behaviour of the IFB model. When stimulus parameters are varied in qualitative agreement with A, the IFB model reproduces many salient features of these responses. With depolarising mean applied current $(1.0 \ \mu A/cm^2 < I_0 < 1.2 \ \mu A/cm^2)$, the IFB model responds in tonic mode and the average number of spikes/cycle increases as I_1 is increased in successive rows. With hyperpolarising mean applied current $(I_0 = -0.05 \ \mu A/cm^2)$, the IFB model responds in burst mode. One burst/cycle is observed over a wide range of I_1. Table 5.1 gives the cellular parameter values unless otherwise stated. [Reproduced with kind permission from Smith [137].]
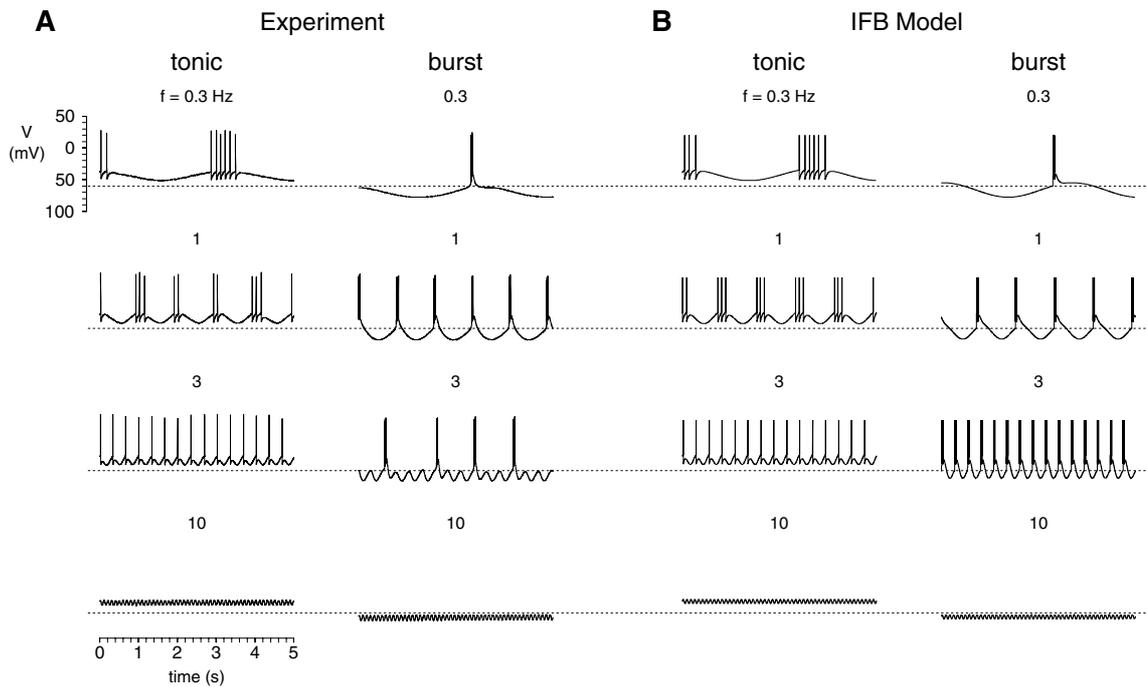
Figure 5.2 A: Intracellular recordings from the same neuron as in figure 5.1 showing responses to sinusoidal current injection over a range of frequencies (f) while the modulation amplitude is held constant ($I_1 = 96$ pA). Relay neuron responds in tonic mode when a depolarising mean applied current ($I_0 = 336$ pA) is applied and responds in burst mode when I_0 is hyperpolarising ($I_0 = -136$ pA). One burst/cycle is observed over a range of frequencies and subharmonic responses are observed as the cut-off frequency of 3Hz is approached. B: IFB model responses that reproduce these firing patterns. IFB model responds in tonic mode when the mean applied current is depolarising ($I_0 = 0.8$ µA/cm^2). Average number of spikes/cycle decreases as f is increased in successive rows; at 10Hz, the model no longer responds with tonic spikes. IFB model responds in burst mode when the mean applied current is hyperpolarising ($I_0 = -0.05$ µA/cm^2). One burst/cycle is observed over a wide range of f; bursts cease at f = 10 Hz, $I_1 = 0.2$ µA/cm^2. The cellular parameter values are given in table 5.1 unless otherwise stated. [Reproduced with kind permission from Smith [137].]

The usual action potential firing mechanism of the integrate-and-fire model is apparent with firing times defined by

$$T^n = \inf\{t \mid V(t) \geq V_\theta \; ; \; t \geq T^{n-1} + \tau_R\},$$

with subsequent discontinuous reset; $\lim_{\delta \to 0} V(T^n + \delta) = V_{\text{reset}}$. Equation (5.2) describes a process whereby the de-inactivation level of I_T relaxes to zero with time constant τ_h^- when $V \geq V_h$ and relaxes to unity with time constant τ_h^+ when $V < V_h$. Hence, sufficient hyperpolarization leads to increasing values of h, representing de-inactivation of I_T. The integrate-and-fire-or-burst dynamics depend strongly on the two thresholds V_h and V_θ, responsible for the activation of burst and tonic spiking respectively. In previous work, Smith *et al.* chose the threshold values, V_h, V_θ, V_{reset}, the time-scales, $\tau_h^\pm$, reversal potentials, V_L, V_T, leakage conductance, g_L and membrane capacitance, C, to fit *in vitro* intracellular recordings of relay neuron responses to sinusoidal current injection (see table 5.1). All intrinsic and applied transmembrane currents are given in units of $\mu A/cm^2$. Of course, in order that the bursting mechanism be represented in this model, the external drive I_{app} must be of a small enough magnitude, since large values of the applied external drive would result in tonic firing. The V_h threshold for activating the T-type calcium current would never be crossed, resulting in ordinary integrate-and-fire dynamics. Ensuring that the voltage in the steady state of equation (5.1) in the absence of the low threshold T-current is not greater than the firing threshold V_θ leads to the condition $I_{\text{app}} < (V_\theta - V_L)g_L = I_{\text{max}}$. A simple bound such that there is enough current driving the system in order that the potential can cross the $V = V_h$ boundary from below is found by considering the steady state of equation (5.1) in the absence of synaptic coupling. This is given by $I_{\text{app}} > g_L(V_h - V_L) = I_{\text{min}}$.

It is useful to rewrite the inactivation and de-inactivation dynamics in the form

$$\tau_h(V)\frac{dh}{dt} = -h + h_\infty(V), \tag{5.3}$$

where $h_\infty(V) = \Theta(V_h - V)$ and $\tau_h(V) = \tau_h^- \Theta(V - V_h) + \tau_h^+ \Theta(V_h - V)$. The form of this equation is reminiscent of a post-inhibitory rebound current described by Wang

Parameter	Value	Unit
Cellular parameters		
V_θ	-35	mV
V_L	-65	mV
C	2	$\mu F/cm^2$
g_L	0.035	mS/cm^2
V_{reset}	-50	mV
V_h	-60	mV
V_T	120	mV
τ_h^-	20	ms
τ_h^+	100	ms
g_T	0.07	mS/cm^2
Stimulus parameters		
I_0	-0.67–2.67	$\mu A/cm^2$
I_1	0–1.33	$\mu A/cm^2$
f	0.1–100	Hz

Table 5.1 Standard cellular parameter values for the integrate-and-fire-or-burst model, obtained from fits with experimental data [137].

and Rinzel [153]. In agreement with voltage-clamp experiments, the low-threshold Ca^{2+} current in their model is given by $I_T = g_T m_\infty^3(V)h(V - V_T)$ with "smooth" equilibrium activation $m_\infty(V)$ and inactivation $h_\infty(V)$ functions,

$$
\begin{aligned}
h_\infty(V) &= \frac{1}{1 + \exp(\beta_h(V - V_h))}, \\
m_\infty(V) &= \frac{1}{1 + \exp(-\beta_m(V - V_h + \epsilon))},
\end{aligned}
$$

for some appropriate constants β_m, β_h and ϵ; and h satisfying (5.3) under the replacement $\tau_h(V) \to h_\infty(V) \exp((V+a)/b)$ (for constants a and b) (see the equations given in (5.7) for the exact form). The smooth activation function $m_\infty(V)$ may be considered as the asymptotic value of a fast activation variable. In the limit $\beta_h \to \infty$, the sigmoidal function $h_\infty(V)$ tends to a step function, so that $h_\infty(V) = \Theta(V_h - V)$. As β_m tends to infinity and ϵ tends to zero, $m_\infty(V) = \Theta(V - V_h)$. Hence, the two models may be identified in the limit $\beta_h, \beta_m \to \infty$, $\epsilon \to 0$ under the replacement $\tau_h(V) \to \tau_h^-\Theta(V - V_h) + \tau_h^+\Theta(V_h - V)$.

For mathematical simplicity, smooth activation $m_\infty(V)$ and inactivation $h_\infty(V)$ functions are avoided and instead, the original integrate-and-fire-or-burst model with piecewise constant activation and inactivation functions are considered. The shunting term, $(V - V_T)$, of the low-threshold Ca^{2+} current is eliminated by assuming $V_T \gg V$. This does not lead to any qualitatively different behaviour to the model with shunting. With these approximations, the slow current I_T takes the form $I_T = -g_T V_T h\Theta(V - V_h)$. It is now convenient to rewrite the integrate-and-fire-or-burst model with the introduction of the relative voltage $v = V - V_L$ and the parameters $g = g_T V_T/C$, $\tau = C/g_L$. Hence, $v_X = V_X - V_L$, where $X \in \{\theta, \text{reset}, h\}$, leading to the re-scaled equations

$$\dot{v} = -\frac{v}{\tau} + gh\Theta(v - v_h) + I(t),$$
$$\tau_h(v)\dot{h} = h_\infty(v) - h,$$

where $I(t) = I_{app}/C$, $h_\infty(v) = \Theta(v_h - v)$ and $\tau_h(v) = \tau_h^-\Theta(v - v_h) + \tau_h^+\Theta(v_h - v)$. Apart from the firing times, there are two types of event which play an important role in the dynamics of this system; namely the times at which v crosses v_h from above or below. At these times the dynamics for h undergoes a switch in behavior (see figure 5.3). If the potential does not cross the lower v_h threshold, then tonic firing occurs.

Throughout this thesis, the membrane time constant has been chosen to be unity. However, timescales have been recorded from 1-100 ms depending upon both the type of neuron and the conditions of the neuron. Neurons which specialise in high-fidelity
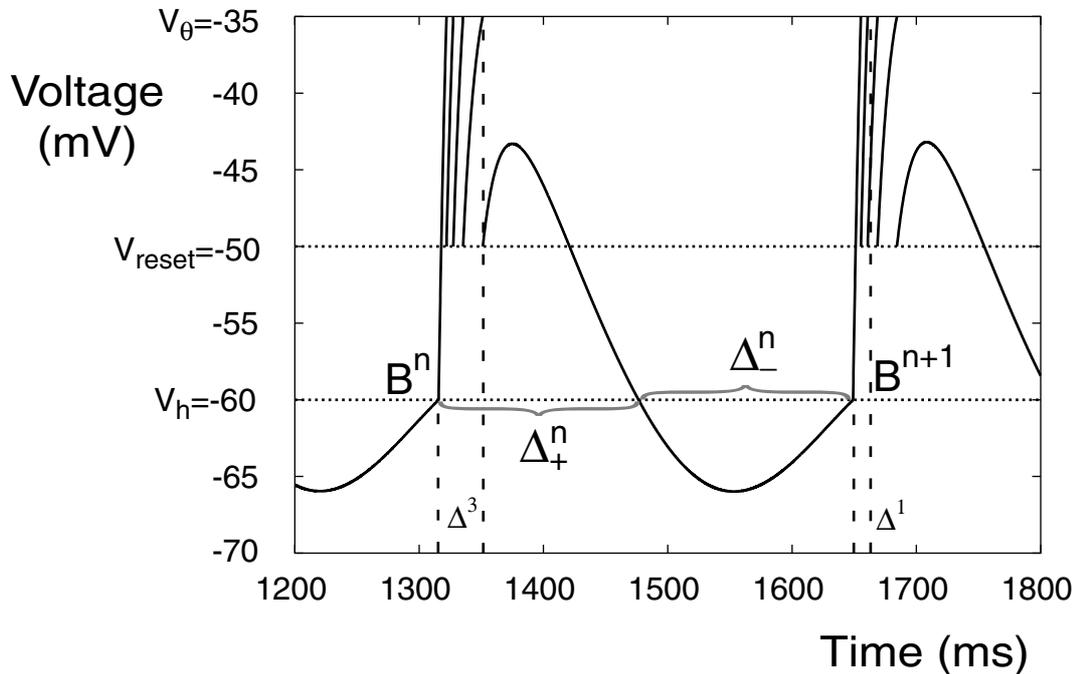
Figure 5.3 The integrate-and-fire-or-burst model of a neuron periodically stimulated by a sinusoid: $I_{app} = 0.1 + 0.25 \cos(6\pi x/1000)$. All other parameter values are given in table 5.1. See the text for an explanation of the various labels.

temporal information have small time constants and cortical neurons have demonstrated time constants of 100 ms or longer for *in vitro* experiments. Cortical cells in live animals (*in vivo*) typically demonstrate time constants between 10 and 20 ms. Since there is such a wide range of values for this constant, and the parameter values of Smith *et al.* indicate a membrane time constant of approximately 57 ms, the analysis will henceforth include this parameter.

Not only does the integrate-and-fire-or-burst model of a neuron provide excellent agreement with experimental results, but is analytically tractable. Network behaviour of

this more biophysical model will be considered in this chapter. The mathematical analysis of a pair of coupled oscillators and travelling waves in the continuum will be addressed. In particular, the study of travelling waves has not been considered previously. In order to generate any rhythm of post-inhibitory rebound spikes, the neurons must be connected inhibitorily, since excitatory connections lead to "normal" integrate-and-fire spikes and the results from the previous chapter carry through (the h current is never switched on).

Denote the number of spikes within a cluster by p. Then, it is convenient to write the set of times for which $v(t)$ crosses through v_h from below (de-inactivation of the low-threshold Ca^{2+} current) as

$$B^n = \inf\{t \mid v(t) \geq v_h, \dot{v} > 0 \; ; \; t \geq B^{n-1}\}.$$

Using this notation, the nth firing event can be written as

$$T^n = B^{\left[\frac{n}{p}\right]} + \Delta^{n(p)}\left(\left[\frac{n}{p}\right]\right), \qquad n(p) = n \bmod p, \tag{5.4}$$

where $[.]$ denotes the integer part and $n \in \mathbb{Z}$. Here, a firing event is decomposed using inter- and intra-cluster firing times. The notation $n(p) = n \bmod p$ is introduced to conveniently label each of the p spikes within a cluster, whilst the index $[n/p]$ keeps track of the cluster to which the set of p spikes belongs. The times $B^{[n/p]}$ signal the onset of a clustered firing pattern, whilst $T^0([n/p])$ signifies the first firing event within a cluster (relative to the start of the clustered firing pattern) and $T^1([n/p]), T^2([n/p]), \ldots, T^{p-1}([n/p])$ signal subsequent intra-cluster firing events. The associated value of $h(t)$ at the time $B^{[n/p]}$ is denoted $h^{[n/p]}$. The evolution of $h^{[n/p]}$ over a cycle is easily calculated in terms of the time spent above and below $v = v_h$.

$$h_{\left[\frac{n}{p}\right]+1} = h_{\left[\frac{n}{p}\right]}\exp\left(-\frac{\Delta_+^{\left[\frac{n}{p}\right]}}{\tau_h^-} - \frac{\Delta_-^{\left[\frac{n}{p}\right]}}{\tau_h^+}\right) + 1 - \exp\left(-\frac{\Delta_-^{\left[\frac{n}{p}\right]}}{\tau_h^+}\right). \tag{5.5}$$

where $\Delta_-^{[n/p]}$ ($\Delta_+^{[n/p]}$) is the time spent below (above) the $v = v_h$ threshold. The crossing times $B^{[n/p]}$ then satisfy $B^{[n/p]+1} = B^{[n/p]} + \Delta^{[n/p]}$ where $\Delta^{[n/p]} = \Delta_+^{[n/p]} + \Delta_-^{[n/p]}$. Having established a mathematical framework for analysing integrate-and-fire-or-burst neurons,
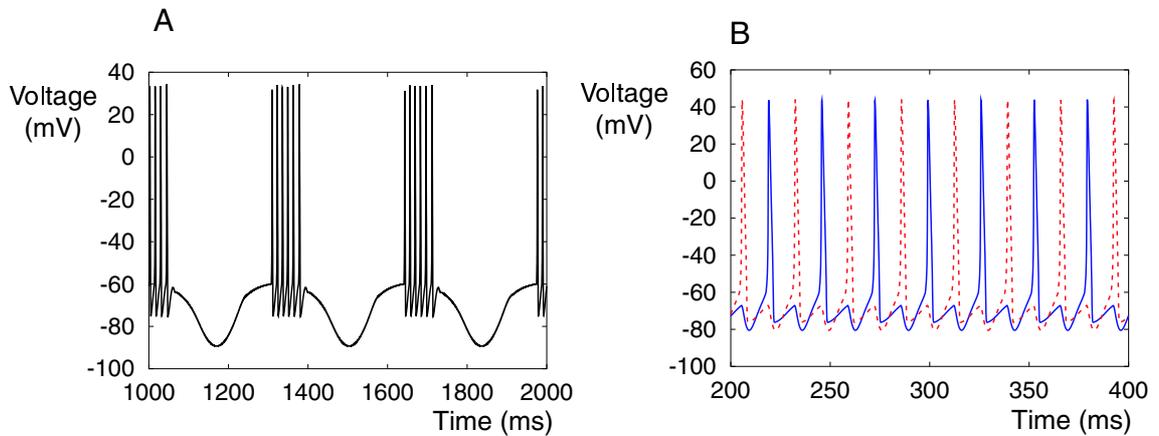
Figure 5.4 A: The sinusoidally driven Hodgkin-Huxley neuron (equations (2.1) and (2.2)) augmented with a T-current identical to that presented in the integrate-and-fire-or-burst model. The stimulus is given by $-0.5 + 10\cos(6\pi x/1000)$. B: Two Hodgkin-Huxley neurons augmented with a T-current identical to that presented in the integrate-and-fire-or-burst model coupled via α-function synaptic responses. The Hodgkin-Huxley parameter values are given in table 2.1.

it is useful to gain insight into a discrete network of these neurons before progressing onto travelling waves in the one-dimensional continuum.

5.2 Discrete integrate-and-fire-or-burst networks

It is interesting to consider the effect of post-inhibitory rebound on the full Hodgkin-Huxley model (equations (2.2)). The Hodgkin-Huxley equations are augmented with the same type of slow calcium T-current which is present in the integrate-and-fire-or-burst model.

107

This adapted Hodgkin-Huxley neuron is sinusoidally driven (figure 5.4(A)) and a packet of action potentials can be seen riding the crest of the sinusoid (cf figure 2.3 and also figure 4 in [30]). In figure 5.4(B), two Hodgkin-Huxley neurons are inhibitorily coupled together using α-function synaptic delay kernels and a half-centre oscillator evolves. This rhythm *only* occurs because the oscillators are coupled.

Qualitatively similar results are obtained with the reduced Hodgkin-Huxley model given by equations (2.6) augmented with the additional calcium current given by I_T, and the Wang-Rinzel model, which is defined as by the equations [153]

$$C\frac{dV_i}{dt} = -g_{pir}m_\infty^3(V_i)h_i(V_i - V_{pir}) - g_L(V_i - V_L) - g_{syn}s_{ji}(V_i - V_{syn}), \quad \text{(5.6a)}$$

$$\frac{dh_i}{dt} = \phi[h_\infty(V_i) - h_i]/\tau_h(V_i), \quad \text{(5.6b)}$$

where s_{ji} is the post-synaptic conductance (fraction of the maximum g_{syn}) in cell i due to the activity in cell j. This conductance is an instantaneous, sigmoid function of the pre-synaptic voltage with a threshold θ_{syn}

$$s_{ji} = S_\infty(V_j) = \frac{1}{1 + exp[-(V_j - \theta_{syn})/k_{syn}]}.$$

The voltage dependent gating functions are given by

$$m_\infty(V) = \frac{1}{1 + exp[-(V + 65)/7.8]}, \quad \text{(5.7a)}$$

$$h_\infty(V) = \frac{1}{1 + exp[(V + 81)/11]}, \quad \text{(5.7b)}$$

$$\tau_h(V) = h_\infty(V)exp[(V + 162.3)/17.8], \quad \text{(5.7c)}$$

and the parameter values are given by $k_{syn} = 2$, $g_{syn} = 0.3$ mS/cm^2, $C = 1$ μF/cm^2, $g_L = 0.1$ mS/cm^2 and reversal potentials (in mV) $V_{pir} = 120$, $V_L = -60$, $V_{syn} = -80$. The factor ϕ scales the kinetics of h and is taken to be 3. This model gives a complete contrast to the integrate-and-fire-or-burst model since all functions are smooth. This model considers the envelope of the burst (as do the Morris-Lecar equations which were originally designed to describe muscle fibre [110]). There is no discontinuous reset when a neuron reaches a pre-determined threshold. The method of synaptic interaction in
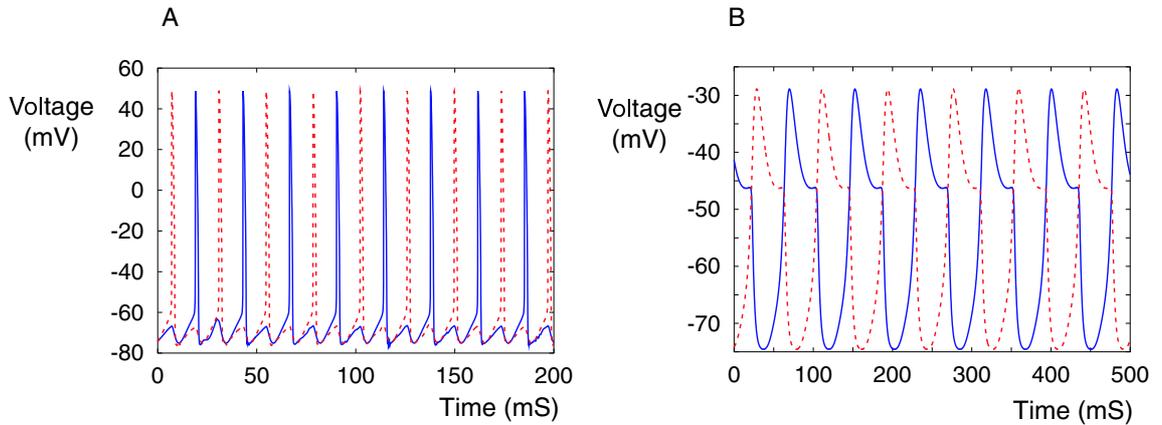
Figure 5.5 A: Half-centre oscillator produced by two synaptically interacting reduced Hodgkin-Huxley neurons (equations (2.6)) neurons with synaptic interaction governed by α-functions and an imposed post-inhibitory rebound current supplied by I_T. B: Two Wang-Rinzel model neurons (equations (5.6)) interacting to produce a half-centre oscillator. The results presented here are qualitatively similar to those created using the augmented Hodgkin-Huxley model (see figure 5.4).

the Wang-Rinzel model is different to synaptic interactions considered previously in this thesis. Instead, it is supposed that the neurons interact for the duration that one neuron is above this threshold. This is similar to fast threshold modulation which was described in section 2.3. The half-centre oscillators produced by these two different models are reproduced in figure 5.5. Half-centre oscillators are the primary method of locomotion and other rhythmic motor behaviour [21, 99, 100].

Now, consider a network of N integrate-and-fire-or-burst neurons and focus on the class of periodic solutions, such that $(v_i(t + \Delta), h_i(t + \Delta)) = (v_i(t), h_i(t))$ in which $p \in \mathbb{Z}$ spikes are fired within a period Δ and $i = 1, \dots, N$. In this case the crossing times

B^n satisfy $B^{n+1} = B^n + \Delta$, and for neurons indexed $i, i = 1, \ldots, N$,

$$B_i^n = n\Delta + \Delta_B + \Delta_i,$$

where Δ_i is the phase difference of the clustered spike packet of neuron i, and Δ_B is the time shift of the onset of the bursting packet with respect to the start of the considered period. The firing times of spikes within a cluster are assumed to have the form

$$T_i^n = B_i^n + \Delta^{n(p)},$$

for all n, where $\Delta^0, \ldots, \Delta^{p-1}$ denote the collection of firing times. The discrete network of integrate-and-fire-or-burst neurons is defined as

$$
\begin{aligned}
\frac{dv_i}{dt} &= -\frac{v_i}{\tau} + gh_i\Theta(v_i - v_h) + I_{inj} + \epsilon \sum_{j=1}^{N} W_{ij} \sum_{m \in \mathbb{Z}} \eta(t - T_j^m), &\text{(5.8a)} \\
\tau_h(v)\frac{h_i}{dt} &= h_\infty(v) - h_i, &\text{(5.8b)}
\end{aligned}
$$

for $i = 1, \ldots, N$ with $\eta(t)$ defined in equation (2.10). Throughout this chapter, synaptic interaction occurs via α-functions for mathematical simplicity.

Consider two synaptically coupled neurons defined by equation (5.8). Simulations of the equations show that a half-centre oscillator evolves (see figure 5.6). This is consistent with the other models which exhibit post-inhibitory rebound shown in figures 5.4 and 5.5. However, the integrate-and-fire-or-burst model can be solved exactly and precise analytical statements can be made about periodic travelling waves in more biophysical neural systems.

Numerical simulations of the integrate-and-fire-or-burst neuron model under sinusoidal forcing predict responses which are typically $p{:}q$ mode-locked solutions [30]. This means that an oscillator fires a packet of p spikes in q multiples of the fundamental period of the sinusoidal signal. For simplicity, further discussion is restricted to the case of $p{:}1$ mode-locked solutions, where the de-inactivation variable h is 1:1 frequency locked to the stimulus, since these define the dominant responses to sinusoidal stimulation. The
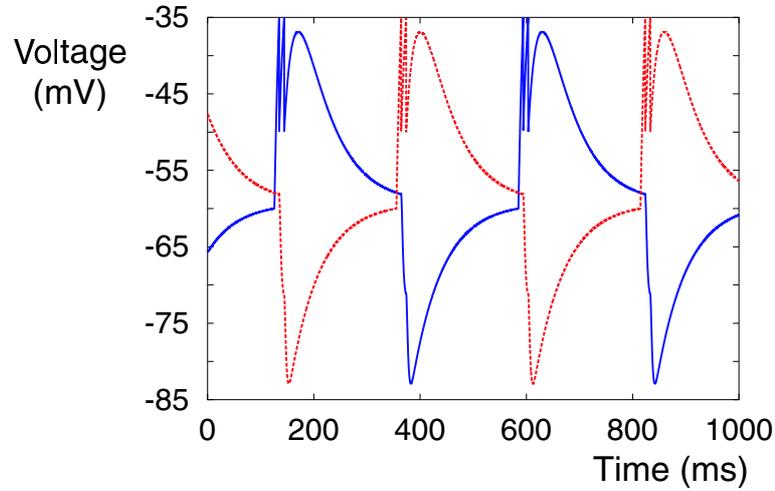
Figure 5.6 Half-centre oscillator produced by two synaptically interacting integrate-and-fire-or-burst neurons. Coupling strength $\epsilon = -30$ and $\alpha = 0.5$, and all other parameter values as in table 5.1. This result is in qualitative agreement with that produced with the augmented Hodgkin-Huxley equations (see figure 5.4).

generalisation to $p{:}q$ type states is straightforward, and for clarity and brevity, will not be pursued here.

Denoting the time spent on the portion of a periodic orbit with $v < v_h$ as Δ_- and the time spent on the orbit with $v > v_h$ as Δ_+ write $\Delta = \Delta_+ + \Delta_-$. More usefully the assumption of a $p{:}1$ periodic orbit allows us to determine $h^{[n/p]}$ using the constraint $h^{[n/p]} = h^{[n/p]+1} = \widetilde{h}$. Using (5.5),

$$\widetilde{h} = \frac{1 - e^{-\Delta_-/\tau_h^+}}{1 - e^{-\Delta_+/\tau_h^-}e^{-\Delta_-/\tau_h^+}}.$$

Hence, $h(t)$ can be written as

$$h(t) = \widetilde{h}e^{-(t-B^n)/\tau_h^-} \quad \text{for } t \in [B^n, B^n + \Delta_+).$$

There are three distinct sections of the voltage path and they have to be considered separately. Hence, equations (5.8) need to be integrated over the regions which define threshold crossings; namely, $[B^n, B^n + \Delta^0)$, $[B^n + \Delta^j, B^n + \Delta^{j+1})$, $[B^n + \Delta^{p-1}, B^n + \Delta_+)$ and $[B^n + \Delta_+, B^n + \Delta)$, where $j = 0, \ldots, p - 2$. It is useful to consider all times relative to B^n, without loss of generality, and thus take $\Delta_B = 0$. The system is integrated over the region $[B^n + y, B^n + z)$ to give,

$$v_i(B^n + z) - v_i(B^n + y)e^{(y-z)/\tau} = \mathrm{PIR}_{\mathrm{disc}}(y, z) + I\tau(1 - e^{(y-z)/\tau}) + \mathrm{SYN}_{\mathrm{disc}}(y, z), \quad (5.9)$$

with

$$
\begin{aligned}
\mathrm{PIR}_{\mathrm{disc}}(y, z) &= g\widetilde{h}\Theta(v - v_h)e^{-z/\tau}\left(e^{z/\tau_0} - e^{y/\tau_0}\right)\tau_0, \\
\mathrm{SYN}_{\mathrm{disc}}(y, z) &= \epsilon \sum_{j=1}^{N} W_{ij} K_j^{\mathrm{disc}}(y, z),
\end{aligned}
$$

where

$$K_j^{\mathrm{disc}}(y, z) = e^{-z/\tau} \int_y^z e^{u/\tau} \sum_{k \in \mathbb{Z}} \sum_{m=0}^{p-1} J(u + k\Delta - \Delta_m + \Delta_i - \Delta_j)\, du,$$

and $1/\tau_0 = 1/\tau - 1/\tau_h^-$. This system of equations produces self-consistent solutions for the firing times along with the periods Δ_+ and Δ (and hence Δ_-).

For analytical simplicity, two neurons are considered. In addition, only a single action potential is produced by each neuron in each bursting packet. The more complex case of multiple spikes is a simple extension and each additional spike considered merely introduces an additional equation to determine the subsequent firing time. The refractory period τ_R will not be included in the analysis for clarity, and indeed it has no effect on these pulse networks (provided it is smaller than the period of inhibition). The self-consistent solutions of equations (5.9) for the periods in the system generated by this mathematical treatment are plotted in figure 5.7. It is clear that critical values of the coupling strength and external drive exist such that a half-centre oscillation occurs. Stability of the solutions will not be considered, but direct numerical simulations suggest that the mode with the smaller period is stable.
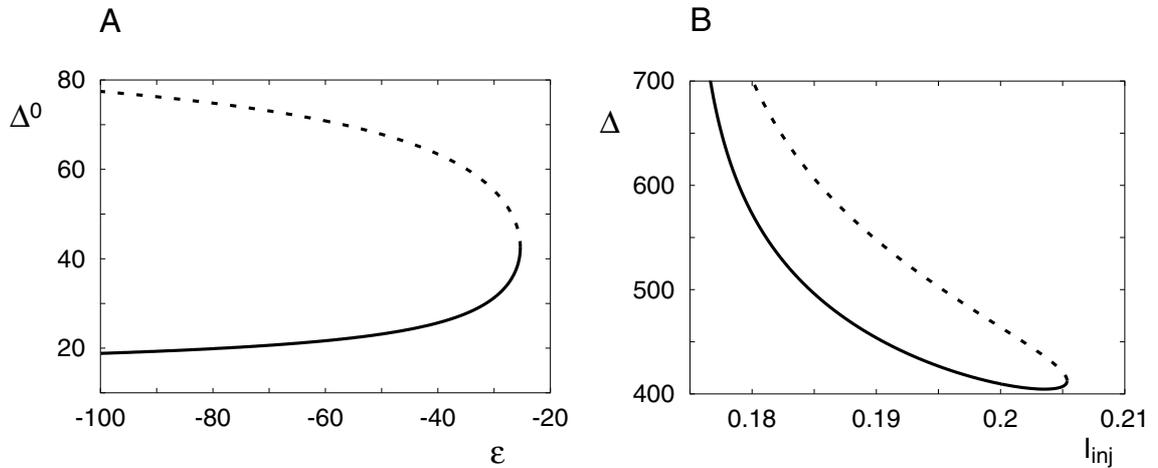
Figure 5.7 A: The self-consistent solution of equations (5.9) for Δ^0 (the relative firing period) for the IFB half-centre oscillator plotted against ϵ. $(I_{inj} = 0.2)$ B: The self-consistent solution of equations (5.9) for Δ (the total firing period) for the IFB half-centre oscillator plotted against I_{inj} ($\epsilon = -30$). In both diagrams, a critical value for the considered parameter exists such that the half-centre oscillator does not exist for larger values. In both diagrams, direct numerical simulations indicate that the lower branch is stable (solid) and the upper branch in unstable (dashed). Parameter values are as in table 5.1 except $\epsilon = -30$, $\alpha = 0.5$, $\tau_h^- = 30$, $\tau_h^+ = 200$ and $g_T = 0.05$ to ensure only a single pulse in each burst.

By considering how the limit point in figure 5.7(A) moves as I_{inj} varies, it is possible to create the existence border of a half-centre oscillator in the $\epsilon - I_{inj}$ plane. Existence of the half-centre oscillator is only apparent for a small window in the drive (see figure 5.8). If the drive is too small $(I_{inj} < I_{min})$, then the voltage will never cross the v_h boundary from below and therefore the T-current will not activate. If the drive is too large $(I_{inj} > I_{max})$, then the voltage will not be pushed below the v_h threshold and/or repetitive
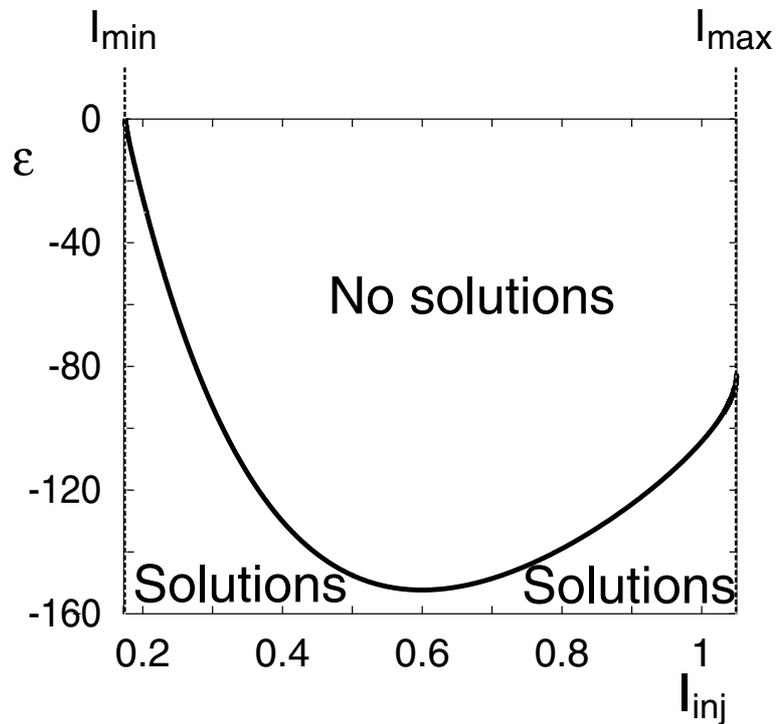
Figure 5.8 Two parameter boundary curve for the integrate-and-fire-or-burst half-centre oscillator. A limit point is taken from figure 5.7 and continued with respect to both parameters. Oscillations exist providing the parameter regime lies below the curve. For values of the injected current greater I_{max}, the half-centre oscillator ceases to exist. Instead, complex firing (where there is a mixture of tonic and burst spikes), or oscillator death can occur. For $I_{inj} < I_{min}$ there is insufficient external drive to ensure the potential crosses the V_h threshold from below.

firings in the oscillatory regime will be created with a mixture of tonic and burst spike. Oscillator death can occur with strong external drive (depending on the initial conditions of each neuron), where, as mentioned in chapter 3, one neuron suppresses the activity of the other. This existence boundary has been verified through numerical simulation.

In simulations, the parameter values can be adjusted in order that a single action potential is released per period. In order to create a single spike, the following parameter values are used: $\tau_h^- = 30, \tau_h^+ = 200, g_T = 0.05$ and all other parameter values are given in table 5.1. A travelling pulse (rather than a travelling packet of spikes) in a continuum will be analysed in the following section.

5.3   An integrate-and-fire-or-burst continuum

The thalamus is typically modelled as two layers of neurons: the thalamocortical cells and the reticularis cells. The membrane is structured such that thalamocortical cells (excitatory) project to the cortex and to reticularis cells, and that reticularis cells (inhibitory) project to thalamocortical cells as well as other reticularis cells. The T-current is the dominant current. Mathematical analysis has been used to study travelling pulses and waves in one-dimensional thalamic models [24, 56, 58, 130, 141]. Reduced models of the thalamus were studied using averaging theory [24] and singular perturbation theory [141]. Both smooth waves and lurching solutions have been found in the one-dimensional continuum limit. Golomb and Ermentrout have recently used a simple integrate-and-fire model with discrete communication delays (see chapter 4) to study the difference between smooth and lurching waves [57]. It was seen in chapter 4 that for increasing delays, smooth waves become unstable in favour of lurching waves. A coupling "gap" in the work of Rinzel *et al.* [130] essentially allows cells to escape from inhibition sooner so that this "delay" is shorter and smooth waves result. The narrower the gap, the slower the propagation of the travelling wave. If the gap is too narrow, then smooth propagation will be impossible. *A priori* estimates on the width of this gap were calculated for a different, but related, model by Terman *et al.* [141]. The reason for requiring this minimum gap is perhaps easiest to visualise if one considers the voltage profile of a neuron. A smooth wave can only propagate if a neuron is not inhibited by its immediate neighbours. As such, a gap

is needed in the synaptic weight kernel in order that communication between cells does not occur in this neighbourhood.

Consider a travelling wave in the one-dimensional continuum of integrate-and-fire-or-burst neurons. The firing time ansatz in this case is given by

$$T^{[\frac{n}{p}]}(x) = \left[\frac{n}{p}\right]\Delta + \Delta^{n(p)} + x/c.$$

In this continuous case, the spatial versions of equations (5.9) are produced when the synaptic input to each neuron is given by I_{inj} and equation (4.2). However, due to the nature of the problem, calculations are eased by shifting the origin of time to where the potential crosses the threshold $v = v_h$ from above rather than from below. In the analytical equations, it is assumed that all neurons start from rest (above v_h) and are subsequently pushed below the v_h threshold via synaptic interactions with the other neurons. In the travelling wave framework $\chi = ct - x$, this system of equations is represented as

$$v(z) - v(y)e^{(y-z)/(c\tau)} = \tau I \left(1 - e^{(y-z)/(c\tau)}\right) + PIR_{cont}(y, z) + SYN(y, z), \qquad (5.10)$$

with

$$PIR_{cont}(y, z) = g(1 - e^{-\Delta_-/\tau_h^+})\Theta(y - c\Delta_-)e^{-z/(c\tau)}e^{\Delta_-/\tau_h^-}\left(e^{-z/(c\tau_0)} - e^{-\Delta_-/\tau_0}\right)\tau_0,$$

$$SYN(y, z) = \frac{\epsilon e^{-z/(c\tau)}}{c}\int_{-\infty}^{\infty} W(v)K^{cont}(v)\,dv,$$

where

$$K^{cont}(v) = \int_y^z e^{\chi/(c\tau)}\sum_{k\in\mathbb{Z}}\sum_{m=0}^{p-1} J\left(\frac{\chi + v}{c} + k\Delta - \Delta^m\right)\,d\chi,$$

and the various integration limits are given by the following intervals

$$(y, z) = \begin{cases} (-\infty, 0], (0, c\Delta_-], (c\Delta_-, c\Delta^0] \\ (c\Delta^j, c\Delta^{j+1}] \text{ for } j = 0, \ldots, p - 2 \\ (c\Delta^p, \Delta_*], (\Delta_*, \Delta_{**}], (\Delta_{**}, \infty] \end{cases}$$

Equations (5.10) then define self-consistent equations for the total period Δ, the time spent below the v_h threshold prior to a bursting packet Δ_-, the times of the p spikes

within the bursting packet Δ^j, for $j = 0, \ldots, p-1$ and the wave speed c. In addition, the periods Δ_* and Δ_{**} are determined self-consistently and these correspond to a subsequent ν_h threshold crossing which does not lead to rebound bursting (see figure 5.10). There may be many such threshold crossings, but only one is illustrated here, motivated by the necessity of a gap in the synaptic weight kernel.

For simplicity, travelling pulse solutions will be calculated in this network. The extension to propagating packets of action potentials purely involves solving more equations simultaneously to determine the self-consistent solutions of the periods in the system. In fact, for each extra action potential considered in the cluster, an additional equation describing the additional ν_θ threshold crossing will be required. Simulations of the network show that the speed of the pulse does not vary greatly if more action potentials are introduced into the bursting packet, and that the speed of the pulse dominates any travelling burst for the same parameter values.

The synaptic weight kernel in this section will be the off-centre square footprint given by

$$W(x) = \frac{1}{4\sigma} \left[\Theta \left(\sigma - |x - \Gamma| \right) + \Theta \left(\sigma - |x + \Gamma| \right) \right],$$

where Γ defines the extent to which the kernel is off-centred, and σ is the usual spatial scaling (see figure 5.9). As $\Gamma \to 0$, the off-centre synaptic weight kernel becomes on-centre and is a scaled version of equation (4.3).

The precise wave profile for the travelling pulse solution is shown in figure 5.10. Only one extra ν_h threshold crossing occurs. This is due to the fact that there is a single pulse propagating in the system and an off-centre synaptic weight kernel. Each half of the footprint leads to a ν_h threshold crossing. This voltage profile was seen in direct numerical simulations.

The self-consistent solution for the speed of a travelling pulse determined from equation (5.10) is plotted in figure 5.11. It is interesting to note that the speed of the
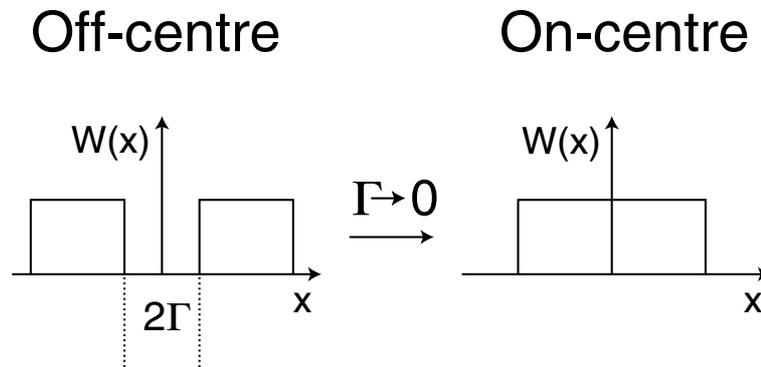
Figure 5.9 The synaptic weight kernel given in terms of a square wave. An off-centre synaptic footprint with gap of 2Γ is shown. As the gap parameter Γ is decreased, the synaptic footprint becomes on-centre.

pulse increases as the inhibitory coupling strength ϵ becomes *weaker*. This is because it takes less time for the neuron to reach the ν_h threshold from below. There exists a critical coupling strength ϵ_{trav} such that a travelling pulse solution exists in this network. For more positive values of the coupling strength, the synaptic input obtained by each neuron is insufficient to hyperpolarise the neuron for a long enough duration. Hence, the slow calcium T-current is not strong enough to cause post-inhibitory rebound. Another interesting point to note is that only a single speed exists for travelling pulses in this regime. This is consistent with other observations [24, 56]. Direct numerical simulations of the network indicate that this travelling pulse solution is stable. However, a second critical value of the coupling strength ϵ exists. Whenever the coupling is *greater* (more negative) than this critical value then the post-inhibitory rebound current caused by the second ν_h crossing is too strong and causes a second action potential to be released. This is easily visualised from figure 5.10. The point A is pushed lower due to the strength of inhibitory connections, and as a result, point B moves upwards. This point will eventually

118
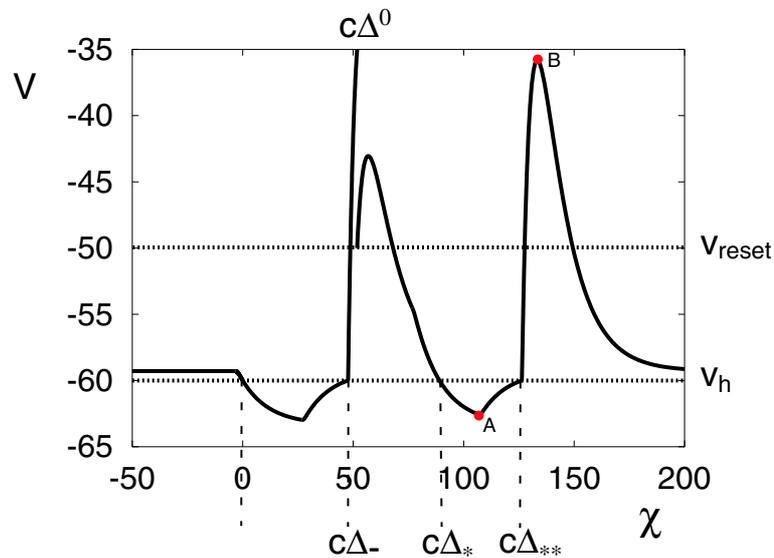
Figure 5.10 The theoretical pulse profile generated by equations (5.10). Parameter values are given in table 5.1 except $\tau_h^- = 200$ and $g_T = 0.06$. The self-consistent solutions for $\epsilon = -40$ with synaptic weight parameters $\Gamma = 40$ and $\sigma = 15$ are given by $\Delta_- = 224.05$, $c = 0.2128$, $\Delta^0 = 243.32$, $\Delta_* = 418.55$ and $\Delta_{**} = 593.8$. For larger coupling values, the self-consistent solution of equations (5.10) create a large post-inhibitory rebound current from the second ν_h threshold crossing and thus the neuron fires a subsequent action potential. This is one way in which a travelling pulse can destabilise into a double pulse solution.

cross the ν_θ threshold and another spike will be produced. This grazing bifurcation is one way that a single pulse can destabilise into a double pulse. The grazing condition is given by $\nu_\chi(\beta) = 0$ and $\nu(\beta) = \nu_\theta$ for some $\beta > c\Delta_{**}$. This was observed in the direct numerical simulations. Subsequent ν_θ threshold crossings can be created through further increasing the ϵ coupling strength leading to triple, or even multiple, pulse solutions.
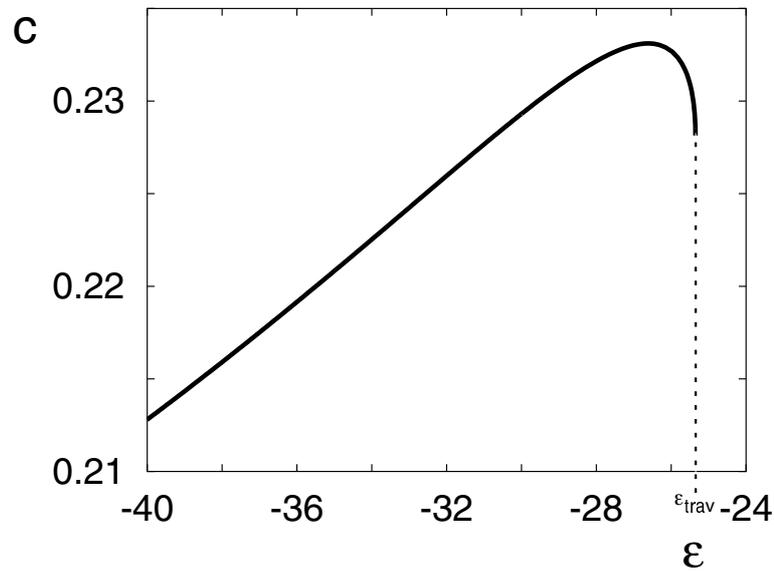
Figure 5.11 Speed plotted against coupling ϵ for the integrate-and-fire-or-burst pulse. An increase in the travelling pulse speed is present for a decrease in the inhibitorial coupling strength. However, the smooth travelling pulse solution does not exist if the global coupling strength is more positive than some critical value. These insights were observed in numerical simulations. Parameter values are given in table 5.1 except that $\tau_h^+ = 200$ and $g_T = 0.06$. The synaptic weight kernel parameter values are given by $\Gamma = 40$ and $\sigma = 15$.

This theoretical mathematical analysis can be extended, as in chapter 4, to periodic travelling wave solutions. One deficiency of this type of theory is that the solution form (in terms of a firing time ansatz) is required to perform the analysis. Of course this is not always possible (as in the case of lurching in section 4.2.1) and so direct numerical simulations need to be performed in order that different waveforms are found and can be examined. The drawback of this simulation approach is that theoretical solutions which

are unstable will never be realised. Some simulations of a one-dimensional continuum are presented in the following section.

5.4   Complex firing patterns

A smooth periodic travelling wave in the one-dimensional integrate-and-fire-or-burst continuum is shown in figure 5.12. Technical details of the computer simulations are presented in appendix A. The analysis in chapter 4 indicated that complex waveforms may exist depending upon the parameter values and the initial conditions chosen.

Intracellular recordings in ferret thalamic slices exhibiting post-inhibitory rebound display spindle waves [36], and simulations of conductance-based models of this typically produce lurching waves (see section 4.2.1 for more details and definitions). Rinzel *et al.* claimed that by reducing the gap in the off-centre coupling it is possible to create lurching phenomena in the sense that clusters of neurons are recruited to fire in a non-smooth fashion [130]. For on-centred coupling, Terman *et al.* analysed the velocity of this lurching phenomena [141]. Rinzel *et al.* also suggested that lurching phenomena can be produced with off-centre coupling, but their example is equivalent to a periodic travelling wave. A smooth wave emerges from the leading cluster, whilst recruitment of the leading clusters takes place non-smoothly in the opposite direction (see figure 2 in [130]).

A reduction of the gap parameter Γ in simulations of the continuum of integrate-and-fire-or-burst neurons leads to a qualitative change in behaviour. Figure 5.13 shows that a single spike is no longer the stable solution. Each neuron fires two action potentials before the next neuron spikes. This could be described as a double pulse solution. Suppose that the refractory period τ_R is re-introduced into the model. Increasing this refractory period to some high level in the travelling wave simulation leads to more obvious lurching waves in the sense that there are periods of propagation at constant speed punctuated by
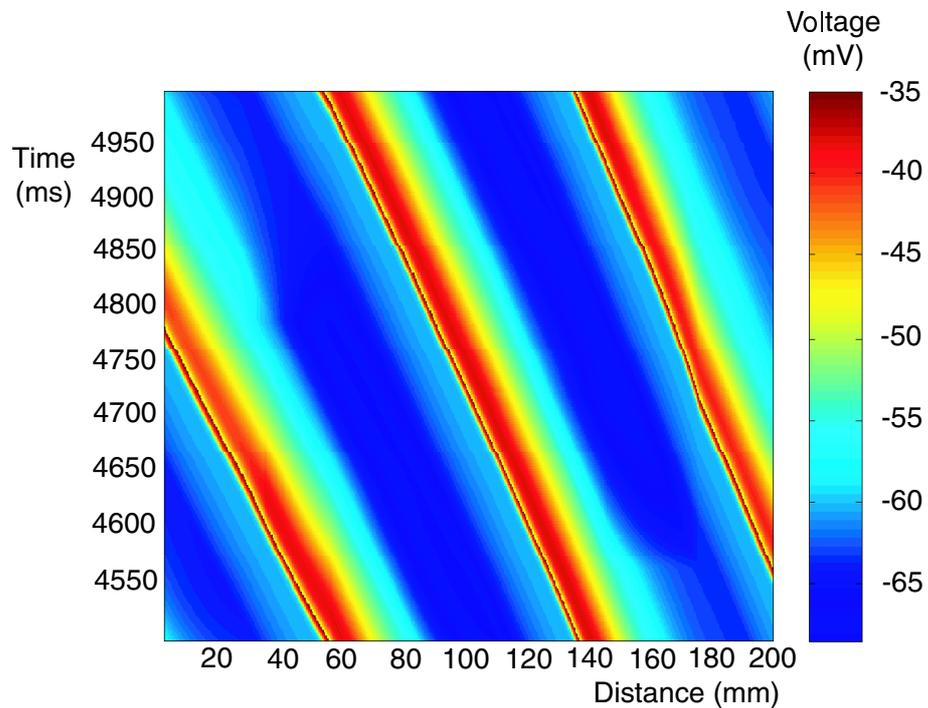
Figure 5.12 The smooth periodic travelling wave solution in an integrate-and-fire-or-burst continuum generated by direct numerical simulation of equations (5.1) and (5.2). Each neuron fires only a single action potential in each smooth wave and these spikes are separated by a constant period. Parameter values are identical to those given in figure 5.11 with the inclusion of $\epsilon = -60$.

stationary intervals (figure 5.14). In this case, more of the travelling waveform is plotted to give a full impression of the rich nature of the interactions. Since the continuum is finite for simulation purposes, sampling sites nearer to the ends of the simulation region will be subject to boundary effects, whereby there will be fewer neighbours than for a central site, and hence a reduced synaptic input current. Boundary conditions do not affect lurching wave propagation away from the boundary.
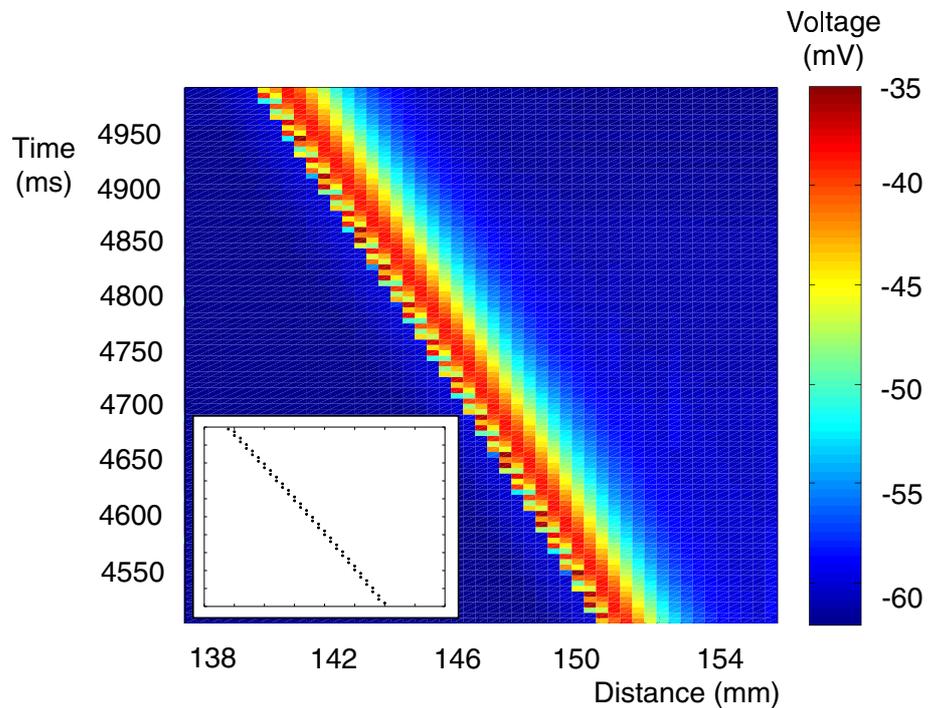
Figure 5.13 A qualitative change in behaviour is noticed as the gap parameter Γ is reduced in a one-dimensional continuum of integrate-and-fire-or-burst model neurons. A packet with two spikes propagating at constant speed is observed. Parameter values are identical to those in figure 5.12 except that $\Gamma = 17$. The insert shows the same region of the continuum, but with only the firing times of each neuron displayed.

If the refractory period is increased in the system with parameter values given in figure 5.12, then a periodic travelling wave with two distinct periods emerges (figure 5.15). This solution could easily be analysed along similar lines to those presented in section 4.4.5. Indeed, higher order multi-periodic waves will exist in this system.
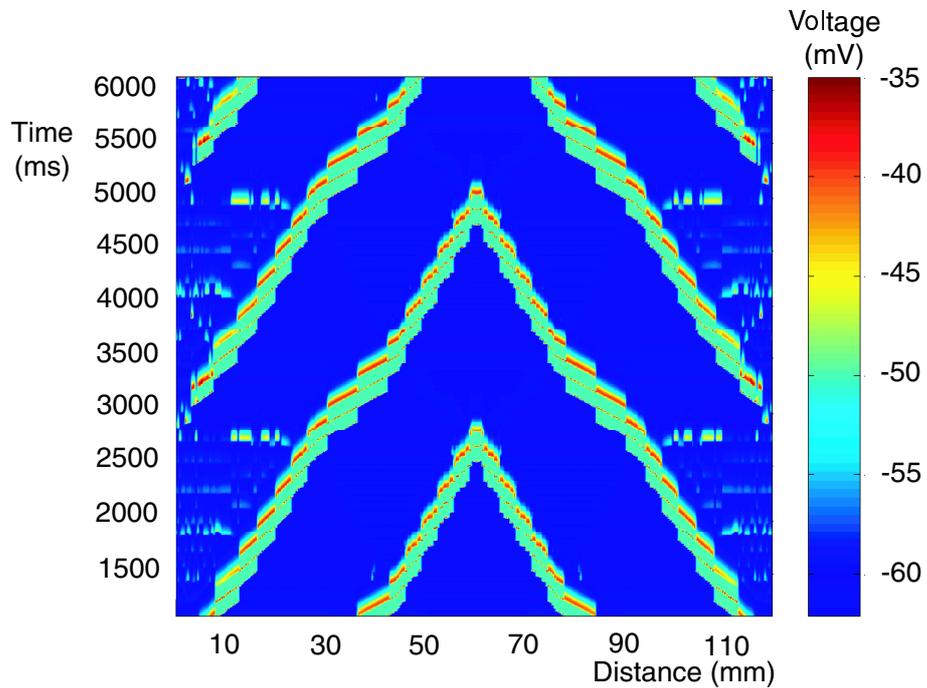
Figure 5.14 Lurching wave phenomena in a one-dimensional continuum of integrate-and-fire-or-burst neurons. Parameter values are identical to those in figure 5.13 with the exception of introducing a refractory time of $\tau_R = 125$. Close examination of the wave suggests that the shape of the waves is reminiscent of the lurching encountered in section 4.2.1. However, the structure of this periodic wave is much more complex and difficult to analyse.

Finally, suppose that all neurons begin the simulation by firing an action potential (figure 5.16). The travelling wave that emerges is periodic, and has a complex structure. Left-right symmetry is apparent, probably through the interaction of the boundaries. The analysis of such a travelling wave, as well as the wave presented in figure 5.14, would be extremely difficult since a firing time ansatz needs to be provided for the asymptotic
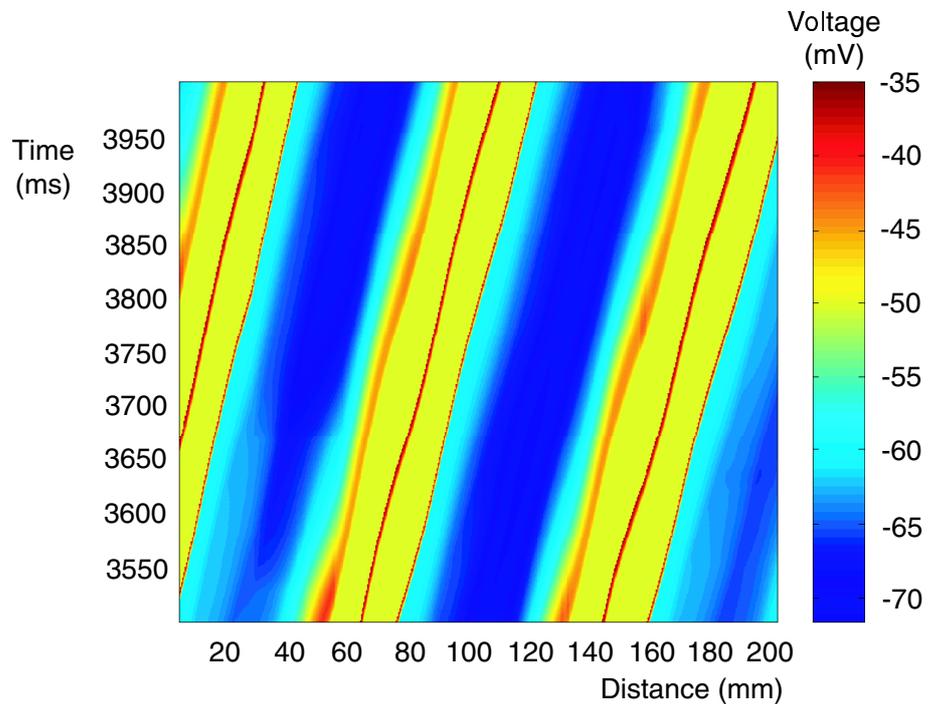
Figure 5.15 A periodic travelling wave with two distinct periods in a one-dimensional continuum of integrate-and-fire-or-burst neurons. Each repeated green band contains two travelling pulses. Parameter values are identical to those in figure 5.13 with the exception of introducing a refractory time of $\tau_R = 125$ and synaptic coupling strength $\epsilon = -80$.

steady state in order to use the framework presented here. The kinematic theory presented in section 4.4.1 would be useful in determining, and giving insight into, these and other exotic travelling wave states.
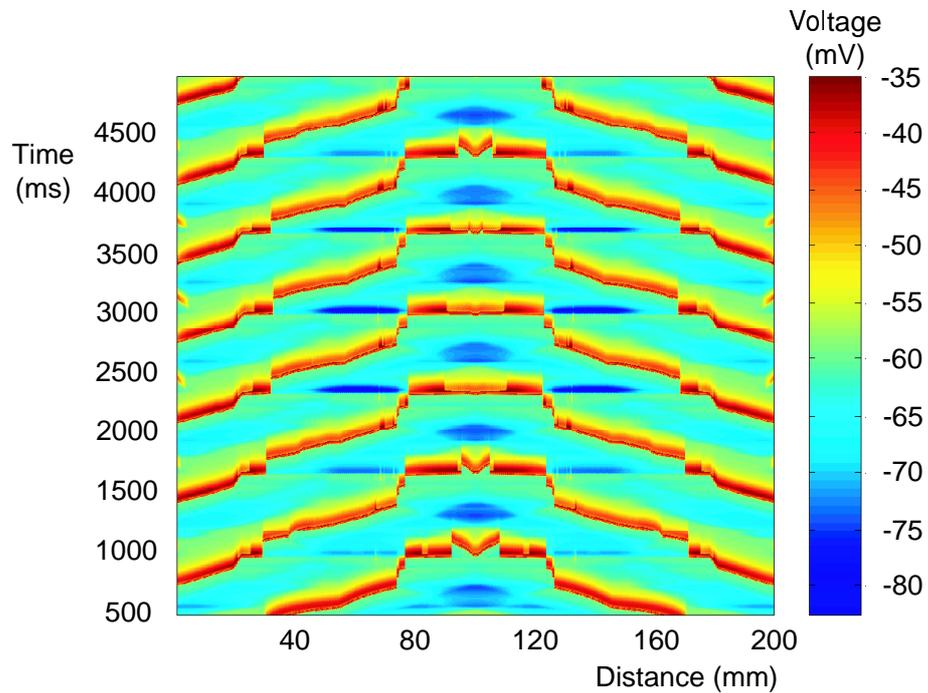
Figure 5.16 A periodic travelling wave solution in the continuum of integrate-and-fire-or-burst neurons. At the onset of the simulation, all neurons were assumed to fire an action potential. Parameter values are identical to those in figure 5.12.

With the exception of the simulation which produces figure 5.16, all simulations in this section are initiated in the same manner. The sampling sites in the closed interval $40 \leq x \leq 80$ are assumed to have fired an action potential. The different solutions obtained through the numerical simulations were obtained by changing the values of various parameters in the system architecture. In figure 5.16, *all* neurons are initially assumed to have fired an action potential.

5.5   Recapitulation

In a manner reminiscent of the analysis presented in chapter 4, a framework for the analysis of networks of integrate-and-fire-or-burst neurons has been developed. The region of existence of a half-centre oscillator has been derived. It is shown that the injected current must take a value between $I_{min} = g_L(V_h - V_L)$ and $I_{max} = g_L(V_\theta - V_L)$ and that coupling must be of a sufficient strength to produce the rhythm. For travelling pulses, a single stable branch was found by self-consistently solving equations (5.10). In integrate-and-fire networks, two branches were found for the travelling pulse solution with the upper branch being stable. Simulations of more varied travelling waves are presented, but these are only a few of the many examples which may be obtained in networks of integrate-and-fire-or-burst neurons. Other varieties of travelling waves may be produced be selecting different parameter values and initial conditions.

Chapter 6

Conclusions and further work

This chapter will mainly describe possible ways in which to extend the work presented in this thesis. The selection of topics is by no means exhaustive, but merely serves to give an insight into the vast number of possibilities for future studies. First, however, it seems prudent to summarise the main contributions to mathematical neuroscience in this thesis.

6.1   Conclusions

The Hodgkin-Huxley model of a nerve cell and its subsequent reduction to the integrate-and-fire model was presented, along with derivations of models which describe biologically realistic synaptic interactions such as the the α-function and dendrites. Linearisation of the Hodgkin-Huxley model led to an appropriate description of quasi-active dendrites.

A simple model of synaptic adaptation was included into an existing theory of discrete integrate-and-fire networks. The primary result of including synaptic adaptation is merely to shift the stability borders of the synchronous state. However, an impor-

tant property of synaptic adaptation is elucidated when the concept of neural coding is considered. Tsodyks and Markram [146] observed that for low rates of depression, the post-synaptic response reflects the rate of firing. As the rate of depression is increased, temporal coherence becomes apparent, in the sense that neuronal bursting output becomes more synchronised. Using the framework presented in this thesis, the claim of Tsodyks and Markram has been extended to the network level. Using the integrate-and-fire model, it has been shown that when the level of depression is increased (for a suitable value of the synaptic adaptation time constant) or when the speed of the dynamics is decreased, the post-synaptic potentials show a transition from primarily refecting a rate code to demonstrating synchronous behaviour. This switch between rate- and spike-coding has been presented for a mixture of excitatory and inhibitory neurons. The case of facilitation has been considered, and no noticeable difference between the analog model and the integrate-and-fire model was detected. This suggests that facilitation does not affect the neural code.

Kistler and van Hemmen [90] stated in some of their work on synaptic adaptation that they had done an extensive parameter search, and could find no parameter set which would destabilise a frequency-locked solution which is stable in the absence of facilitation. From figures 3.1 and 3.2 it is easy to counter their claim with the integrate-and-fire model and this particular model of adaptation. All stability boundaries generated for facilitation lie below those for no adaptation, and never intersect. The area underneath the stability boundary denotes stable behaviour. Thus (at least for the case of *balanced* neurons) there is always a region below the non-adapting stability border but above the facilitation stability border. Hence a region which was stable in the non-adapting case is unstable for facilitation.

Travelling pulses and waves have been analysed within a one-dimensional continuum of integrate-and-fire neurons. For biologically realistic synaptic interactions, existence and linear stability was calculated. It was found that for travelling pulses, two branches

were apparent for the speed of the pulse (as a function of the global coupling strength) with the uppermost (fast) branch being linearly stable and the lower (slow) branch being unstable. These branches culminate at a limit point defining the critical value of the coupling strength such that a travelling pulse exists. In the case of a travelling pulse propagating via α-functions with temporal delay, it was found that an extra instability occurred on the upper branch. When the network was simulated within the region of instability in the upper branch, lurching waves were produced. These waves propagate in a saltatory fashion. No such phenomena was apparent in the dendritic cases.

For periodic travelling waves, dispersion curves relating the speed of the wave to its period, were constructed. These curves initially highlighted that a refractory period should be included into the integrate-and-fire model to avoid an arbitrarily high firing rate. Various methods to incorporate this refractory period were considered and all produced qualitatively similar shapes for the dispersion curves. A kinematic theory was introduced to determine the stability with a positive gradient in the dispersion curve indicating a stable wave. Similar shapes for the dispersion curves were observed for all forms of axo-dendritic connections. For smaller values of the refractory period, stationary points could be created in the upper branch. From these local maxima, multi-periodic states emerged whereby the periodic traveling wave has a number of different periods in its wave train. Resonance in systems selects certain frequencies of oscillation. There are circumstances in the inferior olive [80] where strongly amplified resonances are used to coordinate the emergent pattern of network activity around some preferred frequency. It may also apply to the thalamic participation in delta- and spindle-wave generation [39, 36]. In the quasi-active dendritic case, many such multiple-periodic branches exist in the dispersion curve since the resonant nature of the circuit creates oscillations in the upper branch. This suggests that more variety of travelling waves could be selected in this regime. Simulations of the network showed broad agreement with the precise analytical statements (see appendix A for more details about the numerical simulations).

A model which describes thalamocortical relay cells with a slow calcium current was defined. An examination of the model followed. Simulations of detailed (Hodgkin-Huxley) and reduced (Reduced Hodgkin-Huxley and Wang Rinzel) models of biophysical systems produce half-centre oscillations in agreement with the integrate-and-fire-or-burst model. Through mathematical analysis, the existence of a half-centre rhythm was shown to occur only for a small band of values for the external drive. Precise analytical statements describing a one-dimensional travelling wave were calculated. Only a single branch was found for a travelling pulse solution in this network. "Off-centre" coupling produced a smooth travelling wave, and by reducing the gap in the synaptic weight kernel, a qualitative change occurred in the smooth wave. A single pulse became a double pulse for small gap sizes. Simulations generated more intricate solutions of the one-dimensional continuum of integrate-and-fire-or-burst neurons.

To conclude, the significant contributions to the field of mathematical neuroscience can be summarised as follows. Synaptic adaptation is not seen to have any quantitative change on the stability properties of synchronous states in discrete integrate-and-fire networks, but may be useful in descriptions of neural coding. An analytical treatment of travelling waves and pulses in a one-dimensional continuum of synaptically interacting integrate-and-fire neurons with an assortment of axo-dendritic connections has been presented. Dispersion curves and stability results broadly agree with numerical presentations in current neuroscience literature. Finally, analytical calculations concerning a continuous network of integrate-and-fire-or-burst neurons have been derived. Travelling wave studies have not previously been undertaken. By combining biologically motivated choices for neurons and neural transmission, and building on existing theory, this thesis presents a framework for analysing periodic travelling waves in a biophysical continuum of neurons exhibiting post-inhibitory rebound. Thereby giving a minimal mathematical framework to study travelling waves in a thalamic slice.

6.2 Further work

6.2.1 Noise in systems with synaptic adaptation

Some interesting extensions can be made to the synaptic adaptation theory presented in chapter 3. Abbot suggests two ways to improve the synaptic adaptation function [2]. In the additive case, $A(t) = 1 + S(t)$, where $S(t) = \sum_{t_i < t} K_2(t - t_i)$ and $K_2(t) = (\gamma - 1)e^{-t/\tau_a}$. Nothing restricts K_2 to be an exponential function, and so optimal functions may be found. The amplitude A can have a nonlinear dependence on the sum $S(t)$ by setting $A(t) = 1 + F(S)$ for some function F.

Many synapses have multiple processes which affect the amplitude of the post-synaptic response. In order to model this, the total post-synaptic response amplitude can be represented by the product of several separate amplitude factors as described above. Then, the fit can be adapted by raising each of the amplitudes to various powers. Thus, the general expression is

$$A = A_1^{p_1} A_2^{p_2} A_3^{p_3} \ldots .$$

In real life, neurons are not clean and noise occurs in the system. It would be interesting to consider the effects of noise in systems of integrate-and-fire neurons, although to some extent this would destroy the usefulness of the model. Namely that it can be solved without the need to resort to numerical simulations. However, a simple formalism for noise could be constructed. From this, it will be possible to examine the robustness of these neural systems. Tiesinga and José have shown that a network of integrate-and-fire-or-burst neurons with the inclusion of noise can synchronise without the need of a strong external drive [143]. Equation (3.1) with the reset condition (3.2) may be written

$$\tau_\gamma \frac{dA_j}{dt} = 1 - A_j + \tau_\gamma(\gamma - 1) \sum_{m \in \mathbb{Z}} \delta(t - T_j^m),$$

in the additive case, and

$$\tau_\gamma \frac{dA_j}{dt} = 1 - A_j + A_j \tau_\gamma \log \gamma \sum_{m \in \mathbb{Z}} \delta(t - T_j^m), \tag{6.1}$$

in the multiplicative case. By using these formulations it is easier to perform analysis in stochastic systems. For example, in the case of additive noise drawn from a given probability density ρ, the averaged equations describing depression take the form of (6.1) with the last term on the right hand side replaced by

$$\begin{aligned} \tau_\gamma \log \gamma \left\langle \sum_{m \in \mathbb{Z}} A_j(T_j^m) \delta(t - T_j^m) \right\rangle &\approx \tau_\gamma \log \gamma \sum_{m \in \mathbb{Z}} \left\langle A_j(T_j^m) \right\rangle \left\langle \delta(t - T_j^m) \right\rangle, \\ &= \tau_\gamma \log \gamma \frac{\left\langle A_\infty^\ddagger(T) \right\rangle_\rho}{T}. \end{aligned}$$

The techniques described by Bressloff [12] and Chance *et al.* [23] may then be used to proceed for a given distribution ρ.

6.2.2 Inhomogeneous neural networks

Until now, a homogeneous network where all neurons react and evolve in the same manner irrespective of position within the system has been considered in all of the calculations. However, the cortex is not homogeneous. As an example, consider the retinotopic mapping of the visual field onto the surface of the cortex. The left and right halves of the visual field are mapped onto the right and left halves of the cortex respectively. There are a number of additional maps that have an approximately periodic structure [140]. For example, some cells tend to respond more strongly to stimuli presented in one eye than in the other. Together with this, most cells in V1 respond optimally to a bar or edge moving at an appropriate orientation and velocity in its receptive field [77, 78]. Cells of similar orientation preference are organised into vertical columns whereas there is a systematic variation of orientation preference transversely across the cortex [79]. Moreover, travelling wave solutions are sensitive to the degree of homogeneity in the connectivity pattern [16].

Motivated by Bressloff, the new weight kernel to describe the inhomogeneities will have the form

$$W^*(x, y) = W(|x - y|)h(|x - y|/\delta)k(y/\delta),$$

where h and k are 2π-periodic functions and δ determines the microscopic length scale. If the function k is the identity, then the homogenoeous network is recovered with the effective connection strength a periodically modulated function of spatial separation. The function h may be absorbed into the definition of W. Additional cortical labels could be added into the weight distribution such as orientation preference $\phi \in S^1$ to give a more detailed analysis [19].

6.2.3 Travelling waves in higher spatial dimensions

Higher spatial dimensions can support more exotic travelling structures. It is straightforward to extend the analysis presented into N dimensional space. Instead of having the spatial variable x, replace this with the N dimensional spatial vector $\mathbf{r}$. However, the difficult part of the formal analysis is choosing a suitable firing time ansatz with which to study the non-trivial geometric structures which arise. Recently, studies have been undertaken to develop the theory of two (or more) dimensional travelling waves [15, 81, 87, 89, 109]. In the majority of these cases, they are extensions of the one-dimensional waves to planar waves in two dimensions. Simulations [47, 89, 93] demonstrate that spirals and target patterns, along with much more unusual patterns, can occur in neural media. It is known that rotating spiral waves occur naturally in a wide variety of biological, physiological and chemical systems ([113] and references within,[123]).

In order to give an impression of the task at hand, consider the case of target patterns in two dimensions. This is perhaps the most simple form of travelling structure in higher spatial dimensions which is not a trivial extension of the work presented. Suppose

that a two-dimensional plane of neural media is silent (no neuron has fired, or is firing). Then, without the addition of external stimulus, the network will remain quiescent. If a sufficiently large current is injected at one point in space, neurons will be stimulated in the immediate neighbourhood of the applied current. This leads to all neighbouring neurons firing, which in turn will stimulate their neighbours, and ever increasing circles will be created. Consider a single ring of this motion. Then, the total spike activity can be written as

$$S(\mathbf{r}, t) = S^{\text{init}}(\mathbf{r}, t) + S^{\text{ring}}(\mathbf{r}, t) = s_0 \delta(\mathbf{r}) \delta(t + \Delta t) + \delta[\| \mathbf{r} \| - \rho(t)],$$

where the radius of the front is given by $\rho(t)$ and s_0 is the strength of the initial perturbation. This firing time ansatz contains an unknown function (the radius of the front), and numerics are the only feasible way to proceed [89].

Lurching waves in the one dimensional continuum of integrate-and-fire networks were found by simulating the system with parameter values which predicted an unstable travelling pulse. Analytical progress into these waveforms is difficult, and the precise shape of the lurch has yet to be formulated. Lurching waves must exist in higher dimensions, but it is practically impossible to predict the structure of these waveforms. It would be interesting to examine higher dimensional systems purely to gain insight into these fascinating, and highly relevant, travelling waves.

Appendix A

Numerical Issues

XPPAUT

XPPAUT is available at http://www.pitt.edu/~phase/ and is a free package written by G. B. Ermentrout [46]. It is an interactive package for numerically solving and analysing differential equations and provides a simple interface to most of the common features of AUTO (ftp://ftp.cs.concordia.ca/pub/doedel/auto). Details on the numerical methods used by XPPAUT can be found in the reference. Simulations in XPPAUT make use of equation (2.11), with $\eta_2 \to \eta_2 + \alpha^2$ whenever the neuron fires, for α-function synaptic delay kernels. This allows the iterations to proceed quickly without the need to store all the firing times in the system. Truncation of the spike train is another way to proceed, but obviously this will lead to numerical errors.

Another benefit of XPPAUT is that auxilliary dynamical systems can be set up in order to find and track roots of nonlinear algebraic equations. This method has been used to produce many of the figures in this thesis and to find bifurcation points of the system. However, truncation of the Fourier representation in chapter 4 was necessary. It

was found that the balance between accuracy and time was achieved when 2001 terms (centred around the zero Fourier coefficient) were considered with an α-function synaptic delay kernel, and 10001 terms were needed for the dendritic kernels.

Chapter 3 - Synaptic adaptation in discrete integrate-and-fire networks

An algorithm was formulated in Mathematica. The benefits of this approach are that the integral equations don't need to be evolved and that arbitrary accuracy can be achieved using the root-finding algorithm of the Mathematica package. However, a closed form expression must exist for the state variable. Equation (3.3) was integrated on the region $(T_i^n, t]$ and evaluated for an α-function delay kernel. For this closed form expression, the system is started at values $V_i(0) = \nu_i$ where $V_{reset} \leq \nu_i < V_\theta$, and initially there are no spikes in the system. The algorithm then proceeds as follows:

- Calculate $V_i(t_i) = 1$ for each i using a root-finding process. This determines all *possible* firing times t_i in the system.

- Calculate $t_k = \min\{t_1, \ldots, t_N\}$.

- Set $V_k(t_k) = V_{reset}$.

- Solve the system with initial data $(V_1(t_k), V_2(t_k), \ldots, V_{reset}, \ldots, V_N(t_k))$ with V_{reset} at the kth position. In addition, the coupling term now contains an extra spike.

- Repeat the process for the desired number of spikes in the system.

Chapter 4 - Synaptic travelling waves in integrate-and-fire systems

Chapter 5 - Biophysical models

An extensive discussion on numerical simulations of neural models has been presented by Mascagni and Sherman [101]. Runge-Kutta methods are presented for the numerical modelling of ordinary differential equations and finite element methods are presented for systems described by partial differential equations. In order to represent the continuum in chapters 4 and 5, a portion of the real line was truncated and a lattice embedded upon the resulting space. Equations (4.1) and (4.2) (or the equivalent system, including the slow T-type calcium current, for the integrate-and-fire-or-burst model) were evolved using a standard Euler scheme

$$V(t + \Delta t) = V(t) + \frac{\Delta t}{C_M} \left(-F + I_s + I \right),$$

(from equation (2.1)) with small step size Δt in accordance with Hansel *et al.* [63]. They show that small time steps are required whenever differential equations describing integrate-and-fire networks are integrated using the standard Euler or second order Runge-Kutta algorithms. As with the XPPAUT simulations, the α-function synaptic delay kernel was represented with equation (2.11) with $\eta_2 \to \eta_2 + \alpha^2$ whenever the neuron fires. Each sampling site in the lattice is represented by the above Euler expression with connectivity determined by the discrete analog of equation (4.2). The network was stimulated by assuming some spikes had already fired in a region of the lattice and adjusting the synaptic current accordingly. Excellent agreement was found with the analytical solutions.

A trade exists between accuracy and CPU time. To be computationally more efficient, it would be possible to use a second-order Runge-Kutta iteration scheme and even to formulate some sort of interpolation for the firing times along the following lines. Suppose there are N lattice sites, and that the time step is given by Δt. A linear interpolation of the firing times is then given by

$$T - \Delta t + \frac{\Delta t (V_\theta - V(t))}{V(t + \Delta t) - V(t)},$$

where T is the value of time at the first iteration such that the potential is greater than the threshold V_θ. These modifications greatly improve the integration performance. However, small time steps are still required.

Other neural packages

Excellent neural modelling packages have been produced over recent years. They involve constructing systems from detailed neural descriptions; even including various types of neuron at the cellular level. GENESIS (the GEneral NEural Simulation System developed by Bower and Beeman [11]) and NEURON (developed by Hines [68, 69]) are two such tools. Additional information can be obtained at http://www.genesis-sim.org/GENESIS/ and http://www.neuron.yale.edu for GENESIS and NEURON respectively.

References

[1] L F Abbott and T B Kepler. Model neurons: From Hodgkin–Huxley to Hopfield. In L Garrido, editor, *Statistical Mechanics of Neural Networks*, pages 5–18. Springer–Verlag, Berlin, 1990.

[2] L F Abbott and Eve Marder. Modelling small networks. In C Koch and I Segev, editors, *Methods in Neuronal Modeling. From Ions to Networks (2nd edition)*, pages 361–410. MIT press, Cambridge, 1998.

[3] M Abeles. *Corticonics: Neuronal Circuits of the Cerebral Cortex*. Cambridge University Press, 1991.

[4] P Andersen and S A Andersen. *Physiological Basis of the Alpha Rhythm*. Appleton-Century-Crofts, New York, 1968.

[5] A Bansal, J H Singer, B J Hwang, W Xu, A Beaudet, and M B Feller. Mice lacking specific nicotinic acetylcholine receptor subunits exhibit dramatically altered spontaneous activity patterns and reveal a limited role for retinal waves in forming ON and OFF circuits in the inner retina. *The Journal of Neuroscience*, 20(20):7672–7681, 2000.

[6] H Berger. ´uber das elektrenkephalogram des menschen. *Arch. f. Psychiat.*, 87:527–570, 1929.

[7] M J Berry, D K Warlund, and M Meister. The structure and precision of retinal spike trains. *Procedures of the National Academy of Science, USA*, 94:5411–5416, 1997.

[8] S R Bishop. Impact oscillators. *Philosophical Transactions of the Royal Society of London A*, 347:345–448, 1994.

[9] G N Borisyuk, R M Borisyuk, A I Khibnik, and D Roose. Dynamics and bifurcations of two coupled neural oscillators with different connection types. *Bulletin of Mathematical Biology*, 57(6):809–840, 1995.

[10] R M Borisyuk and L M Urzhumtseva. Dynamical regimes in a system of interacting neural oscillators. In A V Holden and V I Kryukov, editors, *Neural Networks: Theory and Architecture*, pages 9–21. Manchester University Press, Manchester, 1990.

[11] J M Bower and D Beeman. *The Book of GENESIS (2nd edition)*. TELOS, New York, 1997.

[12] P C Bressloff. Mean field theory of globally coupled integrate-and-fire oscillators with dynamic synapses. *Physical Review E*, 60:2160–2170, 1999.

[13] P C Bressloff. Resonantlike synchronization and bursting in a model of pulse-coupled neurons with active dendrites. *Journal of Computational Neuroscience*, 6:237–249, 1999.

[14] P C Bressloff. Synaptically generated wave propagation in excitable neural media. *Physical Review Letters*, 82:2979–2982, 1999.

[15] P C Bressloff. Traveling waves and pulses in a one-dimensional network of excitable integrate-and-fire neurons. *Journal of Mathematical Biology*, 40(2):169–198, 2000.

[16] P C Bressloff. Traveling fronts and wave propagation failure in an inhomogeneous neural network. *Physica D*, 155(1/2):83–100, 2001.

[17] P C Bressloff and S Coombes. A dynamical theory of spike train transitions in networks of integrate-and-fire oscillators. *Physical Review Letters*, 81:2384–2387, 1998.

[18] P C Bressloff and S Coombes. Dynamics of strongly-coupled spiking neurons. *Neural Computation*, 12:91–129, 2000.

[19] P C Bressloff, J D Cowan, M Golubitsky, P J Thomas, and M Wiener. Geometrical hallucination, Euclidean symmetry and the functional architecture of striate cortex. *Philosophical Transactions of the Royal Society B*, 356(1407):299–330, 2001.

[20] C J Budd. Non-smooth dynamical systems and the grazing bifurcation. In P J Aston, editor, *Nonlinear Mathematics and its Applications*, pages 219–235. Cambridge University Press, Cambridge, UK, 1996.

[21] R L Calabrese. Half-centre oscillators underlying rhythmic movements. In M A Arbib, editor, *The Handbook of Brain Theory and Neural Networks*, pages 444–447. MIT Press, Cambridge, Massachusetts, 1995.

[22] C E Carr and M Konishi. A circuit for detection of interaural differences in the brain stem of the barn owl. *Journal of Neuroscience*, 10:3227–3246, 1990.

[23] F S Chance, S B Nelson, and L F Abbott. Synaptic depression and the temporal response characteristics of V1 cells. *The Journal and Neuroscience*, 18(12):4785–4799, 1998.

[24] Z Chen, B Ermentrout, and X-J Wang. Wave propagation mediated by $GABA_B$ synapse and rebound excitation in an inhibitory network: A reduced model approach. *Journal of Computational Neuroscience*, 5:53–69, 1998.

[25] R D Chervin, P A Pierce, and B W Connors. Periodicity and directionality in the propagation of epileptiform discharges across neocortex. *Journal of Neurophysiology*, 60:1695–1713, 1998.

[26] K S Cole. *Membranes, Ions and Impulses.* University of California Press, Los Angeles, 1968.

[27] B W Connors and Y Amitai. Generation of epileptiform discharges by local circuits in neocortex. In P A Schwartzkroin, editor, *Epilepsy: Models, Mechanisms and Concepts*, pages 388–424. Cambridge University Press, Cambridge, UK, 1993.

[28] S Coombes. From periodic travelling waves to travelling fronts in the spike-diffuse-spike model of dendritic waves. *Mathematical Biosciences*, 170:155–172, 2001.

[29] S Coombes and P C Bressloff. Mode-locking and Arnold tongues in integrate-and-fire neural oscillators. *Physical Review E*, 60:2086–2096, 1999.

[30] S Coombes, M R Owen, and G D Smith. Mode-locking in a periodically forced integrate-and-fire-or-burst neuron model. *Physical Review E*, 64(4):04194, 2001.

[31] A C Crawford and R Fettiplace. An electrical tuning mechanism in turtle cochlear hair cells. *Journal of Physiology*, 312:377–412, 1981.

[32] S Crook, G B Ermentrout, M C Vanier, and J M Bower. The role of axonal delay in the synchronization of networks of coupled cortical oscillators. *Journal of Computational Neuroscience*, 4:161–172, 1997.

[33] R R de Ruyter van Steveninck, G D Lewen, S P Strong, R Koberle, and W Bialek. Reproducibility and variability in neural spike trains. *Science*, 275:1805–1808, 1997.

[34] K R Delaney, A Gelperin, M S Fee, J A Flores, R Gervais, D W Tank, and D Kleinfeld. Waves and stimulus-modulated dynamics in an oscillating olfactory network. *Proceedings of the National Academy of Science USA*, 91:669–673, 1994.

[35] A Destexhe. Conductance-based integrate and fire models. *Neural Computation*, 9:503–514, 1997.

[36] A Destexhe, T Bal, D A McCormick, and T J Sejnowski. Ionic mechanisms underlying synchronized oscillations and propagating waves in a model of ferret thalamic slices. *Journal of Neurophysiology*, 76:2049–2070, 1996.

[37] A Destexhe, Z F Mainen, and T J Sejnowski. Synthesis of models for excitable membranes, synaptic transmission and neuromodulation using a common kinetic formalism. *Journal of Computational Neuroscience*, 1:195–231, 1994.

[38] J S Dittman, A C Kreitzer, and W G Regehr. Interplay between facilitation, depression, and residual calcium at three presynaptic terminals. *The Journal of Neuroscience*, 20(4):1374–1385, 2000.

[39] R C Dossi, A Nunez, and M Steriade. Electrophysiology of a slow (0.5-4 Hz) intrinsic oscillation of cat thalamocortical neurons in vivo. *Journal of Physiology*, 447:215–234, 1992.

[40] C Elphick, E Meron, J Rinzel, and E A Spiegel. Impulse patterning and relaxational propagation in excitable media. *Journal of Theoretical Biology*, 146:249–268, 1990.

[41] G B Ermentrout. n:m phase-locking of weakly coupled oscillators. *Journal of Mathematical Biology*, 12:327–342, 1981.

[42] G B Ermentrout. Asymptotic behaviour of stationary homogeneous neuronal nets. In S Amari and M A Arbib, editors, *Competition and Cooperation in Neural Nets*, pages 57–70. Springer-Verlag, Heidelberg, Germany, 1982.

[43] G B Ermentrout. An adaptive model for synchrony in the firefly *pteroptyx mallacae*. *Journal of Mathematical Biology*, 29:571–585, 1991.

[44] G B Ermentrout. Firefly synchrony. *Nature*, 353(6341):220–220, 1991.

[45] G B Ermentrout. The analysis of synaptically generated travelling waves. *Journal of Computational Neuroscience*, 5:191–208, 1998.

[46] G B Ermentrout. *Simulating, Analyzing, and Animating Dynamical Systems: A Guide to XPPAUT for Researchers and Students*. SIAM, Philadelphia, 2002.

[47] G B Ermentrout and D Kleinfeld. Travelling electrical waves in cortex: Insights from phase dynamics and speculation on a computational role. *Neuron*, 29:33–44, 2001.

[48] G B Ermentrout and N Kopell. Frequency plateaus in a chain of weakly coupled oscillators. *SIAM Journal on Mathematical Analysis*, 15:215–237, 1984.

[49] G B Ermentrout and N Kopell. Oscillator death in systems of coupled neural oscillators. *SIAM Journal on Mathematical Analysis*, 50(1):125–146, 1990.

[50] Y-S Fan and T R Chay. Generation of periodic and chaotic bursting in an excitable cell model. *Biological Cybernetics*, 71:417–431, 1994.

[51] J C Fiala, S Grossberg, and D Bullock. Metabotropic glutamate receptor activation in cerebellar Purkinje cells as substrate for adaptive timing of the classically conditioned eye-blink response. *The Journal of Neuroscience*, 16(11):3760–3774, 1996.

[52] R Fitzhugh. Impulses and physiological states in theoretical models of nerve membrane. *Biophysical Journal*, 1:445–466, 1961.

[53] R Fitzhugh. Mathematical models for excitation and propagation in nerve. In H P Schwan, editor, *Biological Engineering*, pages 1–85. McGraw Hill, New York, New York, 1969.

[54] W Gerstner, J Leo van Hemmen, and Jack D Cowan. What matters in neuronal locking? *Neural Computation*, 94:1653–1676, 1996.

[55] D Golomb and Y Amitai. Propagating neuronal discharges in neocortical slices: computational and experimental study. *Journal of Neurophysiology*, 78:1199–1211, 1997.

[56] D Golomb and G B Ermentrout. Continuous and lurching traveling pulses in neuronal networks with delay and spatially decaying connectivity. *Proceedings of the National Academy of Science USA*, 96(23):13480–13485, 1999.

[57] D Golomb and G B Ermentrout. Effects of delay on the type and velocity of travelling pulses in neuronal networks with spatially decaying connectivity. *Network: Computation in Neural Systems*, 11:221–246, 2000.

[58] D Golomb and G B Ermentrout. Bistability in pulse propagation in networks of excitatory and inhibitory populations. *Physical Review Letters*, 86(18):4179–4182, 2001.

[59] D Golomb, X-J Wang, and J Rinzel. Propagation of spindle waves in a thalamic slice model. *Journal of Neurophysiology*, 75(2):750–769, 1996.

[60] D Hansel, G Mato, and C Meunier. Phase dynamics for weakly coupled Hodgkin-Huxley neurons. *Europhysics Letters*, 23(5):367–372, 1993.

[61] D Hansel, G Mato, and C Meunier. Phase reduction and neural modelling. *Concepts in Neuroscience*, 4(2):193–210, 1993.

[62] D Hansel, G Mato, and C Meunier. Synchrony in excitatory neural networks. *Neural Computation*, 7:307–337, 1995.

[63] D Hansel, G Mato, C Meunier, and L Neltner. On numerical simulation of integrate-and-fire neural networks. *Neural Computation*, 10(2):467–483, 1998.

[64] J L Hindmarsh and R M Rose. A model of neuronal bursting using three coupled first order differential equations. *Philosophical Transactions of the Royal Society London B*, 221:87–102, 1984.

[65] J L Hindmarsh and R M Rose. A model for rebound bursting in mammalian neurons. *Philosophical Transactions of the Royal Society London B*, 346:129–150, 1994.

[66] J L Hindmarsh and R M Rose. A model of intrinsic and driven spindling in thalamocortical neurons. *Philosophical Transactions of the Royal Society London B*, 346:165–183, 1994.

[67] J L Hindmarsh and R M Rose. Resonance in a model of mammalian neuron. *Philosophical Transactions of the Royal Society London B*, 346:151–163, 1994.

[68] M Hines. NEURON – a program for simulation of nerve equations. In F Eeckman, editor, *Neural Systems: Analysis and Modeling*, pages 127–136. Kluwer, Norwell, MA, 1993.

[69] M Hines and N T Carnevale. The NEURON simulation environment. *Neural Computation*, 9:1179–1209, 1997.

[70] A L Hodgkin and A F Huxley. The components of membrane conductance in the giant axon of *loligo*. *Journal of Physiology*, 116:473–496, 1952.

[71] A L Hodgkin and A F Huxley. Currents carried by sodium and potassium ions through the membrane of the giant axon of *loligo*. *Journal of Physiology*, 116:449–472, 1952.

[72] A L Hodgkin and A F Huxley. The dual effect of membrane potential on sodium conductance in the giant axon of *loligo*. *Journal of Physiology*, 116:497–506, 1952.

[73] A L Hodgkin and A F Huxley. A quantitative description of membrane current and its application to conduction and excitation in nerve. *Journal of Physiology*, 117(4):500–544, 1952.

[74] A V Holden. *Models of the Stochastic Activity of Neurones*. Lecture Notes in Biomathematics. Springer-Verlag, Berlin, 1976.

[75] F C Hoppensteadt and E M Izhikevich. *Weakly Connected Neural Networks*. Applied Mathematical Sciences;126. Springer-Verlag, New York, 1997.

[76] Yo Horikawa. A spike train with a step change in the interspike intervals in the Fitzhugh-Nagumo model. *Physica D*, 82:365–370, 1995.

[77] D H Hubel and T N Wiesel. Receptive fields, binocular interaction and functional architecture in the cat's visual cortex. *Journal of Physiology London*, 160:106–154, 1962.

[78] D H Hubel and T N Wiesel. Receptive fields and functional architecture of monkey striate cortex. *Journal of Physiology London*, 195:215–243, 1968.

[79] D H Hubel and T N Wiesel. Sequence regularity and geometry of orientation columns in the monkey striate cortex. *Journal of Computational Neuroscience*, 158:295–306, 1974.

[80] B Hutcheon and Y Yarom. Resonance, oscillation and the intrinsic frequency preferences of neurons. *Trends in Neurosciences*, 23(5):216–222, 2000.

[81] M A P Idiart and L F Abbott. Propagation of excitation in neural network models. *Network*, 4:285–294, 1993.

[82] H Jahnsen and R Llinás. Electrophysiological properties of guinea-pig thalamic neurons: An *in vitro* study. *Journal of Physiology*, 349:205–226, 1984.

[83] H Jahnsen and R Llinás. Ionic basis for the electroresponsiveness and oscillatory properties of guinea-pig thalamic neurons *in vitro*. *Journal of Physiology*, 349:227–247, 1984.

[84] T B Kepler, L F Abbott, and E Marder. Reduction of conductance-based neuron models. *Biological Cybernetics*, 66:381–387, 1992.

[85] U Kim, T Bal, and D A McCormick. Spindle waves are propagating synchronized oscillations in the ferret LGNd in vitro. *Journal of Neurophysiology*, 74(3):1301–1323, 1995.

[86] U Kim and D A McCormick. The functional influence of burst and tonic firing mode on synaptic interactions in the thalamus. *The Journal of Neuroscience*, 18(22):9500–9516, 1998.

[87] W M Kistler. Stability properties of solitary waves and periodic wave trains in a two-dimensional network of spiking neurons. *Physical Review E*, 62(6):8834–8837, 2000.

[88] W M Kistler, W Gerstner, and J L van Hemmen. Reduction of the Hodgkin-Huxley equations to a single-variable threshold model. *Neural Computation*, 9(5):1015–1045, 1997.

[89] W M Kistler, R Seitz, and J L van Hemmen. Modelling collective excitations in cortical tissue. *Physica D*, 114:273–295, 1997.

[90] W M Kistler and J L van Hemmen. Short-term synaptic plasticity and network behaviour. *Neural Computation*, 11:1579–1594, 1999.

[91] C Koch. Cable theory in neurons with active, linearized membranes. *Biological Cybernetics*, 50:15–33, 1984.

[92] Christof Koch. *Biophysics of Computation : Information Processing in Single Neurons*. Oxford University Press, New York, 1999.

[93] S Komineas, F Heilmann, and L Kramer. Patterns formed by spiral pairs in oscillatory media. *Physical Review E*, 63:011103–1–011301–5, 2000.

[94] Y Kuramoto. *Chemical Oscillations, Waves and Turbulence*. Springer-Verlag, Berlin, 1984.

[95] S Kuroda, N Schweighofer, and M Kawato. Exploration of signal transduction pathways in cerebellar long-term depression by kinetic simulation. *The Journal of Neuroscience*, 21(15):5693–5702, 2001.

[96] L Lapicque. Recherches quantitatives l'excitation electrique des nerfs traitee comme une polarization. *Journal de Physiologie et Pathologie General*, 9:620–635, 1907.

[97] W C Lemon and W M Getz. Neural coding of general odors in insects. *Annals of the Entomological Society of America*, 92(6):861–872, 1999.

[98] Z F Mainen and T J Sejnowski. Influence of dendritic structure on firing pattern in model neocortical neurons. *Nature*, 382(6594):759–760, 1996.

[99] E Marder and R L Calabrese. Principles of rhythmic motor pattern generation. *Physiology Review*, 76:687–717, 1996.

[100] E Marder, N Kopell, and K Sigvardt. How computation aids in understanding biological networks. In P S G Stein, S Grillner, A I Selverston, and D G Stuart, editors, *Neurons, Networks and Motor Behavior*, pages 139–150. MIT Press, Cambridge, MA, 1999.

[101] M V Mascagni and A Sherman. Numerical methods for neuronal modeling. In C Koch and I Segev, editors, *Methods in Neuronal Modeling. From Ions to Networks (2nd edition)*, pages 569–606. MIT Press, Cambridge, MA, 1998.

[102] K Matsuoka. Sustained oscillations generated by mutually inhibiting neurons with adaptation. *Biological Cybernetics*, 52(6):367–376, 1985.

[103] D A McCormick and T Bal. Sleep and arousal: Thalamocortical mechanisms. *Annual Review of Neurosciences*, 20:185–215, 1997.

[104] D R McMillen, G M T D'Eleuterio, and J R P Halperin. A simple central pattern generator model using phasic analog neurons. *Physical Review E.*, 59(6):6994–6999, 1999.

[105] B W Mel. Information processing in dendritic trees. *Neural Computation*, 6:1031–1085, 1994.

[106] R N Miller and J Rinzel. The dependence of impulse propagation speed on firing frequency, dispersion, for the Hodgkin-Huxley model. *Biophysical Journal*, 34:227–259, 1981.

[107] B Milner, L R Squire, and E R Kandel. Cognitive neuroscience and the study of memory. *Neuron*, 20:445–468, 1998.

[108] R E Mirollo and S H Strogatz. Synchronisation of pulse-coupled biological oscillators. *SIAM Journal on Applied Mathematics*, 50(6):1645–1662, 1990.

[109] H Mori and Y Kuramoto. *Dissipative Structures and Chaos*. Springer-Verlag, Berlin, 1998.

[110] C Morris and H Lecar. Voltage oscillations in the barnacle giant muscle fiber. *Biophysical journal*, 35:193–213, 1981.

[111] B Mulloney, D H Perkel, and R W Budelli. Motor-pattern production: Interaction of chemical and electrical synapses. *Brain Research*, 229:25–33, 1981.

[112] D Mumford. Thalamus. In M A Arbib, editor, *The Handbook of Brain Theory and Neural Networks*, pages 981–984. MIT Press, Cambridge, Massachusetts, 1995.

[113] J D Murray. *Mathematical Biology*. Springer-Verlag, Berlin, 1989.

[114] J S Nagumo, S Arimoto, and S Yoshizawa. An active pulse transmission line simulating nerve axon. *Proc. IRE*, 50:2061–2070, 1962.

[115] M Oestreich, N Hinrichs, K Popp, and C J Budd. Analytical and experimental investigation of an impact oscillator. In *Proceedings of DETC'97*, pages 1–11. ASME Design Engineering Technical Conferences, Sacramento, 1997.

[116] R Osan and B Ermentrout. The evolution of synaptically generated waves in one- and two-dimensions. *Physica D*, 163(3/4):217–235, 2002.

[117] R Osan, J Rubin, and B Ermentrout. Regular travelling waves in a one-dimensional network of theta neurons. *SIAM Journal on Applied Mathematics*, 62(4):1197–1221, 2002.

[118] S Panzeri, R S Petersen, S R Schultz, M Lebedev, and M E Diamond. The role of spike timing in the coding of stimulus location in rat somatosensory cortex. *Neuron*, 29:769–777, 2001.

[119] D H Perkel and B Mulloney. Motor-pattern production in reciprocally inhibitory neurons exhibiting postinhibitory rebound. *Science*, 185:181–183, 1974.

[120] R S Petersen, S Panzeri, and M E Diamond. Population coding of stimulus location in rat somatosensory cortex. *Neuron*, 32:503–514, 2001.

[121] P Poirazi and B W Mel. Impact of active dendrites and structural plasticity on the memory capacity of neural tissue. *Neuron*, 29:779–796, 2001.

[122] J C Prechtl, T H Bullock, and D Kleinfeld. Direct evidence for local oscillatory current sources and intracortical phase gradients in turtle visual cortex. *Proceedings of the National Academy of Science USA*, 97(2):877–882, 2000.

[123] J C Prechtl, L B Cohen, P P Mitra, B Pesaran, and D Kleinfeld. Visual stimuli induce waves of electrical activity in turtle cortex. *Proceedings of the National Academy of Science USA*, 94(14):7621–7626, 1997.

[124] W Rall. Theory of physiological properties of dendrites. *Annals New York Academy of Science*, 96:1071–1092, 1962.

[125] W Rall. Theoretical significance of dendritic trees for neuronal input-output relations. In R F Reiss, editor, *Neural Theory and Modeling*, pages 73–97. Stanford University Press, Stanford, CA, 1964.

[126] W Rall. Distinguishing theoretical synaptic potentials computed for different soma-dendritic distributions of synaptic input. *Journal of Neurophysiology*, 30:1138–1168, 1967.

[127] W Rall and H Agmon-Snir. Cable theory for dendritic neurons. In C Koch and I Segev, editors, *Methods in Neuronal Modeling. From Ions to Networks (2nd edition)*, pages 27–92. MIT Press, Cambridge, Massachusetts, 1998.

[128] U Ribary, A A Ioannides, K D Singh, R Hasson, J P R Bolton, F Lado, A Mogilner, and R Llinás. Magnetic field tomography of coherent thalamocortical 40-Hz oscillations in humans. *Proceedings of the National Academy Sciences, USA*, 88:11037–11041, 1991.

[129] J Rinzel and K Maginu. Kinematic analysis of wave pattern formation in excitable media. In C Vidal and A Pacault, editors, *Non-equilibrium Dynamics in Chemical Systems*, pages 107–113. Springer–Verlag, Berlin, 1984.

[130] J Rinzel, D Terman, X-J Wang, and B Ermentrout. Propagating activity patterns in large-scale inhibitory neuronal networks. *Science*, 279:1351–1355, 1998.

[131] J Rubin and D Terman. Geometric analysis of neuronal firing patterns in network models with fast inhibitory synapses. *Neurocomputing*, 26–27:491–498, 1999.

[132] M A Seager, L D Johnson, E S Chabot, Y Asaka, and S D Berry. Oscillatory brain states and learning: Impact of hippocampal theta-contingent training. *Proceedings of the National Academy of Science USA*, 99(3):1616–1620, 2002.

[133] T J Sejnowski, D A McCormick, and M Steriade. Thalamocortical oscillations in sleep and wakefulness. In M A Arbib, editor, *The Handbook of Brain Theory and Neural Networks*, pages 444–447. MIT Press, Cambridge, Massachusetts, 1995.

[134] G M Shepherd. *The Synaptic Organization of the Brain (4th edition)*. Oxford University Press, Oxford, UK, 1998.

[135] S M Sherman and R W Guillery. On the actions that one nerve cell can have on another: Distinguishing "drivers" from "modulators". *Proceedings of the National Academy of Science USA*, 95:7121–7126, 1998.

[136] C S Sherrington. *The Integrative Action of the Nervous System*. Yale University Press, New Haven, USA, 1906.

[137] G D Smith, C L Cox, S M Sherman, and J Rinzel. Fourier analysis of sinusoidally driven thalamocortical relay neurons and a minimal integrate-and-fire-or-burst model. *Journal of Neurophysiology*, 83:588–610, 2000.

[138] G D Smith, C L Cox, S M Sherman, and J Rinzel. A firing-rate model of spike-frequency adaptation in sinusoidally-driven thalamocortical relay neurons. *Thalamus and Related Systems*, 11:1–22, 2001.

[139] D Somers and N Kopell. Rapid synchronization through fast threshold modulation. *Biological Cybernetics*, 68:393–407, 1993.

[140] N V Swindale. The development of topography in visual cortex: a review of models. *Network*, 7(2):161–247, 1996.

[141] D H Terman, G B Ermentrout, and A C Yew. Propagating activity patterns in thalamic neuronal networks. *SIAM Journal on Applied Mathematics*, 61(5):1578–1604, 2001.

[142] A M Thomson. Molecular frequency filters at central synapses. *Progress in Neurobiology*, 62:159–196, 2000.

[143] P H E Tiesinga and J V José. Synchronous clusters in a noisy inhibitory neural network. *Journal of Computational Neuroscience*, 9(1):49–65, 2000.

[144] V Torre and W G Owen. High-pass filtering of small signals by the rod network in the retina of the toad Bufo Marinus. *Journal of Biophysics*, 41:305–324, 1983.

[145] A Treves and E T Rolls. Computational analysis of the role of hippocampus in memory. *Hippocampus*, 4(3):374–391, 1994.

[146] M V Tsodyks and H Markram. The neural code between neocortical pyramidal neurons depends on neurotransmitter release probability. *Proceedings of the National Academy of Sciences, USA*, 94:719–723, 1997.

[147] M V Tsodyks, K Pawelzik, and H Markram. Neural networks with dynamic synapses. *Neural Computation*, 10:821–835, 1998.

[148] M V Tsodyks, A Uziel, and H Markram. Synchrony generation in recurrent networks with frequency-dependent synapses. *Journal of Neuroscience*, 20:RC50(1–5), 2000.

[149] H C Tuckwell. *Introduction to Theoretical Neurobiology*, volume I. Cambridge University Press, Cambridge, 1988.

[150] C van Vreeswijk, L F Abbott, and G B Ermentrout. When inhibition not excitation synchronizes neural firing. *Journal of Computational Neuroscience*, 1:313–321, 1994.

[151] J Volkmann, M Joliot, A Mogilner, A A Ioannides, F Lado, E Fazzini, U Ribary, and R Llinás. Central motor loop oscillations in parkinsonian resting tremor revealed by magnetoencephalography. *Neurology*, 46:1359–1370, 1996.

[152] K E Voskamp, N Noorman, H A K Mastebroek, N E G Van Schoot, and C J Den Otter. Neural coding in antennal olfactory cells of tsetse flies (glossin spp.). *Chemical Senses*, 23:521–530, 1998.

[153] X-J Wang and J Rinzel. Alternating and synchronous rhythms in reciprocally inhibitory model neurons. *Neural Computation*, 4:84–97, 1992.

[154] X-J Wang and J Rinzel. Oscillatory and bursting properties of neurons. In M A Arbib, editor, *The Handbook of Brain Theory and Neural Networks*, pages 686–691. MIT Press, Cambridge, Massachusetts, 1995.

[155] M Wehr and G Laurent. Odour encoding by temporal sequences of firing in oscillating neural assemblies. *Nature*, 384:162–166, 1996.

[156] H R Wilson and J D Cowan. Excitatory and inhibitory interactions in localized populations of model neurons. *Biophysical Journal*, 12:1–24, 1972.

[157] Z J Zhou. A critical role of the strychnine-sensitive glycinergic system in spontaneous retinal waves of the developing rabbit. *The Journal of Neuroscience*, 21(14):5158–5168, 2001.